LM-00K072
September 5, 2000

Shallow Cavity Flow Tone Experiments: Onset of Locked-On States

D. Rockwell, J.C. Lin, P. Oshkai, M. Reiss, M. Pollack

NOTICE

L-M MS1 071900

SHALLOW CAVITY FLOW TONE EXPERIMENTS: ONSET OF LOCKED-ON STATES

by

D. Rockwell* J.-C. Lin* P. Oshkai*

M. Reiss* M. Pollack†

*Lehigh University
Department of Mechanical Engineering
and Mechanics
354 Packard Laboratory
19 Memorial Drive West
Bethlehem, PA 18015

†Lockheed- Martin
P. O. Box 1072
Schenectady, NY 12301

Fully turbulent inflow past a shallow cavity is investigated for the configuration of an axisymmetric cavity mounted in a pipe. Emphasis is on conditions giving rise to coherent oscillations, which can lead to locked-on states of flow tones in the pipe-cavity system. Unsteady surface pressure measurements are interpreted using three-dimensional representations of amplitude-frequency-inflow velocity; these representations are constructed for a range of cavity depth. Assessment of these data involves a variety of approaches. Evaluation of pressure gradients on plan views of the three-dimensional representations allows extraction of the frequencies of the instability (Strouhal) modes of the cavity oscillation. These frequency components are correlated with traditional models originally formulated for cavities in a free-stream. In addition, they are normalized using two length scales: inflow boundary-layer thickness and pipe diameter. These scales are consistent with those employed for the hydrodynamic instability of the separated shear layer, and are linked to the large-scale mode of the shear layer oscillation, which occurs at relatively long cavity length. In fact, a simple scaling based on pipe diameter can correlate the frequencies of the dominant peaks over a range of cavity depth.

The foregoing considerations provide evidence that pronounced flow tones can be generated from a fully-turbulent inflow at very low Mach number, including the limiting case of fully-developed turbulent flow in a pipe. These tones can arise even for the extreme case of a cavity having a length over an order of magnitude longer than its depth. Suppression of tones is generally achieved if the cavity is sufficiently shallow.

1. INTRODUCTION

A conceptual framework for the generation of flow tones requires, first of all, consideration of strictly hydrodynamic oscillations in an acoustic-free system, then the coupling of such

oscillations with the acoustic mode(s) of a resonator. These concepts, as well as related issues and objectives, are described below.

1.1 CAVITY OSCILLATIONS IN AN ACOUSTIC-FREE SYSTEM

The origin, or stimulus, of locked-on flow tones is the inherent, organized unsteadiness of the velocity and vorticity fields along the cavity. Figure 1a shows the essential features of self-sustaining cavity oscillations: (a) vorticity concentration(s) incident upon the trailing corner of the cavity; (b) upstream influence of the vorticity distortion at the trailing corner to the sensitive region of the shear layer formed from the leading corner of the cavity; (c) conversion of the upstream disturbance arriving at the leading-edge to a fluctuation in the separating shear layer; and (d) amplification of this fluctuation in the shear layer as it develops in the streamwise direction. To be sure, for the case of fully turbulent inflow, organized unsteadiness of the shear layer along the cavity may not be immediately evident; nevertheless, the shear layer may exhibit a predisposition for broadband undulations. The basic elements associated with self-sustained oscillations described in Figure 1a were defined in the early investigation of Powell (1961) for the simpler case of a planar jet impinging upon a leading-edge. Since then, Rockwell and Naudascher (1978, 1979), Rockwell (1983), Blake (1986), Howe (1997), and Rockwell (1998) have described these elements for a variety of configurations of impinging shear layers, including the cavity configuration.

1.2 CAVITY OSCILLATIONS IN AN ACOUSTIC-RESONANT SYSTEM

Flow past a cavity in presence of an acoustic resonator, such as a long pipe, can exhibit coupling with one or more resonant modes of the pipe. This type of lock-on has conceptual similarities to that occurring in a wide variety of other flow-acoustic configurations. Rockwell and Naudascher (1978, 1979), Rockwell (1983, 1998) and Blake (1986) summarize extensive investigations of lock-on flow past cavity configurations, including not only quasi-two-dimensional geometries, but also circular, triangular, and whistle-shaped cavities. Representative systems that exhibit lock-on behavior are described below.

Jet excitation of a long organ pipe. Large amplitude oscillations of the jet at the mouth of an organ pipe occur during resonant coupling with a pipe mode(s). Cremer and Ising (1967) visualize the jet oscillations and analyze the jet-organ pipe as a controlled system. Techniques for determining the amplitude and phase of the controller are also addressed. This same class of resonant coupling is reviewed by Fletcher (1979), who describes further aspects of the jet-organ

pipe configuration from a systems perspective. Moreover, further aspects of nonlinear interactions in organ flue pipes are analyzed in works summarized by Fletcher (1979).

Jet-sequential orifice plates. Resonant coupling of the jet instability through a series of orifice plates, i.e., baffles, simulates the coupling that occurs in segmented solid rocket motors. In this case, the acoustic wavelength is the same order, or less than, the baffle spacing. In other words, the resonator is the cavity. Flatau and Van Moorham (1990) emphasize the importance of distinguishing between the resonance of inlet and nozzle cavities, relative to resonance of the total test section. Further insight into this type of lock-on configuration is provided by Hourigan, Welsh, Thompson and Stokes (1990). They employ a discrete vortex simulation, in conjunction with the theoretical concept of Howe (1975, 1980), to assess the generation of instantaneous acoustic power. A recent investigation of locked-on flow tone generation in a baffle system by Stoubos, Benocci, Palli, Stoubos, and Olivari (1999) emphasizes the empirically-determined amplitude and frequency response characteristics of the tone as a function of flow velocity through the baffle system. All of the foregoing investigations are, in certain respects, related to early experiments on the fluid mechanics of whistling undertaken by Wilson, Beavers, DeCoster, Holger, and Regenfuss (1971). In their work, a set of two sequential orifice plates, each having rounded edges, gives rise to well-defined whistles or tones, and the nature of the jet instability related to these types of flow tones is similar to those of the foregoing studies.

Wake from a flat plate in a test section. Vortex shedding from the blunt trailing-edge of a flat plate in the test section of a wind tunnel gives rise to highly coherent resonant coupling with the acoustic mode(s) of the plate-test section system. These modes are often referred to as Parker modes, based on investigations of Parker (1966), which are summarized by Cumpsty and Whitehead (1971). The latter provide a theory that allows the amplitude of the forced acoustic mode to be predicted from the pressure field below resonance and the measured damping factor of the acoustic mode. Stoneman, Hourigan, Stokes, and Welsh (1988) have recently undertaken an additional, in-depth investigation of a similar lock-on phenomena involving two plates in tandem in a duct.

Cavity shear layer - cavity resonator. For the case of an orifice in a wall bounded by a closed cavity, DeMetz and Farabee (1977) determined the response characteristics of the coupled shear layer-cavity resonance as a function of the character of the inflow boundary layer, i.e., whether it is laminar or turbulent. Elder (1978) provides a systems model in conjunction with

measurements. Elder, Farabee, and DeMetz (1982) give detailed spectra and mode characterization of flow tone generation due to both laminar and turbulent boundary layers approaching the cavity. Moreover, a model is formulated for the self-excited oscillations. Nelson, Halliwell, and Doak (1981, 1983) have undertaken detailed measurements of the time-averaged unsteady shear layer in relation to the overall response characteristics of the coupled system. In their more recent study, momentum and energy balances are employed to characterize the physics of these oscillations.

Cavity shear layer - side branch duct/pipe. Early characterization of the frequency and amplitude characteristics in a jet-pipe (side branch) resonator was undertaken by Pollack (1980). Coupled resonant oscillations that occur in a pipe branch system have been addressed both theoretically and experimentally by Bruggeman, Hirschberg, van Dongen, Wijnands, and Gorter (1989, 1991) and Kriesels, Peters, Hirschberg, Wijnands, Iafrati, Riccaradi, Piva and Bruggemann (1995). In essence, this configuration represents the flow past a deep cavity. Both experiments and theory are employed to explain the acoustic and hydrodynamic conditions for resonance. This analysis leads to a concept that provides the ratio of acoustic to steady flow amplitudes. Ziada and Buehlmann (1992) and Ziada and Shine (1999) characterize this class of coupling for various side branch configurations.

Cavity shear layer - long pipeline. The radiated sound due to lock-on of flow past a cavity inserted in a long pipeline has been experimentally characterized in a series of investigations extending from Davies (1981) to Davies (1996a,b). Sound propagation within, and radiation from, various configurations is summarized therein. The primary emphasis of these investigations has been identification of the locked-on resonant frequencies. Virtually no attention was given to the underlying physics. Rockwell and Schachenmann (1982, 1983) provided the first measurements of the physical behavior of the unsteady shear layer along the mouth of a circular cavity at the end of a long pipe, in conjunction with the locked-on and non-locked-on states. Concepts of linearized, inviscid stability theory were employed as a guide to determining the phase shifts and amplitude spikes across the shear layer. In addition, they characterized the streamwise phase difference, which is essential to the locked-on condition. Moreover, they also showed that during lock-on, the magnitude of the fluctuating velocity due to acoustic resonance can be of the same order as that associated with the hydrodynamic (vorticity) fluctuations. This coexistence of acoustic and instability waves can give rise to false standing

wave patterns along the core of the jet in an acoustically-resonant system, as emphasized by Rockwell and Schachenmann (1980). Such false, short wavelength patterns are not limited to locked-on, self-excited cavity oscillations. They also occur in acoustically-forced jets investigated by the Berlin group, originating with Pfizenmaier (1973).

Further insight into the lock-on phenomena that occur in the cavity-pipeline system is provided by Rockwell and Karadogan (1982). Using zero-crossing statistics, in conjunction with recursive digital filtering, they determined the self- and cross-probability density of velocity and pressure. The degree of phase fluctuation of organized oscillations of turbulent jet flow through the cavity was characterized in terms of a mean phase deviation from the locked-on condition. In this manner, it is possible to characterize phase fluctuations as the phase-locked condition is approached.

Finally, attenuation of pipeline-cavity oscillations has been undertaken by Rockwell and Karadogan (1983). A variety of attenuation configurations were considered. Among them, small-scale vortex generators were shown to be very effective in attenuating the lock-on oscillations.

1.3 CAVITY OSCILLATIONS IN AN ACOUSTIC-RESONANT PIPE SYSTEM: UNRESOLVED ISSUES AND OBJECTIVES

Very little is known of self-excited oscillations of a fully turbulent inflow past a cavity, which is bounded on either side by a pipe. Coherent oscillations are expected to occur when an acoustic resonant mode of the pipe-cavity system is compatible with an inherent instability of the turbulent shear layer past the cavity. The major unresolved issues are:

(a) The possibility of locked-on flow tones arising from a fully turbulent inflow and, in the limiting case, of a fully developed turbulent flow in a pipe, has not been clarified. The onset of such flow tones would require growth of an inviscid instability on the turbulent background of the separated shear layer past the cavity.

(b) Flow tones in relatively shallow cavities at very low values of Mach number have not been addressed. More specifically, when the acoustic wavelength is much longer than the length of the cavity, then acoustic resonance cannot occur within the cavity. Most investigations of flow tones at low Mach number have involved sufficiently deep cavities, such that the large-scale instability of the separated shear layer develops in a relatively unhindered fashion. As the cavity becomes relatively shallow, it is anticipated that the growth of large-scale vortical

structures is hindered, and conditions for the onset of shear layer-resonator coupling, leading to flow tones, may not be attainable.

(c) The appropriate dimensionless scaling for the frequencies of dominant pressure amplitude peaks of flow tones, provided they exist, has not been established. It is expected that, for a relatively deep cavity, which is sufficiently long such that the large-scale vortical structures develop, scaling based on pipe diameter D would be appropriate. In this case, it is anticipated that the vortical structures would correspond to the fully-developed axisymmetric instability of the jet-like shear layer through the cavity. The possibility of extending this type of scaling to extremely shallow cavities has not been addressed. Furthermore, the sensitivity of this scaling based on diameter D to variations in the inflow boundary layer thickness has not been clarified. If the large-scale instability evolves to the same form along a relatively long cavity, irrespective of the initial boundary layer thickness, the case for scaling of the dimensionless frequency based on D would be even more compelling.

(d) The manner in which the amplitudes of flow tones are attenuated as a function of depth of a shallow cavity is unknown. Furthermore, the possibility of the non-existence of flow tones at a very small cavity depth is an important limit that has not been defined. A further, important aspect is whether discernible spectral peaks, which would represent a low level instability in absence of flow tone generation, can be detected in very shallow cavities.

(e) The effect of mode spacing of the resonant modes of the pipe-cavity system, as well as the absolute frequency of the lowest mode of the pipe-cavity system, may influence the types of transformation between the resonant modes of the pipe-cavity system when the inflow velocity is altered. This feature has not been addressed for either deep or shallow cavity-pipe configurations.

The objectives of the present investigation are centered on these unresolved issues. Pressure measurement techniques will be employed in conjunction with: three-dimensional images of the pressure amplitude response; and techniques for assessing these images.

2. EXPERIMENTAL SYSTEM AND TECHNIQUES

2.1 OVERVIEW OF EXPERIMENTAL SYSTEM

The experimental system was designed and manufactured in the Fluid Mechanics Laboratories at Lehigh University. In essence, the system consists of two principal subsystems. The first is the air supply system, and the second is the actual pipeline-cavity system. These two subsystems are located in different rooms, with a thick ceramic wall between them, in order to isolate mechanical vibrations associated with the compressor system.

2.2 AIR SUPPLY SYSTEM

The air supply system involves an air compressor, which provides air to a compressed air plenum. Within the compressed air plenum, the air is maintained at a gauge pressure of 552-689 kPa (80-100 psig). The air exhausts from the plenum into an air dryer where water is separated from the air. A filter system extracts undesirable particles from the air. The air is then transmitted through the isolation wall into the room housing the main experimental facility.

An overview of the pipeline-cavity system is given in Figure 2a. A pipe-valve arrangement for regulating low and high flow rates to the pipeline-cavity system is located at its upstream end. When low velocities through the pipeline-cavity system are desired, air is sent through a series of two pressure regulators to accurately control the flow rate. The first regulator operates at high pressures and takes the air input from approximately 621 kPa gauge (90 psig) to 138 kPa gauge (20 psig). The second regulator then limits the air output to a maximum of approximately 14 kPa gauge (2 psig), which corresponds roughly to a maximum of 9.1 m/s (30 ft/s) through the pipe. When it is desired to generate higher velocities through the pipeline-cavity system, the second regulator, which operates at lower pressures, is bypassed. In this case, the maximum centerline velocity through the pipe system is approximately 61 m/s (200 ft/s). In summary, the role of this pipe-valve system is to provide a regulated, constant air supply to the inlet plenum of the main pipeline-cavity system, as indicated in Figure 2a.

2.3 PIPELINE-CAVITY SYSTEM

Inlet plenum. The inlet plenum of the pipeline-cavity system is shown in the plan and side views of Figure 2a. It is constructed from Plexiglas, and houses a 2.5-inch thick layer of honeycomb, which acts as a flow straightener. Moreover, the inside of the plenum is lined with acoustic damping foam to minimize local acoustic resonances. The exit of the plenum contains a contraction, which was designed to prevent localized separation in the pipe inlet. To ensure that

the large changes in pressure gradient near the exit of the nozzle did not produce localized perturbations that would propagate downstream and, furthermore, to generate a fully-turbulent boundary layer, a trip ring was located immediately downstream of the exit of the plenum contraction. This ring was located a distance of 35 mm from the pipe inlet. It had a thickness of 1 mm, and was 4 mm long. Its geometry involved a series of adjacent triangular cuts along the leading-edge of the ring.

Pipeline-cavity arrangement. The main pipeline-cavity arrangement was located downstream of the inlet plenum, as indicated in Figure 2a. The first version of this system, shown in Figure 2a, consists of two 2.4 m (8 ft) segments of 25.4 mm (1 in) ID aluminum piping, located on the upstream and downstream sides of the Plexiglas cavity. This aluminum pipe had a thickness of 3.2 mm. A total of three pressure transducers were located in the inlet (upstream) pipe. They were positioned at distances of 127, 1213, and 2365 mm upstream of the exit of the inlet (upstream) pipe. Furthermore, a similar system of transducers was mounted on the exhaust (downstream) pipe. They were located at distances of 78 mm and 1218 mm upstream of the exit of the pipe.

The second version of the pipeline-cavity system employed the same inlet plenum and cavity; however, shorter inlet (upstream) and exhaust (downstream) pipe sections were employed. These sections had a length of 30.48 cm (12 in). One pressure transducer was located in the inlet (upstream) pipe at a distance of 125 mm from the pipe exit. Regarding the exhaust (downstream) pipe, one transducer was also mounted along this pipe at a distance of 152 mm from the pipe exit.

Mounting arrangement for pressure transducers. The pressure transducers located along the inlet (upstream) and exhaust (downstream) pipes were PCB high sensitivity transducers (Model U103AO2); the same transducers were employed for measurements within the cavity system, as described subsequently in Section 2.4. The design for mounting the transducers on the pipe was based on the recommendations of PCB. The diameter and depth of the hole drilled into the aluminum piping was kept as small as possible, so that the flow was not distorted. Moreover, the mounting arrangement shown ensures, for the range of frequencies of interest in this investigation, that no acoustic resonant effects were generated in the region between the face of the transducer and the surface of the pressure tap at the interior of the pipe.

2.4 CAVITY SUBSYSTEM

The cavity system is shown in Figure 2b. The inlet (upstream) aluminum pipe, designated as pipe A, is maintained in a fixed position on the pipe supports. The left end of the Plexiglas tube slides along the exterior of a smoothly-machined exterior surface of the inlet (upstream) pipe A. In essence, this sliding arrangement allows adjustment of the cavity length L with a high degree of accuracy and repeatability. This adjustment was achieved by employing a traverse mechanism (see the pipe translation system in Figure 2a), which translated the entire pipe B and the Plexiglas tube attached to it. The junction between the interior of the Plexiglas tube and the exterior of the exhaust (downstream) aluminum pipe B is fixed. The internal diameter D of the two pipes A and B is 25.4 mm (1 in).

The downstream end of pipe A and the upstream end of pipe B form the leading- and trailing-edges of the cavity, respectively. In order to obtain different values of cavity depth W, the exterior diameters of pipes A and B were altered. This was accomplished by placing Plexiglas sleeves around the ends of pipes A and B. Correspondingly, the interior diameter of the Plexiglas tube was altered as well. Since it was desired to investigate a total of four values of cavity depth $W^* = W/D = 1.25$, 0.5, 0.25 and 0.125, in which D = 25.4 mm (1 in) this meant that four different aluminum pipe-Plexiglas-tube combinations were manufactured.

Pressure transducers were deployed in order to obtain pressure measurements on the trailing- (impingement-) corner of the cavity, as well as on the floor of the cavity. In subsequent notations of pressure measurements, the pressure transducer in the pipe upstream of the cavity is designated as p_3, that at the corner as p_5, and that on the cavity floor as p_4 (see Figure 2b). Since both of these transducers (p_4 and p_5) were fixed with respect to pipe B and the Plexiglas tube attached to it, their position, relative to the trailing-corner of the cavity, remained unaltered when the cavity length L was varied.

2.5 PRESSURE MEASUREMENTS

Pressure transducers. PCB transducers (Model No. U103A02) were employed for pressure measurement. These transducers have a nominal sensitivity of 1727 mv/psi. The outputs from the transducers were connected to a PCB Piezotronics multi-channel signal conditioner, Model 48A. This multi-channel conditioner allowed independent adjustment of the gains of the pressure transducer signals. Generally speaking, however, it was possible to employ the same value of

gain for all pressure measurements. This gain adjustment is important in order the meet the required voltage input levels of the A/D (analog/digital) board.

Acquisition of pressure signals. The conditioned pressure signals were transmitted to ports on a National Instruments board (Model PCI-MI0-16E-4). This board, when operating in the single channel acquisition mode, can sample at the rate of 250 KS/sec, in which K = 10^3 and S is the number of samples. In the present scenario, a total of eight pressure transducers were employed, so the effective sampling rate is reduced by a factor of eight, i.e., it takes on a value of 31 KS/sec per channel. In essence, there are two considerations to determine whether this sampling rate is adequate. First of all, for characterization of pressure in the frequency domain, the sampling rate should be at least twice the maximum frequency of interest. For representations in the time domain, a minimum of five samples per cycle is required, but a minimum of ten samples per cycle is desirable. Considering these requirements together, the acquisition system should have a sampling rate at least ten times as high as the maximum typical frequency of interest in the present investigation, which corresponds approximately to 1.5×10^3 Hz. This requirement is approximately a factor of twenty lower than the acquisition rate of 31 KS/sec per channel. It is also important to realize that this type of board basically consists of one A/D (analog digital) converter, and the acquisition of eight pressure signals is accomplished using a multiplexing technique. The scan interval is defined as the time required to go from a recorded point corresponding to pressure transducer No. 1, through the sequence of the other seven transducers, and return to the channel of transducer No.1. This scan interval is basically the inverse of the maximum data acquisition rate per channel from i.e. $1/(31.25 \times 10^3)$, which corresponds approximately to 32 microseconds.

Processing of pressure signals. A Pentium II 350 MHz computer and LabView software were used to process the pressure transducer signals. The major parameters for spectral analysis using the Fast Fourier Transform (FFT) must be properly defined so that adequate resolution in the frequency domain is accomplished, while at the same time minimizing the amount of collected data. In order to determine which values of each parameter were adequate, a series of averaging tests were performed using broadband noise input. For a given set of parameters, the number of averaged files was varied to determine the minimum number of files and, hence, the minimum number of data samples needed to properly represent the system response.

The parameters were: (i) the number of samples acquired per data set; (ii) the sampling rate; and (iii) the number of data sets employed to obtain an average. The sampling rate must be twice as high as the maximum frequency of interest. Therefore, the necessary sampling rate varied directly with the maximum frequency of interest for each experiment. The value of the frequency resolution (Δf) is equal to the sampling rate (f_s) divided by the number of samples per data set (n_s). Once the sampling rate was determined for each experiment, the number of samples was calculated according to $n_s = f_s/\Delta f$.

In order to determine the value for Δf, another set of averaging experiments was performed. Values of Δf were varied. These tests showed that Δf = 0.5 Hz adequately characterized the system response, while providing acceptable frequency resolution at both the low and high ends of the frequency range of interest in this research program. At the lowest and highest frequencies of interest, approximately 35 and 1,500 Hz, $\Delta f/f$ has its maximum and minimum values of 0.014 and 0.00034 respectively.

During acquisition of final experimental data, the sampling rate was set to 4,096 samples per second, which resulted in a Nyquist frequency of 2,048 Hz, well above the maximum frequency component of interest for this research, which was approximately 1,500 Hz. The number of samples per data set (n_s) was then specified, while maintaining Δf = 0.5 Hz, resulting in 2^{13} = 8,192 samples per data set. Each of the spectra represented herein was obtained by averaging a total of 42 data sets.

Unless otherwise indicated, all pressure measurements herein correspond to a reference location (i.e., at pressure transducer p_3 as defined in Section 2.4) in the pipe resonator. Comparisons of measurements at different locations are given in Section 6.

2.6 VELOCITY MEASUREMENTS

In order to characterize in detail the mean and fluctuating velocity distributions at the exit of the inlet (upstream) pipe A, hot wire anemometry was employed. A miniature hot-wire probe was traversed across the pipe exit. The traverse system was equipped with a linear variable displacement transducer (LVDT), so that the position of the hot-wire probe could be positioned with a precision of approximately 0.1 mm. In-house software was used to calculate the mean and fluctuating velocity components from the raw hot-wire signal.

For the wide range of measurements during the course of this investigation, it was necessary to have an accurate and repeatable means to determine the time-averaged centerline

velocity $\bar{u}_m$. This was accomplished by using a pressure tap on the side of the inlet plenum and a tap located at the exit of the orifice plate, which was attached to the downstream end of the plenum. The difference between these two pressure measurements provided a reference value for calculating the centerline velocity of the flow through the pipe. This pressure difference was calibrated against the centerline velocity at the exit of the exhaust (downstream) pipe B using two different approaches. The first involved the calibrated hot-wire, described in the above, and the second was based on the measurement of total pressure by means of a Pitot probe at the exit of the pipe. The total pressure was measured using one of two Validyne transducers, model DP103-104 for smaller values of flow velocity and model DP15-24 for higher values of flow velocity.

3. INFLOW CONDITIONS

A major purpose of the present investigation is to determine whether self-excited flow tones can be generated when the inflow conditions are fully turbulent. Proper specification of the inflow conditions is important in several respects. First of all, it is desirable to ensure that quasi-laminar or transitional phenomena do not exist in the approach flow. For the limiting case of laminar inflow, i.e., a laminar boundary layer, self-excited coherent oscillations, which have pronounced spectral peaks, can be generated even in the absence of a coexisting acoustic resonance of the cavity or an adjacent pipe.

A second reason for specifying details of the inflow conditions is to facilitate the scaling of the dimensionless frequencies of oscillation. Geometric parameters are often used to characterize the frequency of oscillation, e.g., fL/U, in which L is the cavity length and U is the characteristic velocity or fD/U, where D is the diameter of the inflow pipe. Such geometric scaling does not account for the variations of boundary layer thickness that exist in different practical configurations.

The momentum thickness $\theta = \int_0^\infty (\bar{u}/\bar{u}_m)(1-\bar{u}/\bar{u}_m)dy$ is typically employed to represent the characteristic thickness of a shear flow. In this investigation, velocity $\bar{u}$ is the average streamwise velocity at any location, and $\bar{u}_m$ is its value at the centerline of the pipe. The value of θ was determined for the extreme cases of velocity distributions described in this section. The distributions of mean and fluctuating velocity are considered for two basic cases: (a) a long pipe, having a length to diameter ratio of 96, which ensures a fully-developed flow at the pipe exit;

and (b) a relatively short pipe having a length to diameter ratio of 12, which has a turbulent boundary layer at its exit that is not fully-developed. As indicated in Section 2, a boundary layer trip ring was located at the pipe inlet for both cases of the long and short pipes. This trip promotes the rapid onset of turbulence, which was especially important for the case of the short pipe.

Prior to characterizing the values of momentum thickness for the long and short inlet pipes, efforts were focused on ascertaining the turbulent nature of the flow at the exit of each pipe. This involved determination of distributions of normalized root-mean-square velocity u_{rms} across the pipe. These distributions were found to be in agreement with established results. In addition, the logarithmic form of the velocity distribution was pursued. The traditional semi-logarithmic representation of the mean velocity distribution at the exit of the long pipe is given in Figure 3a. In this plot, $\phi = \bar{u}/u_*$. That is, the local mean velocity $\bar{u}$ is normalized with respect to the wall friction velocity u_*. This dimensionless velocity is plotted as a function of log η, in which, $\eta = y u_*/\nu$. The purpose of this type of plot is to show the nature of the logarithmic and inner viscous layers. These data are compared with the standard distributions provided by Schlichting (1968). The log region is represented by $\phi = 5.75 \log \eta + 5.5$. In addition, this region of the boundary layer is compared with the so-called one-seventh power law distribution $\phi = 8.74\ \eta^{1/7}$. In the innermost region of the boundary layer, i.e., the viscous sublayer, the dimensionless velocity is according to $\phi = \eta$. This region corresponds to an extremely thin layer next to the wall.

Considering first the log region of the boundary layer, the data exhibit a generally linear variation in this region, corresponding to an actual logarithmic distribution. In the inner layer, the data generally follow the reference curve $\phi = \eta$, except for departures at the highest value of velocity.

Distributions of dimensionless mean velocity $\bar{u}/\bar{u}_m$ as a function of dimensionless distance y/R from the pipe wall are exhibited in Figure 3b for the short (top plot) and long (bottom plot) inlet pipes. Considering first of all the distributions of mean velocity given at the top of Figure 3b, a relatively flat region exists from approximately y/R = 0.4 to 1.0, corresponding to the "core" region of the pipe flow. Data for the velocities $70.7 \le \bar{u}_m \le 131.5$ are remarkably coincident. For these velocity distributions, the dimensionless momentum

thickness falls in the range of $0.029 \leq \theta_o/R \leq 0.035$. The definition of $\theta_o = \int_{y=0}^{y=R} (\bar{u}/\bar{u}_m)(1-\bar{u}/\bar{u}_m)dy$ was employed.

The bottom plot of Figure 3b represents the corresponding velocity distribution for the case of the long inlet pipe. The values of momentum thickness θ_o normalized by the pipe radius R lie in the range $0.088 \leq \theta_o/R \leq 0.096$.

4. OVERVIEW OF CHARACTERISTICS OF PRESSURE FLUCTUATIONS

The nature of unsteady pressure fluctuations arising from flow past a shallow cavity is complicated by variations in the cavity depth. In contrast to the overwhelming share of previous investigations, where the cavity depth is much larger than the characteristic thickness of the inflow shear layer, the existence of a sufficiently shallow cavity is expected to substantially alter the onset and growth of instabilities in the separating shear layer. The consequence is a rich variety of possible flow states within the cavity. In the present investigation, emphasis is on the case of a sufficiently long cavity length L_m such that, for a deep cavity, the fully-evolved axisymmetric instability of the separated shear layer occurs. This limiting case is well studied for the corresponding case of a free axisymmetric jet. In fact, as will be discussed, the scaled frequencies of a sufficiently deep cavity agree remarkably well with this limiting, reference case. Moreover, preliminary diagnostics showed that the largest amplitude spectral peaks occurred for this long cavity length L_m, irrespective of the cavity depth W. The present results provide extensive characterization of the unsteady pressures as a function of inflow velocity U, cavity depth W, and the thickness of the inflow shear layer.

4.1 SUMMARY OF RANGES OF PARAMETERS

The cavity length was adjusted to a fixed value of $L_m^* = L_m/D = 2.5$, which, as indicated in the foregoing, allowed the fully-evolved axisymmetric instability mode to develop in the deepest cavity. The cavity depth was then varied according to $W^* = W/D = 1.25$, 0.5, 0.25, and 0.125. The largest value of depth $W^* = 1.25$ should, in concept, represent a sufficiently deep cavity, such that the instability in the free shear layer develops in a relatively unhindered fashion. At the other extreme, $W^* = 0.125$ is small in comparison with the pipe diameter D, and thereby represents the case of a very shallow cavity. The inflow velocity U was varied up to a maximum value of approximately 200 ft/sec, depending upon the particular experimental configuration.

Furthermore, the characteristic thickness of the inflow boundary layer was altered by attaching both long and short inlet pipes; this approach led to extreme values of momentum thickness θ_o, as described in Section 3.

The pressure amplitude is averaged over the effective bandwidth Δf of the spectral amplitudes

4.2 METHODS OF PRESENTATION OF DATA

Features of the fluctuations are represented by pressure spectra. For a given experimental run, a relatively large number of spectra are acquired. It is therefore useful to develop a unified, comprehensive presentation of families of spectra. This was accomplished by developing a color-coded, isometric view; a representative image of this type is given in Figure 4a. In constructing these representations, a total of 37 to 40 spectra were employed. In the case where velocity was varied during the experimental run, values of spectral amplitude were interpolated along the velocity axis. Similarly, for the case where the cavity length was altered, interpolation was carried out in the direction of the cavity length. The magnitudes of pressure were color-coded, such that gradations of color are evident in three-dimensional space, thereby providing an overview of the conditions for which relatively high-pressure amplitudes are generated. Since the focus of this program is on conditions for the onset of flow tones, most of the changes in color level are concentrated at lower values of pressure amplitude. Once a threshold value of amplitude is exceeded, the color magnitude is maintained the same for all higher values. This color was, in fact, white. As a consequence of this approach, it is not possible to determine, in certain cases, the maximum amplitude of the pressure spectra based on the three-dimensional color plots. Complete families of spectra are therefore provided in a separate compendium, so that the reader can easily deduce details of each individual spectrum.

A plan view of each isometric, three-dimensional color plot is also provided in each case. It allows a perspective on a plane of velocity vs. frequency and identification of high values of pressure amplitude. This type of view also gives a rapid indication of the extent of each locked-on mode of a flow tone.

Further representations of the pressure variations involve either isometric or plan views of logarithmic, as opposed to linear, pressure amplitude. This type of view emphasizes the variation of the background fluctuations, in addition to the resonant values associated with generation of flow tones.

Finally, effort was devoted to implementing a means of detecting peaks in the plot of logarithmic pressure amplitude. The principal aim here was to educe low-level peaks of pressure, which otherwise remain undetected in simple plots of logarithmic pressure amplitude

or linear pressure amplitude. Once these peaks were identified, they could be represented on the plane of velocity vs. frequency, in order to determine the variation of the inherent instability frequency of the shear layer, i.e., Strouhal frequency, that gives rise to vortex formation. A successful approach to educing low level peaks involved, first of all, taking the derivative of the logarithmic pressure amplitude with respect to velocity. This derivative may be written as:

$$\partial(\log p)/\partial U \tag{4.1}$$

Once this derivative is evaluated, it is plotted in a color-coded form on either the velocity vs. frequency plane or the velocity vs. cavity length plane. The magnitudes of the derivatives are color coded in such a manner that a pressure peak, which corresponds to an essentially discontinuous change in the sign of the slope, according to equation (4.1), is represented by a sharp junction between two distinctive colors. A line passing through these detected peaks is then plotted on the aforementioned plan view of pressure amplitude as a function of velocity vs. frequency or, alternately, on the plan view of pressure amplitude in relation to cavity length vs. velocity. This is a very effective approach to identify a low amplitude peak that is not associated with a flow tone, but nevertheless represents a localized peak due to the inherent instability mode of the shear layer, which is accentuated by presence of the resonator.

In the following, the types of color representations described in the foregoing are shown, first of all, for: (a) variations of the inflow velocity; and (b) alterations of the cavity length L.

4.3 PRESSURE FLUCTUATIONS FOR VARIATIONS OF INFLOW VELOCITY

The pressure response characteristics of the pipeline-cavity that correspond to variations of inflow velocity are examined for the two extreme inflow shear layers defined in Section 3. As described therein, these different inflow conditions are generated via attachments of long and short inlet pipes.

4.3.1 Long Inlet Pipe-Cavity System

Figures 4a through 4f exhibit the pressure amplitude response that corresponds to variations of inflow velocity $U \equiv \bar{u}_m$, i.e., the averaged velocity at the centerline of the pipe. The cavity length L is maintained at its maximum value, designated as L_m. Variations of cavity depth W are considered. Figures 4a,b show the case of a relatively deep cavity and, at the other extreme, Figure 4f represents the shallowest cavity.

For the case of the deepest cavity exhibited in the top image of Figure 4a, pronounced peaks of pressure amplitude are evident at values of inflow velocity of the order of 70 ft/sec and higher. Harmonics of these peaks are either very small or indistinguishable. The peaks shown in this image coincide with the resonant modes of the long pipe-cavity system having frequencies approximately in the range from 300 to 600 Hz. The bottom image of Figure 4a, which shows a plan view of the variation of pressure amplitude over the plane of frequency versus inflow velocity U, indicates clearly the sequential excitation of higher modes of the resonant pipe-cavity system with increasing velocity. The thin, elongated white regions correspond to the peaks exhibited in the isometric view, i.e., in the top image of Figure 4a. At the center of each of these peak (white) regions, the amplitude of the pressure in the neighboring resonant modes is small. On the other hand, near the edges of a given peak (white) region, there is clearly simultaneous excitation of two neighboring resonant modes. This feature is inherent to excitation of flow tones in resonant systems having multiple resonant modes. The black lines indicated in the bottom image of Figure 4a represent constant values of dimensionless frequency fL/U. They pass through the pressure peaks. Although the line having the largest slope passes through distinct and highly visible peaks, the remaining two lines pass through peaks that are less well defined. In order to extract these peaks, the plan view corresponding to the bottom image of Figure 4a was directly compared with the bottom image of Figure 4b, which employs the criterion for identification of peaks.

The top image of Figure 4b shows a plan view of the pressure amplitude on the velocity-frequency plane. It is based on the same data as Figure 4a, except the pressure is expressed in terms of its logarithmic value, i.e., log p. This plot shows further features of locally high values of pressure amplitude outside the clearly distinct peaks. The bottom image of Figure 4b is a plan view of the variation of the parameter $\partial(\log p)/\partial U$ over the velocity vs. frequency plane. As addressed in the foregoing, this parameter aids in peak identification. At locations of the peaks, the slopes on either side of the peak abruptly change from positive to negative values, and thereby the colors show an abrupt change. It should be emphasized that this type of representation shown in the bottom image of Figure 4b is simply intended to serve as an aid in extracting peaks. By no means does it provide an indication of lock-on associated with generation of flow tones. This concept of lock-on will be addressed subsequently.

Figures 4c,d represent the case of a shallower cavity having a depth $W^* = 0.5$. The most striking feature of the top image of Figure 4c, in comparison with the case of the deeper cavity

corresponding to Figure 4a, is that the velocity for onset of a pronounced peak is shifted to a higher value of approximately 120 ft/sec, which is approximately 50% larger than the onset velocity for the deep cavity of Figure 4a. Generally speaking, however, the overall form of the distribution of peaks is similar to that of Figure 4a for the deep cavity. Observations of the bottom image of Figure 4c are, in many respects, similar to the corresponding plan view of Figure 4a. Lines of constant fL/U are linear and pass through the sequence of pressure peaks. In Figure 4d, the plot of logarithmic pressure amplitude is shown in an isometric view (top image), in order to further emphasize the locally large values of pressure amplitude, in addition to the well-defined peaks evident in Figure 4c. This plot also clearly shows the increase in background pressure fluctuation amplitude as the velocity is increased. The plot of magnitude of $\partial(\log p)/\partial U$ on the plane of velocity versus frequency, represented by the bottom image of Figure 4d, is directly analogous to the corresponding plot of Figure 4b.

A further decrease in cavity depth to a value of $W^* = 0.25$ is represented in Figure 4e. The top image of Figure 4e shows the generation of a number of well-defined peaks, which are coincident with the resonant modes of the pipe-cavity system. An important observation is that these peaks are generated only at very high values of inflow velocity, i.e., of the order of U = 150 ft/sec and larger. Although there may be a tendency to interpret these peaks as an indication of locked-on flow tones, this may not be the case; further assessments are required and are addressed in Section 6. The plan view of linear pressure amplitude on the plane of velocity vs. frequency is represented in the bottom image of Figure 4e. The white regions, which indicate the highest amplitude peaks, generally do not have the same sharply-defined symmetrical form as exhibited previously in the bottom images of Figure 4a and 4c. Nevertheless, there is a tendency for these white, peak-like regions to follow a constant fL/U, i.e., the black line having the greatest slope in the bottom image of Figure 4e. As in the previously described cases corresponding to deeper cavities, the black line of the lower slope was constructed with the aid of the pressure gradient concept defined by equation (4.1).

The case of the shallowest cavity, $W^* = 0.125$, is shown in Figure 4f. The top image of Figure 4f reveals that significant peaks are attainable only at the highest values of flow velocity of the order of U = 200 ft/sec. Since these peaks have very low amplitude, it is possible to observe an increase in pressure amplitude for all of the pipe-cavity modes as the inflow velocity increases. Considering the bottom image of Figure 4f, which shows the plan view of linear pressure amplitude p on the plane of velocity vs. frequency, it is clear that isolated, distinct

pressure peaks cannot be defined in the same manner as for deeper cavities, i.e., in the bottom images of Figure 4a through 4e. It is therefore not possible to construct lines of constant fL/U. This lack of a clearly defined Strouhal line of constant fL/U was further reaffirmed by examination of contours of constant pressure gradient calculated according to equation (4.1).

An overview of the pressure amplitude response for extreme values of cavity depth W is given in Figure 4g. These three-dimensional images are taken from Figures 4a, 4e and 4f. The transformation from sharply-defined pressure peaks to a larger number of less sharply-defined peaks having much lower amplitude is clearly indicated for decreasing values of cavity depth. Further observations are as follows: shallower cavities require a higher value of minimum flow velocity to attain a locked-on flow tone; for a sufficiently small cavity depth, lock-on is not attainable; and, for deeper cavities, lower order resonant modes lock-on because the critical flow velocity decreases. All of these features are most likely related to the manner in which the unsteady shear layer develops along the cavity. Presumably, for deeper cavities, the occurrence of large-scale vortex formation proceeds in a relatively uninhibited fashion, whereas for the shallowest cavity, it may not occur. This aspect will be addressed in a forthcoming investigation.

4.3.2 Short Inlet Pipe-Cavity System

A short inlet pipe to the cavity system was employed to: (i) examine the consequence of a smaller characteristic thickness of the inlet boundary layer; (ii) address the consequence of a higher value of absolute frequency for the lowest pipe-cavity resonant modes, i.e., N = 1, 2 and 3; and (iii) resolve the manner in which widely spaced resonant modes, which are attainable for the short pipe system, influence the onset of flow tones, relative to the closely-packed modes existing in the long pipe-cavity system, shown in Figures 4a through 4f.

The top image of Figure 5a represents the case of the deepest cavity. Clearly-defined peaks of pressure occur at resonant pipe modes centered approximately at 550 Hz, 1100 Hz, and 1600 Hz. These excited modes are clearly much more widely spaced than for the corresponding case of the long pipe-cavity system shown in the top image of Figure 4a. Two remarkable similarities exist, however, between the plots of Figure 5a and Figure 4a. First of all, the value of inflow velocity U for the onset of a clearly-definable peak of pressure amplitude is of the order of 70 ft/sec for both cases of Figures 5a and 4a. This similarity is perhaps more evident by comparing the plan view of pressure amplitude on the plane of velocity versus frequency, represented by the bottom image of Figure 5a, with the corresponding image at the bottom of Figure 4a. Note that, at a given velocity, as many as three well-defined peaks exist; moreover,

they are, in an approximate sense, harmonically related. This suggests that multiple Strouhal modes may coexist in the separated shear layer. In the absence of an acoustic resonator, it is known that an unstable shear layer can exhibit a number of coexisting, well-defined frequency components as shown by Knisely and Rockwell (1982).

The second notable feature of the plots of Figure 5a is that the dominant resonant mode in Figure 5a is of the order of 550 Hz, while in Figure 4a, the excited modes extend from approximately 300 to 600 Hz. The same range of frequencies is therefore associated with the generation of large-amplitude pressure peaks. This observation, which suggests that the same mechanism of shear-layer instability is present in both cases, will be addressed subsequently. The plan view of pressure amplitude p shown in the bottom image of 5a exhibits a black line passing through the peak pressure amplitude. As in the previous cases for the long pipe-cavity system, this line corresponds to a constant value of fL/U..

In Figure 5b, the top image shows further features of the pressure amplitude response, in the form of log p on the plane of velocity U versus frequency f. In this plot, the increase in amplitude of the pressure fluctuation as flow velocity increases is clearly evident. Regarding the plot at the bottom of Figure 5b, a number of sharp changes in sign of $\partial(\log p)/\partial U$ occur along each band of constant frequencies as velocity is increased. As in the corresponding figures for the long pipe-cavity system, the abrupt change in color corresponds to the locations of the peaks.

For the case of a shallower cavity, represented by $W^* = 0.5$ and shown in Figure 5c, the overall response characteristics are generally similar to those of the deeper cavity of Figure 5a. Considering, first of all, the top image of Figure 5c, the pressure peaks are not quite as consistent with variations of velocity, relative to those of Figure 5a. With regard to the plan view of the pressure amplitude p, shown in Figure 5c, the value of velocity for the onset of the first, large amplitude peak, is of the order of U = 100 ft/sec. This compares with an approximate value of U = 120 ft/sec for the first, large amplitude peak of Figure 4c.

The plot of logarithmic pressure amplitude log p shown in the top image of Figure 5d clearly shows the increase in background amplitude with the increase of velocity and the emergence of well-defined peaks above the background level at sufficiently high values of velocity. The variation of the amplitude of $\partial(\log p)/\partial U$, shown in the bottom image of Figure 5d, exhibits correspondence between abrupt changes in slope (i.e., color) and the pressure amplitude peaks evident in the plan view of the bottom image of Figure 5c.

If the cavity depth W is decreased still further to a value of $W^* = 0.25$, as represented by the images of Figure 5e, sharply-defined pressure peaks are still evident. At the same value of $W^* = 0.25$ for the long inlet pipe, shown in Figure 4e, such sharply-defined peaks do not occur. Note, however, that the peak occurring at the lowest value of velocity in the top image of Figure 5e, further evident in the bottom image of Figure 5e, is within the band of approximately 500 to 600 Hz. For the case of the long inlet pipe, shown in Figures 5a and 5c, resonant peaks occur in this same band of frequencies. A similar instability mechanism therefore appears to be operative in both cases. The instability mechanism most likely associated with the generation of large-scale vortical structures will be addressed subsequently. The manner in which these large-scale structures develop may be a function of the momentum thickness θ_o at separation, which, as described in Section 3, differs for the long and short inlet pipes. The momentum thickness θ_o of the short pipe system is one-third that of the long pipe-cavity system. A further factor that may influence the difference between Figures 4e and 5e is the difference of damping of the long and short pipe-cavity systems.

The variation of the logarithmic pressure amplitude, $\log p$, over the velocity vs. frequency plane, is represented by the top image of Figure 5f. The increase in the pressure amplitude, along a line of constant frequency, say a frequency of the order of 500 Hz, is evident at a relatively low value of velocity U of the order of 35 ft/sec; this situation contrasts with excitation of sharply-defined peaks at higher velocities. This observation suggests that an inherent instability mode of the shear layer is effective in buffeting the resonator of the pipe-cavity system at lower values of velocity. Confirmation of the peaks of pressure amplitude, which are indicated in the bottom image of Figure 5e, is evident in the abrupt change in sign of $\partial(\log p)/\partial U$ in the bottom image of Figure 5f. Moreover, this parameter $\partial(\log p)/\partial U$ brings out additional peaks at lower value of flow velocity for the first two resonant modes; these peaks are not evident in the raw pressure plot at the bottom of Figure 5e.

Finally, the case of the shallowest cavity, $W^* = 0.125$, is represented in Figure 5g. The values of pressure amplitude generally remain very small, of the order of 2×10^{-4} psi. Moreover, sharply-defined peaks are not evident. It is possible, however, to identify a broader peak, as shown in the plan view of the bottom image of Figure 5g; this broader peak serves as the basis for the construction of a black line representing a constant value of fL/U. This peak, as well as others that might be inferred from the bottom image of Figure 5g, are not sufficiently sharp to produce a

consistent pattern of large gradients of $\partial(\log p)/\partial U$, evident from examination of the corresponding image of these gradients, which is not shown herein.

4.4 SCALING OF PRESSURE FLUCTUATIONS: AMPLITUDE LIMITS AND CONDITIONS FOR ONSET, PERSISTENCE, AND SUPPRESSION

In the foregoing sections, emphasis has been on the description of the organized peaks of pressure fluctuations that emerge above the background. These pronounced peaks are evident in most of the three-dimensional (isometric) plots of the respective images of Figures 4a through 5g. In the summaries that follow, the focus is on the dimensionless representations that dictate the onset and existence of well-defined peaks. They are: dimensionless frequencies; dimensionless cavity length and depth; dimensionless pressure amplitudes; and values of velocity. All of these parameters are characterized using detectable peaks in Figures 4a through 5g.

The modes of oscillation observed in the present investigation are defined as large-scale modes. That is, the present emphasis is on oscillations occurring for a limiting value of cavity length L_m, such that for a sufficiently deep cavity, the fully-evolved axisymmetric instability mode is allowed to develop. As indicated in the foregoing, this asymptotic case corresponds to the largest pressure amplitudes observed in preliminary experiments over a range of cavity length. In view of the fact that they occur for relatively long cavities, i.e., cavities of length L significantly larger than the pipe (or jet) diameter D, these oscillations are designated as large-scale modes. Furthermore, as will be addressed, when the frequencies at which the peaks occur are scaled according to fD/U, then the values lie within a range corresponding to fully-evolved (large-scale) vortex formation in an unbounded free-jet. This observation provides a further reason for characterizing these oscillations as large-scale modes along sufficiently deep cavities. In the following, several characteristics of these large-scale modes are addressed.

Frequency of oscillation. Considering the data shown in Figures 4a through 5g, the values of frequency for the observed peaks extend over the range of approximately 300 Hz to 600 Hz. In turn, these frequencies correspond approximately to dimensionless values in the band $0.3 \leq fD/U \leq 0.6$. This issue of frequency scaling is addressed in further detail at the end of Section 5, i.e. Section 5.2.

Pressure amplitudes. The magnitude p of the pressure fluctuations can be normalized in two physically significant ways. The first involves normalization by the dynamic pressure of the

inflow, defined as $\rho U^2/2$, in which ρ is the density of air under standard conditions and U is the averaged centerline velocity, i.e. $U \equiv \overline{u}_m$. This normalization involved the range of data for which detectable peaks were observed in Figures 4a through 5g. Peak pressure amplitudes as high as $p/(\rho U^2/2) \cong 0.6$ can be attained for the short inlet pipe, the deepest cavity, and a high inflow velocity (Figure 5a). At the other extreme, values as low as $p/(\rho U^2/2) \cong 0.007$ were observed for the long inlet pipe, a moderate depth cavity, and a relatively low inflow velocity corresponding to the onset of an initial peak amplitude (Figure 4c).

An alternate normalization for pressure is of the form $p/\rho Uc$, in which c is the speed of sound. For the ideal case of one-dimensional wave propagation, this normalization may be interpreted as u_{ac}/U, in which u_{ac} is the magnitude of the acoustic velocity. In other words, this pressure normalization represents the ratio of the acoustic velocity u_{ac} to the mean inflow velocity U at the centerline of the pipe. Values of $p/\rho Uc = 0.04$ (Figure 5a) are attainable. On the other hand, values as low as $p/\rho Uc = 0.0003$ (Figure 4c) occur. These extreme values correspond to the same conditions as for the aforementioned values of $p/(\rho U^2/2)$.

The extreme values of dimensionless pressure described in the foregoing are compared at the top of Table 1; they are designated as *large-scale modes* therein. A further comparison of peak values of pressure amplitude using individual spectra, as well as the plots discussed in Section 4.3, reveals that, for a given cavity length and depth, the shorter pipe system yielded significantly higher amplitudes than the longer pipe system. This general observation is due to the difference of damping of the short and long pipe systems; it is proportional to the pipe length. The experiments of Kriesels, Peters, Hirschberg, Wijnands, Iafrati, Riccaradi, Piva and Bruggemann (1995) show the consequence of damping, represented by pipe length, for the configuration of a closed side branch resonator. Extreme values of dimensionless pressure attained with long and short pipes in their investigation are indicated at the bottom of Table 1.

Additional investigations of Rockwell and Schachenman (1982), Elder, Farabee, and DeMetz (1982) and Hourigan, Welsh, Thompson and Stokes (1990) are also included in Table 1, in order to illustrate that the values of dimensionless pressure attained in the present investigation can have values of the same order of magnitude as found in other flow tone investigations, despite differences in system configuration and damping.

When comparing values of normalized pressure, as in the foregoing, it should be emphasized that the intermittency of the instantaneous states of the flow past the cavity, and

thereby intermittency of the instantaneous pressure signals, can contribute to a substantially lower value of time-averaged peak pressure, relative to the cases where the instantaneous states are locked-on, with no intermittency. This issue has not been accounted for in any investigation to date.

Persistence of pressure peaks. Examination of the plots of Figures 4a through 5g reveals that as the cavity depth W decreases, the peak pressure amplitude tends to decrease as well. Pronounced peaks can occur, however, at values of cavity depth as low as W/D = 0.25, i.e., even for very shallow cavities having a length to depth ratio of 10.

Suppression of amplitude peaks. For values of cavity depth sufficiently small, pronounced amplitude peaks are no longer evident. This range of suppression occurs for $W^* = W/D \lesssim 0.125$. It should be noted, however, that the occurrence of preferentially-excited pipe modes is still identifiable at $W^* = 0.125$, over the aforementioned range of frequencies falling roughly in the band $0.3 \lesssim fD/U \lesssim 0.6$. These preferentially excited modes exist in absence of any apparent lock-on.

Threshold velocities. Considering the range of data exhibited in Figures 4a through 5g, the velocities for onset of pronounced peaks, accounting for both short and long inlet pipes, range from approximately 70 ft/sec to 120 ft/sec. These velocities represent the values required to trigger the first amplitude peak, and presumably the first occurrence of a flow tone (addressed in Section 6), over a range of cavity depths, for both short and long inlet pipes. Dimensionless representations of these velocities, based on power concepts, is currently under consideration. In essence, one expects the vorticity-based contribution to the acoustic power P_{ac} to scale according to $P_{ac} \sim \rho U^2 u_{ac}$ for a given value of cavity length L. Sufficiently large values of P_{ac} can be achieved either by increasing the value of inflow velocity U or the self-excited acoustic velocity u_{ac}. These features must be taken into consideration for dimensionless representation.

Preferred modes of resonator. The foregoing considerations have addressed the scaling and limiting values of the system parameters. An additional consideration is the determination of whether all modes of the acoustic resonator, i.e., pipe-cavity system, are susceptible to coupling phenomena that lead to generation of flow tones. For the entire range of experiments, tones are generated only for the even modes, i.e., n = 2, 4, ... of the pipe-cavity system. This observation is compatible with the existence of a pressure node and a velocity antinode at the location of the cavity. An interpretation of the excitation of even modes is as follows. Effective perturbation of

the separating shear layer requires relatively large amplitudes of acoustic velocity fluctuations in the vicinity of shear layer separation, i.e., in the most sensitive, or receptive, region of the shear layer along the mouth of the cavity. This occurs for even resonant modes. With this concept in mind, an interesting issue is the effect of asymmetry of the pipe sections located at either end of the cavity, and whether a small amount of asymmetry can effectively attenuate the amplitude of the self-excited oscillations, presumably by displacing the pressure node, i.e., the velocity antinode, away from its most effective location. This matter will be addressed in a forthcoming stage of the investigation.

AUTHORS/ CONFIGURATION	**$p/\rho U^2/2$**	**$P/\rho Uc$**	**U(ft/sec)**	**Notes**
Present *Cavity in pipeline*	~0.6	0.04	160	Large-scale mode [L/D = 2.5]
	[Short pipe; deepest cavity (Figure 5a)]			
	0.007	0.0003	130	Large-scale mode [L/D = 2.5]
	[Long pipe; shallow cavity (Figure 4c)]			
Rockwell and Schachenmann (1982) *Pipeline-cavity-orifice*	0.36	0.017	65	
Elder et al. (1982) *Side-cavity in wall*	0.24	0.022	200	Large-amplitude mode
	0.014	0.00055	82	Initial mode
Hourigan et al. (1990) *Orifice-baffle system*	0.192	0.048	35	
Kriesels et al. (1995) *Closed side pipe*	NA	0.79	202	
	[Short side pipe]			
	NA	0.02	54	
	[Long side pipe]			

Table 1: Comparison of representative values of dimensionless pressure.

5. FREQUENCIES OF OSCILLATION: CORRELATION AND SCALING

Identifiable peaks in the data given in Section 4.3, and the manner in which they vary with either inflow velocity or cavity length, provide a basis for: (i) correlations with traditional models; and (ii) frequency scaling based on concepts of inviscid stability. In the following, these two classes of assessments are addressed in detail.

5.1 CORRELATIONS OF FREQUENCIES OF OSCILLATION WITH EXISTING MODELS BASED ON CAVITY LENGTH

5.1.1 Overview of Models

Over the years, a great deal of effort has been devoted to the development and revision of models for the dimensionless frequency of oscillation. They have the general form:

$$fL/U = (U_c/U)(n \pm a), \tag{5.1}$$

in which U is taken to be the freestream velocity, U_c is the convective speed of a vortex or instability wave through the shear layer, n is the stage of oscillation and a is an end correction. This type of model has its genesis in the early formulations of Rossiter (1962, 1964), whose more general formulation accounted for variations of Mach number, and Powell (1961, 1964), who actually employed this type of relationship for a jet-edge, as opposed to a cavity configuration. In the application of most models, the ratio U_c/U and a are viewed to be adjustable constants. Various types of arguments have been made, however, for relating the dimensionless phase velocity U_c/U to values determined from stability theory. In doing so, however, a constant value of U_c/U is defined; in contrast, inviscid spatial stability theory indicates that U_c/U is actually a function of frequency. Recent efforts in the theoretical direction aim to specify values of U_c/U and a without recourse to empiricism. Such models employ an infinitesimally thin shear layer. They include the works of Crighton (1992) for the case of a jet-edge configuration and Howe (1997, 1998) for edge and cavity configurations.

For purposes of correlating the present experimental data, the following relations will be employed:

(a) $fL/U = 0.61(n - 1/4)$, which is due to Elder (1978) and Pollack (1980);

(b) $f/L/U = 0.6(n + 1/6)$, which is due to Howe (1997, 1998); and

(c) $f/L/U = 0.6n$, which serves as a reference correlation that does not account for any end effects, i.e., $a = 0$. This correlation was also deduced on the basis of phase measurements by Rockwell and Schachenmann (1982).

It should be emphasized that the correlations (a) and (b) have been employed almost exclusively for the case where there is a well-defined freestream, as opposed to the present situation of flow through a pipe. When the pipe flow is fully-developed, a freestream velocity does not exist. The characteristic velocity, $0.86U = 0.86\bar{u}_m$, which represents the spatially-averaged or bulk-averaged velocity through the pipe, is employed herein. It should be noted that use of this normalizing velocity 0.86U can also be interpreted as follows. It is equivalent to employing an equivalent freestream velocity U and a lower value of a dimensionless phase speed $0.86\ U_c/U$.

5.1.2 Correlations for Variations of Inflow Velocity

Figures 6a through 6c show comparisons between the correlations of Section 5.1.1 and the data of Figures 4a through 4e, which exhibit well-defined peaks. In each figure, the top plot represents a best fit through the data of the form $fL/U = K$, in which K is simply the constant that provides the best linear fit. In other words, this fit does not involve any of the aforementioned correlations. In the bottom plot of each figure, direct correlation with the foregoing models (a) through (c) is given. In all figures presented herein, the normalizing velocity is $0.86\ U = 0.86\ \bar{u}_m$ which, as described in the previous section, corresponds to the bulk velocity at the pipe exit.

Figure 6a represents the case of the deepest cavity $W^* = 1.25$. The top plot shows that the normalized frequencies fL/U are related to each other in an approximately harmonic fashion. The lower plot of Figure 6a shows correlations with stages n = 2, 4, and 6. Reasonable agreement is attained with the correlation $fL/(0.86\ U) = 0.6\ n$.

The correlations of Figure 6b correspond to the shallower cavity $W^* = 0.5$. In this case the upper plot shows fits according to $fL/U = 1.00$, 1.45 and 1.98. In other words, in addition to a harmonic mode, an apparent intermediate mode $fL/U = 1.45$ exists. In the lower plot of Figure 6b, however, the data are recently well fitted using stage, or mode, numbers n = 2, 3 and 4 and with the end correction corresponding to n = 1/4.

For the case of the shallowest cavity, $W^* = 0.25$, for which detectable peaks could still be identified, the data are represented in Figure 6c. The correlation at the top of Figure 6c shows that harmonics of the fundamental mode $fL/U = 1.0$ are not present. Rather, only a so-called intermediate mode $fL/U = 1.47$ is apparent. As indicated in the bottom plot of Figure 6c, the case of n = 2 is well correlated for the equation with (n = 1/4), while neither n = 2 or n = 3 shows

an acceptable correlation with the intermediate mode, represented as $fL/U = 1.47$ in the corresponding upper plot of Figure 6c.

5.1.3 Coexistence of Multiple Modes

A common feature of the correlations discussed in Sections 5.1.2 is the coexistence of two or more frequency components at a given value of velocity U. The criterion employed for defining these frequency components simply involves detection of an organized peak(s) in the pressure spectrum. These peaks are associated with the hydrodynamic unsteadiness of the shear layer past the cavity. In other words, only selected frequency components in the corresponding figures of Section 5.1.2 represent flow tones for which the organized unsteadiness of the shear layer, i.e., a Strouhal mode, couples with the acoustic resonant mode of the pipe-cavity system.

It is important to recognize that multiple hydrodynamic modes can exist in absence of acoustic resonant phenomena. This is evident from the early correlations of Rossiter (1962, 1964) for the limiting case of zero Mach number, and the wide range of theoretical and experimental investigations of impinging flows over the past two decades, including not only cavity, but also jet-edge and jet-orifice systems. Most recently, the theoretical model of Howe (1997) analyzes, using a vortex sheet representation, the multiple modes present for the case of flow past a cavity at low Mach number. As shown by Knisely and Rockwell (1982), actual experimental characterization of the unstable shear layer past a cavity, emerging from initially laminar conditions, show the existence of a substantial number of frequency components at a given value of cavity length. These multiple frequency components need not be harmonically related to each other; in fact, sum and difference frequency components are also present. Such strictly hydrodynamic considerations provide a basis for interpreting the multiple frequency components, or modes, present at a given value of inflow velocity U in Section 5.1.2. Detectable frequency components generally line up with one of the resonant acoustic modes of the pipe-cavity system. If conditions are appropriate for coupling, a pronounced flow tone may result.

5.2 SCALING OF FREQUENCY OF OSCILLATION ON BASIS OF JET DIAMETER

The correlations of the preceding section attempt to provide overall guidance for the occurrence of self-sustaining oscillations in accordance with variations of inflow velocity. An alternate, and more rigorous, indicator of the origin of the oscillation involves scaling the frequencies on the basis of stability concepts. It should be emphasized again that, for all cases considered herein, the inflow is fully turbulent, and it is assumed that application of inviscid stability theory to the

time-averaged base flow, which itself is influenced by the presence of turbulence, can provide guidance for determining the frequency of the predominant fluctuation. This type of scaling is based on a representative thickness of the shear layer, in contrast to the use of a geometrical scale such as cavity length or depth. These scaling parameters are: momentum thickness θ_0, evaluated at the exit of the inlet pipe (see Section 3); and the pipe diameter D, which is an approximation to the jet diameter, i.e., the distance between the inflection points of the jet shear layer. Generally speaking, use of the momentum thickness θ_0 is most relevant for the case of a thin shear layer instability, which initially occurs in the immediate vicinity of the nozzle exit, and is expected to give rise to formation of smaller-scale vortices. On the other hand, the jet diameter D provides a suitable scale for a fully-evolved instability of the entire jet, typically associated with large-scale vortex formation.

The present emphasis is on the large-scale mode of oscillation. This mode is defined to occur at a long cavity length, which allows development of a fully-evolved axisymmetric instability (Section 4.4). It is expected to scale on the jet diameter D. Considerable experimental work for the case of a free axisymmetric jet subjected to loudspeaker excitation or, alternately, to feedback from an impinging jet, allows one to deduce the predominant frequency fD/U, which is taken to represent the generation of large-scale vortical structures, often referred to as "puffs". These experiments, along with an overall correlation of the data, are described by Blake (1986). Relevant investigations include Browand and Laufer (1975), Crow and Champagne (1971), Lau, Fisher and Fuchs (1972), and Nossier and Ho (1982). Based on this range of experimental studies, the dimensionless frequency of the large-scale vortex formation in the jet is expected to lie in the range of $0.3 \leq fD/U \leq 0.6$.

Scaling of the frequencies of the predominant peaks exhibited in Figures 4a through 5g according to fD/U showed that they generally lie in the range of $0.35 \leq fD/U \leq 0.4$. These values are in remarkable agreement with the expected values of $0.3 \leq fD/U \leq 0.6$ defined in the foregoing. Figure 7 exhibits the data corresponding to the predominant amplitudes, which have dimensionless frequencies fD/U in this range. This plot emphasizes the collapse of the data for different thicknesses of the inflow boundary layer, and its relative invariance with flow velocity, or more appropriately, with Reynolds number UD/ν.

Perhaps the most remarkable observation, if one views the entire set of data, is that the scaling relation fD/U proves accurate irrespective of the cavity depth. That is, the unstable

frequency of these so-called large-scale modes is fD/U ≅ 0.4, even for relatively shallow cavities for which large-scale vortex formation is not expected to occur. Peaks of the large-scale mode at fD/U ≅ 0.4 are detectable for values of cavity depth as small as W/D = 0.25. Moreover, even for the shallowest cavity W/D = 0.125, for which pronounced peaks do not occur, the excitation of the pipe modes shows preferential values clustered in the vicinity of fD/U = 0.4. Details of the development of this instability, and mechanisms for sustaining it, deserve further consideration.

In this regard, the possible existence of a global (absolute) instability should be addressed. It contrasts with the aforementioned instabilities, which are of the convective type. In essence, this type of instability is likely to occur in configurations where regions of negative streamwise velocity occur as a result of, for example, the local reverse flow in the recirculation zone in a shallow cavity. In an analogy with the corresponding global (absolute) instability occurring in the wake behind a cylinder of diameter D, for which the instability scales according to fD/U, it is expected that the cavity unsteadiness would scale according to fW/U if it is globally unstable. That is, the only representative transverse length scale would be the cavity depth W. Preliminary indications suggest that such a global instability does not exist, since the frequency scales remarkably well according to fD/U = 0.4 for all values of cavity depth W. Scaling of the form fW/U would produce a fivefold variation of the values of fW/U, corresponding to the range of W/D extending from 1.25 to 0.25. Nevertheless, the role of the recirculation zone in maintaining the cavity oscillations is worthy of further consideration.

6. ONSET OF LOCKED-ON FLOW TONES

A primary issue is whether highly coherent, locked-on flow tones can arise in the presence of a fully-turbulent inflow, as described in the references cited in Section 1. Nearly all previous investigations of this class of flows have considered the case of laminar, transitional, or undefined inflow conditions. Moreover, even in those limited cases where the inflow boundary layer was fully turbulent, means to characterize the onset of lock-on were not explicitly addressed using simple criterion.

6.1 GENERAL FEATURES OF LOCK-ON

It is generally accepted that locked-on flow tones exhibit the following characteristics:

(a) ***Amplitude increase with increase of inflow velocity.*** An abrupt increase in amplitude of the unsteady pressure occurs as the flow velocity is increased in the region of the onset of lock-on. It is expected that, if spatial resolution along the velocity coordinate is adequate, the plot

of unsteady pressure amplitude versus velocity will not necessarily be a discontinuity. Rather, it should be possible to characterize a slope of peak pressure amplitude P versus U associated with the occurrence of locked-on flow tones. This slope could be considered as a deviation from the slope prior to the onset of lock-on, where it is due to a change in either the background turbulence level or an underlying coherent instability, i.e., the Strouhal source.

(b) ***Amplitude peak above background.*** Attainment of sufficiently high amplitude of the pressure peak P above the background pressure level p_{bg} would be a further criterion for identification of a locked-on flow tone. As noted in (a), this background pressure amplitude would be due to either the underlying turbulence or the inherent instability (Strouhal source), or a combination of them. It is expected that the incompressible pressure amplitude due both to turbulence and to the inherent instability will change with velocity according to a power law. The exponent in the power law would take on different values for each of these two origins. It is, however, difficult to decompose the background pressure into turbulence and inherent instability components, due to the manner in which the instability wave grows upon the turbulent background. Nevertheless, it would be desirable to characterize the peak pressure amplitude P that occurs for locked-on flow tones in terms of a value of excess pressure above the background p_{bg}, i.e., turbulence/inherent instability wave components. An important issue regarding the pressure amplitude is the fact that not only the magnitude of the inherent instability (Strouhal source), but also the magnitude of the turbulence will be enhanced by the presence of a resonator, even when lock-on does not occur. It is therefore desirable to have a criterion that would allow a straightforward estimate of the maximum attainable pressure amplitude due to turbulent/instability excitation of a resonator in the absence of lock-on; then, any excess pressure p above this value would presumably be associated with the lock-on features of the inherent instability (Strouhal source).

(c) ***Frequency coincidence.*** Coincidence of the frequency of the inherent instability wave, which presumably gives rise to vortex formation, with the frequency of a given mode of the resonator, is a further criterion for the occurrence of locked-on flow tones. In situations where the inflow is laminar, it is relatively easy to distinguish between the frequency of the inherent instability and the resonator frequency prior to the occurrence of lock-on. Although well-defined peaks due to both of these origins may exist in the region away from lock-on, a

single frequency occurs during lock-on. In the event that the inflow is fully turbulent, the frequency of the inherent instability is more difficult to detect. In fact, a pre-existing coherent oscillation may not be readily detectable prior to coupling with the resonator.

6.2 NON-LOCKED-ON BUFFETING OF A RESONATOR: A MECHANICAL ANALOGY

Incompressible turbulence or an instability wave can effectively excite a resonator. A consequence of this excitation may be a detectable peak or bump in the spectrum of the pressure fluctuation. A mechanical analogy to this process involves flow-structure interaction, or more explicitly, turbulent buffeting of an elastically-mounted body. Whereas very little effort has been devoted to understanding the nature of turbulent buffeting of a resonator, the buffeting of a body or structure has received considerable attention. It can serve as a basis for characterizing the limiting pressure amplitude due to turbulent buffeting of a resonator.

Consider a discrete mechanical system with a mass m, a spring having a stiffness C, and a dashpot having damping coefficient B. This system has a natural frequency $f_n \equiv \omega_n/2\pi$. The Q-factor of this mechanical system is determined by the damping coefficient ζ, i.e., $Q = 1/2\zeta$. This system may be excited by, for example: a relatively broadband turbulence, a combination of turbulence and an instability wave; or simply an instability in the form of a vortex. Irrespective of the type of excitation, one may represent the spectrum of the consequent turbulent/instability force F as $S_F(f)$. The mechanical admittance χ_m of the system is, in accordance with the terminology of Naudascher and Rockwell (1994):

$$|\chi_m(\omega)| = [1/C]/\{[1-(\omega/\omega_n)^2]^2 + [\omega/Q\omega_n]^2\}^{1/2} \qquad (6.1)$$

in which C is the mechanical stiffness of the spring. The relationship between the spectrum of the displacement response $S_x(f)$ and the turbulent forcing function is simply:

$$S_x(f) = |\chi_m(f)|^2 \; S_F(f). \qquad (6.2)$$

The form of $S_F(f)$ is arbitrary. According to equation (6.1), for defined values of C and ω_n, the magnitude of the displacement at a given value of frequency $\omega = 2\pi f$ will be maximized when the value of Q takes on its largest value. In other words, when the Q-factor becomes large, it represents a very lightly damped system and the displacement amplitude becomes large. The converse holds, of course, when Q is small. An analogous relationship to equation (6.1), and similar reasoning, holds for a distributed (multi-degree freedom) resonator as well.

In a general sense, a fluid resonator can be considered analogous to the resonant structural system described in the foregoing. All resonators of the standing wave type are inherently distributed, rather than discrete. Nevertheless, these distributed resonators do have, at a single value of excitation frequency, a specific value of damping, or Q-factor. If an analogous linear relationship between spectra of the response pressure amplitude, resonator admittance, and the incompressible turbulence/ instability wave exists in parallel with equation (6.2), it is possible to make the following, simple argument. Consider the schematic of the pressure spectrum and its Q-factor defined in Figure 8. The response pressure amplitude at frequency f_o, i.e., $S_p(f_o)$, due to buffeting of a resonator having a quality-factor Q can itself have a maximum quality factor of Q. In other words, for the case of linearized, turbulent buffeting of a resonator, no mechanism exists for inducing a pressure amplitude response having a Q-factor in excess of the Q-factor of the resonator. It is known from an earlier phase of this investigation that the maximum Q-factor of a resonator occurs in absence of mean flow; therefore, the no flow value of Q would provide an upper (bounding) limit for the Q-factor of the pressure amplitude response, i.e., the Q-factor of the spectrum of the pressure. In essence, this means that if the spectrum of the response pressure has a Q-factor in excess of this upper bound, a mechanism for coupling, i.e., the onset of locked-on flow tone generation, must be present.

6.3 CRITERIA FOR EVALUATION OF FLOW TONE LOCK-ON

The background information outlined in the foregoing leads to several criteria for characterizing the onset of locked-on flow tones. Generic cases were selected from the relatively large number of experiments described in Section 4.3. The following types of assessments are expected to lead to identification of locked-on flow tones.

(a) Variation, i.e., slope, of peak pressure amplitude P of the pressure spectrum as a function of inflow velocity U;

(b) Value of the peak pressure amplitude P relative to the local amplitude of the background pressure p_{bg};

(c) Variation of the Quality (Q)-factor of the pressure spectrum as a function of either inflow velocity U or cavity length L; this type of Q-factor is defined in Figure 8.

Emphasis herein will be on criteria (b) and (c).

6.4 *CHARACTERIZATION OF THE ONSET OF LOCK-ON FOR A GIVEN RESONANT ACOUSTIC MODE*

The range of data described in Section 4.3 can be examined in order to determine the onset of lock-on, in accord with the approaches defined in Section 6.3. Of particular interest with regard to the onset and eventual attainment of lock-on are the following:

(a) The consequence of cavity depth on the lock-on process, and the nature of lock-on at a sufficiently large flow velocity such that a relatively large pressure peak is generated.

(b) The initial onset of a locked-on state as flow velocity is varied. This initial state will most likely exhibit a relatively low amplitude peak of pressure amplitude.

In the following, these features are addressed using selected data from Section 4.

6.4.1 *Effect of Cavity Depth on the Lock-on of Large-Scale Mode*

Figure 9a shows the variation of peak pressure amplitude P (determined from spectra $p^2(f)$) and quality factor Q as a function of the flow velocity for various values of cavity depth W. The cavity length L^* has its largest value $L^*_m = L_m / D = 2.5$ and is maintained constant. The plots of P in the left column are to be compared respectively with Figures 4c, 4e and 4f representing plots of cavity depths $W^* = 0.5$, 0.25, and 0.125. The peak pressure amplitude P may occur at a frequency that deviates from the frequency of the resonant acoustic mode when flow velocity is increased. It is therefore necessary to search for the peak P over a defined band of frequencies at a given velocity. The lower and upper frequencies of this band are designated by f_L and f_H, and are defined in the inset of each figure. Moreover, a zoomed-in view, which corresponds to stretching of a portion of the image of amplitude response in a corresponding figure in Section 4, is provided for each of the plots in the left column of Figure 9a. In each of these insets, the direction of increasing velocity is vertically upwards and the left and right margins correspond to values of f_L and f_H. Considering the peak magnitude in each of the pressure plots in the first column, it is evident that as the cavity depth is decreased, this amplitude decreases as well. Moreover, only for the deepest cavity, $W^* = 0.5$, represented by the top plot, does a well-defined peak region exist. Milder peaks are evident in the middle and bottom plots.

Variations of the Q-factor with velocity are given in the right column of Figure 9a. The Q-factor is calculated from the spectrum, $p^2(f)$ versus f, as defined in Figure 8. Let f_o be the frequency at which the peak occurs and f_2 and f_1 represent the frequencies at which half-values of $p^2(f)$ occur. The quality Q-factor is $f_o/(f_2 - f_1)$. As determined in the preliminary stage of this

program, substantial uncertainties in Q-factor are unavoidable, and the Q-factor plots of Figure 9a show significant deviations. For the top plot of the Q-factor, corresponding to the cavity depth $W^* = W/D = 0.5$, large values of Q of the order of 10^3 are attainable. Since the theoretically determined Q-factor for a simple pipe, in absence of both a cavity and throughflow, has a much lower value of approximately 80, and in accordance with the discussion of Section 6.2, the peak having $Q = 10^3$ is therefore taken to represent a locked-on flow tone. In contrast, at smaller values of cavity depths $W^* = W/D = 0.25$ and 0.125, discernible, small-amplitude and rounded peaks of the Q-factor are generally evident at locations of the corresponding mild peaks of the pressure amplitude distributions in the left column of Figure 9a. It is clear, however, that sufficiently large Q-factor above the background value are not attained, and it is therefore concluded that no locked-on flow tone exists for these states. It should be cautioned, however, that these observations are only for the longest cavity length, for which the large-scale mode of vortex formation presumably becomes well-developed. At short values of cavity length, where smaller-scale vortices may be present, locked-on states may be attainable. This issue is currently under investigation.

Figure 9b provides further representations of the variation of peak pressure amplitude P. The top left plot directly compares P versus velocity U. Note that the values of P for the shallower cavities $W^* = W/D = 0.25$ and 0.125 have been multiplied by a factor of 10 for this comparison. The case of the deepest cavity $W^* = 0.5$ produces a sharply-defined peak at a relatively low value of velocity U = 130 ft/sec. For the case of the shallower cavity $W^* = 0.25$, a peak is not obtained until a much higher velocity of U = 200 ft/sec and, moreover, this peak is not sharply-defined. Finally, for the shallowest cavity $W^* = 0.125$, the peak is extremely mild at a velocity of approximately U = 170 ft/sec.

The upper right plot of Figure 9b compares the shape of each peak on ordinates of peak amplitude P versus normalized velocity U/U_{max}. This plot again brings forth the sharpest response for the deepest cavity. In the lower plot Figure 9b, the plot of log P versus log U emphasizes the increase in the pressure amplitude prior to attainment of the pressure peak. Curves of approximately the same slope are fitted through each set of data for each value of cavity depth W.

Finally, Figure 9c shows the variation of slope dP/dU for the two deepest cavities $W^* = 0.5$ and 0.25. Both the magnitude and gradient of the slope are sharpest for the deeper cavity. The magnitude of the maximum slope is approximately two orders of magnitude higher

for $W^* = 0.5$, relative to $W^* = 0.25$. The individual data points on each of these plots correspond to the local value of slope calculated from the original data set, and the smooth curves represent a best fit through these independently determined, local slopes.

6.4.2 Initial States of Lock-on

The series of plots shown in Figure 10 address the nature of the initial locked-on state as the velocity is varied for several representative inflow and cavity configurations. Often, these states have relatively low amplitude peaks. The pressure amplitude plots shown in the left column correspond respectively, from top to bottom, to Figures 4c, 5c, and 4a. The top and bottom plots of peak pressure amplitude P versus flow velocity U in Figure 10 compare the effect of cavity depths $W^* = W/D = 0.5$ and 1.25. It is evident that, for the larger value of cavity depth $W^* = 1.25$, the onset of a first, pronounced pressure peak occurs at a relatively low inflow velocity of the order of U = 70 ft/sec (bottom plot), in comparison with the case $W^* = 0.5$, for which the first peak is at U = 120 ft/sec (top plot). The presumption is that the deeper cavity allows more effective development of a large-scale vortex over the relatively long cavity. For both the $W^* = 1.25$ and 0.5 cavities, the magnitude of the Q-factor shows a relatively large value at the location of the first peak.

The middle set of plots of Figure 10 corresponds to the case of the cavity depth $W^* = 0.5$ with the short inlet pipe, for which the momentum thickness is approximately one-third the value of the long inlet pipe employed for the case of the top row of plots of Figure 10. In this case, a detectable peak is evident at a relatively low velocity U = 60 ft/sec and, correspondingly, the plot of Q-factor shows a significant peak as well. This low value of onset velocity may be due to the lower total damping of the short pipe-cavity system, relative to the long pipe-cavity system. In addition, the initial development of the separated shear layer from the short inlet pipe has an influence on the manner in which large-scale vortices eventually evolve; this difference in evolution might promote a well-defined oscillation at a substantially lower velocity.

In summary, these results of Figure 10 suggest that larger values of ratio of cavity depth to pipe diameter, i.e., larger $W^* = W/D$, promote the onset of flow tones at significantly lower velocities for a pipe-cavity system of constant length. In addition, larger W/θ together with a shorter length of the pipe-cavity system promote lower onset velocities.

6.5 SUMMARY OF OBSERVATIONS OF LOCK-ON BASED ON SELECTED CRITERIA

The evaluations of lock-on, presented in Figures 9a and 10, are representative of those occurring over a broad range of inflow velocity and cavity length, and it is possible to arrive at general observations, which should be applicable to all of the specific cases addressed in this program. Two principal criteria for defining lock-on are the focus of our present considerations: (a) a quality Q-factor of the square of the pressure amplitude as a function of frequency, i.e., the spectrum of the power $p^2(f)$ of the pressure fluctuation; and (b) the amplitude of the pressure peak P normalized by the background pressure p_{bg}, i.e., P/p_{bg}. The background pressure p_{bg} is defined in the top plot of Figure 9a. It represents the value, obtained by extrapolation, of the magnitude of the background pressure that would exist at the frequency of the peak pressure in the absence of any significant lock-on. In the following, these criteria are defined, then assessed for representative cases.

6.5.1 Definition of Lock-on According to Quality Q-Factor

According to the concept described in Section 6.2, in the absence of any coupling between flow unsteadiness and a resonator, the quality-factor Q of the pressure response spectrum cannot have a value exceeding the Q of the resonator. In principle, this criterion provides a basis for determining the occurrence of the initial state of lock-on, provided uncertainties in deviations of evaluated Q-factors are accounted for. In an initial phase of the present investigation, values of Q-factor were determined for the pipe-cavity system subjected to external excitation, as well as to self-excited excitation via throughflow. Despite use of adequate frequency resolution and averaging over a very large number of cycles, significant deviations about a mean value were discernible. In fact, these deviations are evident in virtually all of the Q-factor plots in Figures 9a and 10. Such deviations are due, at least in part, to the uncertainty of evaluating the Q-factor.

In the present investigation, the nominal upper limit of the Q-factor approximately corresponds to the theoretically-determined value in the absence of mean flow, if one excludes regions where either well-defined peaks or certain "bumps" occur. Values of Q-factor can extend substantially below this limit due to the effects of mean flow. Inspection of the trends of Q-factors for the data of Figures 9a and 10 suggest the occurrence of organized "bumps". The maximum values of these "bumps" do not exceed a value of Q of approximately 180, i.e., $Q \cong 180$.

On the basis of these data, values of Q-factor substantially in excess of $Q = 180$ are taken to represent occurrence of a locked-on state. In fact, considering the entire range of data

displayed in Figures 9a and 10, the smallest value of Q-factor of the well-defined peak amplitudes is Q = 500, and the maximum value is Q = 2,000.

6.5.2 Lock-on According to Peak Pressure Amplitude

The variations of peak pressure amplitude P can be directly compared with the corresponding variations of Q in each of the plots of Figures 9a and 10. It is readily apparent that large peaks of Q essentially correspond to large values of peak pressure P above the background.

Values of $(P/p_{bg})_{max}$ were evaluated for each of the cases of 9a and 10. The background pressure p_{bg} is defined in the top plot of Figure 9a. Parallel with the aforementioned considerations for the Q-factor, where small-amplitude "bumps" of Q-factor are discernible, it is possible to consider the corresponding "bumps" of the distributions of peak pressure P versus velocity U in 9a and 10. For all cases considered, the maximum dimensionless amplitude of a "bump" was $P/p_{bg} \cong 2.0$.

Consider the well-defined peaks of distributions of amplitude P, given in 9a and 10. The values of $(P/p_{bg})_{max}$ range from 40 to 100. In parallel with reasoning for the aforementioned Q-factor criterion, a peak amplitude ratio P/p_{bg} in excess of 2.0 is taken to be an indication of a pronounced lock-on and, in fact, the smallest value of 40 indicates that this limit is indeed well exceeded.

6.6 CHARACTERIZATION OF LOCK-ON FOR A GIVEN STROUHAL NUMBER

In the foregoing sections, 6.4 and 6.5, emphasis has been on the onset of lock-on along a given resonant mode, i.e., pipe mode of the pipe-cavity system. The inflow velocity U was varied, and the consequent variations of the peak pressure amplitude P and quality factor Q were observed as a function of U. This approach provides the most straightforward, and conventional, interpretation of lock-on. It does not, however, provide a comparison of pressure peaks corresponding to a number of pipe modes, which are negotiated by varying the inflow velocity U, while maintaining a constant value of Strouhal number fL/U. A further reason for considering this type of representation is the possible occurrence of ordered deviations of pressure amplitude p between resonant modes as either inflow velocity U or cavity length L is increased.

This type of representation involves taking vertical cuts through the types of three-dimensional plots shown in Section 4. These cuts are taken coincident with a constant Strouhal line, i.e., a line corresponding to constant value of fL/U. They are represented as straight black

lines on the plan views of Figures 4a, 4c, and 4e for a long pipe on either end of the cavity and Figures 5a, 5c, and 5e for a short pipe on either end of the cavity.

Consider first the case corresponding to Figure 4c, i.e., a cavity length $L^* = 2.5$ and depth $W^* = 0.5$. The plan view of Figure 11a is the same view as Figure 4c, but with different reference lines, corresponding to the straight black solid and dashed lines. The dashed line indicated by the symbol I passes through the peak values of pressure amplitude. Lines designated as $a = -0.5$ and $a = -0.742$ define the boundaries of the domain on the velocity versus frequency plane. Vertical cuts are made through these lines, as well as lines lying between them. Representations of these cuts are given in Figure 11b. It is a three-dimensional plot of log p as a function of log f and log u. The bold lines therein represent typical spectra on the log p versus log f axes. Orthogonal to these bold black lines are thin black lines, which correspond to the aforementioned vertical cuts.

Cuts at various values of a, using the data of Figure 11a, are given in Figure 11c. For all values of a, over the lower range of inflow velocity U, the pressure peaks are not sharp. For the cuts corresponding to $a = -0.66$, -0.68 and -0.70, there is onset of large amplitude, sharply-defined peaks at a sufficiently high value of flow velocity.

A zoomed-in view of case $a = -0.68$ is shown in Figure 11d. As the value of velocity U is increased, peaks tend to occur in pairs, and these paired peaks coalesce at the highest values of velocity to produce single, sharply-defined peaks. In analogy with the classical Q-factor for a typical spectrum, $p^2(f)$, it is possible to define a sharpness factor as: $S_1 = U_o/(U_2 - U_1)$. In addition, an alternate sharpness factor may be defined according to: $S_2 = A/(U_2 - U_1)$, in which A is the amplitude of the local pressure peak. Representative values of S_1 and S_2 are indicated adjacent to the two peaks designated in Figure 11d, one occurring at a relatively low value of velocity U, and the other at the relatively high value of U. The values of both S_1 and S_2 increase by approximately a factor of 5 as velocity U is increased.

The results for a shallower cavity are represented by Figure 12a, which is the same data set as exhibited in Figure 4f. A reference line is indicated as I, and boundaries of the region considered extend from $a = -0.5$ to $a = -0.7$. Sectional cuts are shown in Figure 12b. Irrespective of the cut employed, sharply-defined peaks do not emerge, suggesting a non-locked-on response. A zoomed-in view of a representative series of peaks, corresponding to the cut $a = -0.76$, is given in Figure 12c. Values of the sharpness factor S_1 exhibit little change over the

relatively wide range of inflow velocity U. In fact, the sharpness factor defined as S_2 actually decreases at the higher value of inflow velocity.

For the case of the short pipe mounted on either end of the cavity, a representative data set corresponding to Figure 5c was selected. The plot of Figure 13a corresponds to Figure 5c. A predominant pressure amplitude peak intersects the line designated as I. The boundaries of the domain extend from $a = -0.6$ to $a = -0.8$. As shown in Figure 13b, emergence of a sharply-defined peak is evident at $a = -0.76$, -0.78 and -0.8. A zoomed-in view of the case $a = -0.78$ is given in Figure 13c. The sharpness factor S_1 increases by approximately a factor of 8 and S_2 by about a factor of 7 as the value of U is increased.

7. CONCLUDING REMARKS

An overview of the principal findings of the present investigation is provided in this section. Detailed values of parameters and other specifics related to these findings are summarized at the end of each of the preceding sections. In the following, the onset of self-excited oscillations is addressed with respect to the inherent instability of the shear layer past the cavity and its relation to the generation of relatively large-scale modes of flow tone lock-on, the dimensionless frequencies and pressure amplitudes associated with these modes, and the criteria for lock-on.

7.1 TRANSFORMATION FROM FULLY-TURBULENT INFLOW TO HIGHLY COHERENT FLOW TONES

A central issue in this investigation is generation of highly coherent flow tones from a fully turbulent inflow. Considerable effort was devoted to the generation of fully turbulent shear flow at the inlet of the cavity, including the case of a fully-developed turbulent pipe flow. For appropriate ranges of parameters, highly coherent flow tones emerge. It is hypothesized that the inherent, inviscid instability of the shear layer past the cavity is reinforced by coupling with an acoustic resonant mode of the pipe. This process would then dominate the background turbulence of the inflow. The fact that the inviscid instability of the shear layer plays a clear role is suggested by agreement between dimensionless frequencies of the flow tone and frequencies of instabilities of the shear layer predicted from inviscid theory. This observation suggests that the time-averaged turbulent background flow can serve as the mean flow for the development of the inviscid instability in the shear layer.

7.2 GENERATION AND SCALING OF FLOW TONES IN THE LARGE-SCALE MODE

Of primary interest in this investigation is generation of flow tones in a large-scale mode, which is defined to occur at relatively long cavity lengths. Its frequency scales with the pipe diameter. This mode occurs for extremes of boundary layer thickness generated at the cavity inlet, thereby reaffirming the scaling based on pipe diameter.

Flow tones in the large-scale mode can be generated in very shallow, long cavities, where the length of the cavity is an order of magnitude larger than its depth, and the cavity depth is as small as one-fourth the pipe diameter. Generally speaking, the peak amplitude of the fluctuating pressure decreases as cavity depth decreases. In the limit, if the cavity depth is sufficiently shallow, of the order of one-eighth of the pipe diameter, flow tones cannot be generated in the large-scale mode.

Scaling of the pressure fluctuations involves two types of dimensionless groups. For sufficiently deep cavities and minimum damping corresponding to the short pipe system, the dimensionless pressure amplitude of a flow tone, using the inflow dynamic pressure for normalization, is $p/(\rho U^2/2) \sim 0.6$; correspondingly, the pressure amplitude normalized on inflow velocity and the speed of sound can attain values as high as $p/(\rho Uc) \sim 0.04$. On the other hand, for shallower cavities and relative high damping corresponding to the long pipe system, flow tones having low amplitudes of $p/(\rho U^2/2) \sim 0.007$ and $p/\rho Uc \sim 0.0003$ can be generated. For this case, it is hypothesized that a degree of intermittency of the lock-on process may contribute to low-pressure magnitudes, even though the pressure response characteristics are sharp and indicate lock-on. A detailed summary of the concepts and issues related to this type of scaling is given in Section 4.4.

Scaling of the frequencies of the flow tones of the large-scale mode involve, first of all, scaling based on the pipe diameter D, i.e., fD/U = constant. Remarkable is the fact that this scaling holds for all values of cavity depth W for which flow tones are generated, even for cavities sufficiently shallow such that large-scale vortex formation is not expected to occur. Apparently, a mechanism for a long wavelength, large-scale mode persists. Moreover, even for the shallowest cavity for which flow tones do not occur, excitation of the pipe modes occurs over a band of preferential frequencies that satisfy the fD/U scaling. This scaling is described in detail in Section 5.2.

The frequencies of flow tones can also be scaled in accordance with the cavity length, i.e., $fL/U = K$. A variety of scaling correlations have been compared with the present set of data,

but no single correlation adequately characterizes the flow tone frequency fL/U over the wide ranges of parameters addressed herein. Generally speaking, however, the large-scale mode tends to occur at the second mode, or stage, n = 2 defined by these correlations. The results of this type of dimensionless scaling are described in Section 5.1.2.

7.3 NATURE OF LOCKED-ON FLOW TONES

Criteria, or indicators, for assessing the occurrence of locked-on flow tones have been addressed and evaluated. The first is the quality Q-factor of the power spectrum of the pressure fluctuation. After considering a range of representative, locked-on flow states, it is apparent that two types of peaks can occur in variations of Q-factor with inflow velocity or cavity length. The first are small amplitude, organized "bumps" of the Q-factor. The maximum value of Q-factor that occurs for these "bumps" is approximately Q = 180. The second type of peak in the variation of Q-factor is much larger; it exceeds by a substantial margin the values of the Q-factors for the so-called bumps. In fact, these Q-factors range from Q = 500 to 2,000. The fact that these values of Q are decisively larger than those occurring in the aforementioned band of Q-factors suggests that they represent robust locked-on flow tones.

The second criterion is the normalized pressure amplitude $(P/p_{bg})_{max}$, in which P is the amplitude peak of the pressure spectrum and p_{pg} is the background pressure magnitude that would exist in the absence of flow tone coupling. Analogous observations hold for the ratio $(P/p_{bg})_{max}$ for cases where inflow velocity is varied. Small "bumps" of this ratio have a maximum value of $(P/p_{bg})_{max} \cong 2.0$. On the other hand, the onset of pronounced peaks yields values of $(P/p_{bg})_{max}$ from 40 to 100. For cases where cavity length is varied, similar bumps and peaks of $(P/p_{bg})_{max}$ occur, but their correspondence with the features of the Q-factor is not as consistent.

REFERENCES

BLAKE, W. K. 1986 Mechanics of Flow-Induced Sound and Vibration, Vols. 1 and 2. Academic Press, Inc., NY.

BROWAND, F. K. & LAUFER, J. 1975 The role of large-scale structures in the initial development of circular jets. *Turbulence of Liquids* **4**, 333-334.

BRUGGEMAN, J. C., HIRSCHBERG, A., VAN DONGEN, M. E. H., WIJNANDS, A. P. J. & GORTER, J. 1989 Flow induced pulsations in gas transport systems: analysis of the influence of closed side branches. *Journal of Fluids Engineering* **111**, 484-491.

BRUGGEMAN, J. C., HIRSCHBERG, A., VAN DONGEN, M. E. H., WIJNANDS, A. P. J. & GORTER, J. 1991 Self-sustained aero-acoustic pulsations in gas transport systems: experimental study of the influence of closed side branches. *Journal of Sound and Vibration* **150**, 371-393.

CREMER, L. & ISING, H. 1967/68 Die selbsterregte schwingungen von orgelpfeifen. *Acustica* **19**, 143-153.

CRIGHTON, D. G. 1992 The jet-edge-tone feedback cycle: linear theory for the operating stages. *Journal of Fluid Dynamics* **1234**, 361-392.

CROW, S. C. & CHAMPAGNE, F. H. 1971 Orderly structure in jet turbulence. *Journal of Fluid Mechanics* **48**, 547-591.

CUMPSTY, N. S. & WHITEHEAD, D. S. 1971 The excitation of acoustic resonances by vortex shedding. *Journal of Sound and Vibration* **18**, 353-369.

DAVIES, P. O. A. L. 1981 Flow-acoustic coupling in ducts. *Journal of Sound and Vibration* **77**, 191-209.

DAVIES, P. O. A. L. 1996a Piston engine intake and exhaust system design. *Journal of Sound and Vibration* **190**, 677-712.

DAVIES, P. O. A. L. 1996b Aeroacoustics and time varying systems. *Journal of Sound and Vibration* **190**, 345-362.

DEMETZ, F. C. & FARABEE, T. M. 1977 Laminar and turbulent shear flow-induced resonances. AIAA Paper 77-1293.

ELDER, S. A. 1978 Self-excited depth-mode resonance for a wall-mounted cavity in turbulent flow. *Journal of Acoustical Society of America* **64**, 877-890.

ELDER, S. A., FARABEE & T. M., DEMETZ, F. C. 1982 Mechanisms of flow-excited cavity tones at low Mach number. *Journal of Acoustical Society of America* **72**, 532-549.

FLATAU, A. AND VAN MOORHAM, W. K. 1990 Prediction of vortex shedding responses in segmented solid rocket motors. AIAA Paper 90-2073.

FLETCHER, N. H. 1979 Air flow and sound generation in musical wind instruments. *Annual Review of Fluid Mechanics* **11**, 123-146.

HOURIGAN, K., WELSH, M. C., THOMPSON, M. C. & STOKES, A. N. 1990 Aerodynamic sources of acoustic resonance in a duct with baffles. *Journal of Fluids and Structures* **4**, 345-370.

HOWE, M. S. 1975 Contributions to the theory of aerodynamic sound with applications to excess jet noise and the theory of the flute. *Journal of Fluid Mechanics* **71**, 625-673.

HOWE, M. S. 1980 The dissipation of sound at an edge. *Journal of Sound and Vibration* **70**, 407-411.

HOWE, M. S. 1997 Edge, cavity and aperture tones at very low mach numbers. *Journal of Fluid Mechanics* **330**, 61-84.

HOWE, M. S. 1998 Acoustics of Fluid-Structure Interaction, Cambridge University Press.

KNISELY, C. & ROCKWELL, D. 1982 Self-sustained low-frequency components in an impinging shear layer. *Journal of Fluid Mechanics* **116**, 157-186.

KRIESELS, P. C., PETERS, M. C. A. M., HIRSCHBERG, A., WIJNANDS, A. P. J., IAFRATI, A., RICCARADI, G., PIVA, R. & BRUGGEMANN, J.-C. 1995 High amplitude vortex-induced pulsations in a gas transport system. *Journal of Sound and Vibration* **184**, 343-368.

LAU, J. C., FISHER, M. J. AND FUCHS, H. V. 1972 the intrinsic structure of turbulent jets. *Journal of Sound and Vibration* **22**, 379-406.

NAUDASCHER, E. & ROCKWELL, D. 1994 Flow-Induced Vibrations: An Engineering Guide, Balkema Press, Rotterdam, April.

NELSON, P. A., HALLIWELL, N. A. & DOAK, P. E. 1981 Fluid dynamics of a flow excited resonance. Part I: Experiment. *Journal of Sound and Vibration* **78**, 15-38.

NELSON, P. A., HALLIWELL, N. AND DOAK, P. E. 1983 Fluid dynamics of a flow excited resonance. Part II: Flow acoustic interaction. The dissipation of sound at an edge. *Journal of Sound and Vibration* **91**, 375-402.

NOSSEIR, N. S. & HO, C.-M. 1982 Dynamics of an impinging jet. Part 2. The noise generation. *Journal of Fluid Mechanics* **116**, 379-391.

PARKER, R. 1966 Resonance effects in wake shedding from parallel plates: some experimental observations. *Journal of Sound and Vibration* **4**, 62-72.

PFIZENMAIER, E. 1973 On the instability of a sound influenced free jet. *E.S.R.O. Technical Transl. 122* (Transl. of *DFVLR Berlin Rep.* DLR-FB 73-69*)*.

POLLACK, M. L. 1980 Flow-induced tones in side-branch pipe resonators. *Journal of the Acoustical Society of America* 7, 1153-1156.

POWELL, A. 1961 On the edgetone. *Journal of the Acoustical Society of America* 33, 395-409.

POWELL, A. 1964 Theory of vortex sound. *Journal of the Acoustical Society of America* **36**, 177-195.

ROCKWELL, D 1983 Oscillations of impinging shear layers. Invited Lecture, 20th Aerospace Sciences Meeting of AIAA, January, 1981, Orlando, FL; AIAA Paper 81-0047; also see *AIAA Journal* **21**, 645-664.

ROCKWELL, D 1998 Vortex-body interactions. Invited contribution to *Annual Review of Fluid Mechanics* **30**, 199-229.

ROCKWELL, D. & KARADOGAN, H. 1982 Oscillations of an impinging turbulent jet: coherence characterization via conditional sampling. *Journal of Sound and Vibration* **83**, 111-124.

ROCKWELL, D. & KARADOGAN, H. 1983 Toward attenuation of self-sustained oscillations of a turbulent jet through a cavity. *ASME Journal of Fluids Engineering* **105**, 335-340.

ROCKWELL, D. AND NAUDASCHER, E. 1978 Review - self-sustaining oscillations of flow past cavities. *ASME Journal of Fluids Engineering* **100**, 152-165.

ROCKWELL, D. & NAUDASCHER, E. 1979 Self-sustained oscillations of impinging free-shear layers. *Annual Review of Fluid Mechanics* **11**, 67-94.

ROCKWELL, D. & SCHACHENMANN, A. 1980 "A Quasi-Standing Wave Phenomenon Due to Oscillating Internal Flow", *Journal of Fluids* Engineering, Vol. 102, pp. 70-77.

ROCKWELL, D. & SCHACHENMANN, A. 1982 Self-generation of organized waves in an impinging turbulent jet at low mach numbers. *Journal of Fluid Mechanics* **117**, 425-441.

ROCKWELL, D. & SCHACHENMANN, A. 1983 The organized shear layer due to oscillations of a turbulent jet through an axisymmetric cavity. *Journal of Sound and Vibration* **87**, 371-382.

ROSSITER, J. E. 1962 The effect of cavities on the buffeting of aircraft. Royal Aircraft Establishment Technical Memorandum 754.

ROSSITER, J. E. 1964 Wind tunnel experiments on the flow over rectangular cavities at subsonic and transonic speeds. Reports and Memoranda No. 3438, October.

SCHLICHTING, H. 1968 Boundary-Layer Theory, Sixth Edition, McGraw-Hill Book Company, New York.

STONEMAN, S. A. T., HOURIGAN, K., STOKES, A. N. & WELSH, M. E. 1988 Resonant sound caused by flow past two plates in tandem in a duct. *Journal of Fluid Mechanics* **192**, 455-484.

STOUBOS, A. K., BENOCCI, C., PALLI, E., STOUBOS, G. K. & OLIVARI, D. 1999 Aerodynamically-generated acoustic resonance in a pipe with annular flow restrictors. *Journal of Fluids and Structures* **13**, 755-778.

WILSON, T. A., BEAVERS, G. S., DECOSTER, M. A., HOLGER, D. K. & REGENFUSS, M. D. 1971 Experiments on the fluid mechanics of whistling. *Journal of the Acoustical Society of America* **50**, 366-372.

ZIADA, S. & BÜHLMAN, E. T. 1992 Self-excited resonances of two-side-branches in close proximity. *Journal of Fluids and Structures* **6**, 583-601.

ZIADA, S. & SHINE, S. 1999 Strouhal numbers of flow-excited acoustic resonance of closed side branches. *Journal of Fluids and Structures* **13**, 127-142.

10. FIGURE CAPTIONS

Figure 1: (a) Principal elements of self-sustaining oscillation of turbulent flow past cavity; and (b) hypothesized flow pattern within a very shallow cavity.

Figure 2a: Overview of pipeline-cavity system

Figure 2b: Details of cavity subsystem.

Figure 3a: Variation of normalized mean velocity across pipe on semi-log coordinates to emphasize region of logarithmic velocity variation.

Figure 3b: Direct comparison of time-mean velocity variations across short inlet pipe (top plot) and long inlet pipe (bottom plot).

Figure 4a: Isometric view (top image) and plan view (bottom image) of pressure amplitude as a function of frequency and velocity. Lines shown on plan view represent fits through peak values of pressure amplitude. Cavity length $L^* = L/D = 2.5$ and depth $W^* = W/D = 1.25$, where D is pipe diameter. Long pipes of equal length are located at either end of the cavity.

Figure 4b: Plan view of logarithmic pressure amplitude as a function of velocity and frequency (top image); and plan view of magnitude of the derivative of the logarithmic pressure amplitude with respect to velocity, $\partial(\log p)/\partial U$ (bottom image). Cavity length $L^* = L/D = 2.5$ and depth $W^* = W/D = 1.25$, where D is pipe diameter. Long pipes of equal length are located at either end of the cavity.

Figure 4c: Isometric view (top image) and plan view (bottom image) of pressure amplitude as a function of frequency and velocity. Lines shown on plan view represent fits through peak values of pressure amplitude. Cavity length $L^* = L/D = 2.5$ and depth $W^* = W/D = 0.5$, where D is pipe diameter. Long pipes of equal length are located at either end of the cavity.

Figure 4d: Isometric view of logarithmic pressure amplitude as a function of velocity and frequency (top image); and plan view of magnitude of the derivative of the logarithmic pressure amplitude with respect to velocity, $\partial(\log p)/\partial U$ (bottom image). Cavity length $L^* = L/D = 2.5$ and depth $W^* = W/D = 0.5$, where D is pipe diameter. Long pipes of equal length are located at either end of the cavity.

Figure 4e: Isometric view (top image) and plan view (bottom image) of pressure amplitude as a function of frequency and velocity. Lines shown on plan view represent fits through peak values of pressure amplitude. Cavity length $L^* = L/D = 2.5$ and depth $W^* = W/D = 0.25$, where D is pipe diameter. Long pipes of equal length are located at either end of the cavity.

Figure 4f: Isometric view (top image) and plan view (bottom image) of pressure amplitude as a function of frequency and velocity. Cavity length $L^* = L/D = 2.5$ and depth $W^* = W/D = 0.125$, where D is pipe diameter. Long pipes of equal length are located at either end of the cavity.

Figure 4g: Overview of effect of cavity depth on three-dimensional representation of pressure amplitude as a function of velocity and frequency. In all cases, cavity length is constant at $L^* = L/D = 2.5$. Cavity depth varies according to $W^* = W/D = 1.25$ (top image), $W^* = W/D = 0.25$ (middle image), and $W^* = W/D = 0.125$ (bottom image).

Figure 5a: Isometric view (top image) and plan view (bottom image) of pressure amplitude as a function of frequency and velocity. Line shown on plan view represents a fit through peak values of pressure amplitude. Cavity length $L^* = L/D = 2.5$ and depth $W^* = W/D = 1.25$, where D is pipe diameter. Short pipes of equal length are located at either end of the cavity.

Figure 5b: Plan view of logarithmic pressure amplitude as a function of velocity and frequency (top image); and plan view of magnitude of the derivative of the logarithmic pressure amplitude with respect to velocity, $\partial(\log p)/\partial U$ (bottom image). Cavity length $L^* = L/D = 2.5$ and depth $W^* = W/D = 1.25$, where D is pipe diameter. Short pipes of equal length are located at either end of the cavity.

Figure 5c: Isometric view (top image) and plan view (bottom image) of pressure amplitude as a function of frequency and velocity. Line shown on plan view represents a fit through peak values of pressure amplitude. Cavity length $L^* = L/D = 2.5$ and depth $W^* = W/D = 0.5$, where D is pipe diameter. Short pipes of equal length are located at either end of the cavity.

Figure 5d: Isometric view of logarithmic pressure amplitude as a function of velocity and frequency (top image); and plan view of magnitude of the derivative of the logarithmic pressure amplitude with respect to velocity, $\partial(\log p)/\partial U$ (bottom image). Cavity length $L^* = L/D = 2.5$ and depth $W^* = W/D = 0.5$, where D is pipe diameter. Short pipes of equal length are located at either end of the cavity.

Figure 5e: Isometric view (top image) and plan view (bottom image) of pressure amplitude as a function of frequency and velocity. Line shown on plan view represents a fit through peak values of pressure amplitude. Cavity length $L^* = L/D = 2.5$ and depth $W^* = W/D = 0.25$, where D is pipe diameter. Short pipes of equal length are located at either end of the cavity.

Figure 5f: Plan view of logarithmic pressure amplitude as a function of velocity and frequency (top image); and plan view of magnitude of the derivative of the logarithmic pressure amplitude with respect to velocity, $\partial(\log p)/\partial U$ (bottom image). Cavity length $L^* = L/D = 2.5$ and depth $W^* = W/D = 0.25$, where D is pipe diameter. Short pipes of equal length are located at either end of the cavity.

Figure 5g: Isometric view (top image) and plan view (bottom image) of pressure amplitude as a function of frequency and velocity. Line shown on plan view represents a fit through peak values of pressure amplitude. Cavity length $L^* = L/D = 2.5$ and depth $W^* = W/D = 0.125$, where D is pipe diameter. Short pipes of equal length are located at either end of the cavity.

Figure 6a: Plots of values of frequency corresponding to amplitude peaks in Figures 4a and 4b. Top plot shows lines corresponding to the best fit of the dimensionless frequency fL/U through each set of data points. Bottom plot shows lines corresponding to three different correlations for fL/U. Velocity U corresponds to the time-mean centerline velocity at the center of the pipe, i.e., $U = \bar{u}_m$. In the lower plot, the bulk velocity of the pipe flow, 0.86 U, is employed as the normalization velocity.

Figure 6b: Plots of values of frequency corresponding to amplitude peaks in Figures 4c and 4d. Top plot shows lines corresponding to the best fit of the dimensionless frequency fL/U through each set of data points. Bottom plot shows lines corresponding to three different correlations for fL/U. Velocity U corresponds to the time-mean centerline velocity at the center of the pipe, i.e., $U = \bar{u}_m$. In the lower plot, the bulk velocity of the pipe flow, 0.86 U, is employed as the normalization velocity.

Figure 6c: Plots of values of frequency corresponding to amplitude peaks in Figure 4e. Top plot shows lines corresponding to the best fit of the dimensionless frequency fL/U through each set of data points. Bottom plot shows lines corresponding to three different correlations for fL/U. Velocity U corresponds to the time-mean centerline velocity at the center of the pipe, i.e., $U = \bar{u}_m$. In the lower plot, the bulk velocity of the pipe flow, 0.86 U, is employed as the normalization velocity.

Figure 7: Superposition of values of dimensionless frequency corresponding to the maximum amplitude peaks for each cavity configuration.

Figure 8: Schematic illustrating definition of Quality (Q) factor based on pressure spectrum $p^2(f)$.

Figure 9a: Effect of cavity depth on onset of flow tones. Plots show peak pressure amplitude P and quality factor Q as a function of centerline velocity U for data corresponding to Figures 4c,d (top set of plots), 4e (middle set of plots), and 4f (bottom set of plots). Images in the inset of each pressure amplitude plot correspond to a zoomed-in version of a portion of the plan view of the aforementioned sets of plots.

Figure 9b: Direct comparison of variations of peak pressure amplitude P with centerline velocity U corresponding to data of Figure 9a.

Figure 9c: Variation of slope of peak pressure amplitude P as a function of velocity U for data corresponding to the top and middle sets of plots in Figure 9a.

Figure 10: Onset of initial flow tones. Plots show peak pressure amplitude P and quality factor Q as a function of centerline velocity U for data corresponding to Figures 4c,d (top set of plots), 5c,d (middle set of plots), and 4a,b (bottom set of plots). Images in the inset of each pressure amplitude plot correspond to a zoomed-in version of a portion of the plan view of the aforementioned sets of plots.

Figure 11a: Plan view of pressure amplitude response on plane of velocity versus frequency corresponding to Figure 4c. Dashed line represents predominant Strouhal mode I. Solid lines correspond to boundaries of vertical cuts through three-dimensional plot of pressure amplitude – velocity – frequency. Values of a are extreme reference values for these cuts. Cavity length $L^* = L/D = 2.5$ and depth $W^* = W/D = 0.5$, where D is pipe diameter. Long pipes of equal length are located at either end of the cavity.

Figure 11b: Three-dimensional representation of vertical cuts defined by extreme values of a in Figure 11a. Bold lines represent spectra. Thin lines are vertical cuts coincident with the constant value of a in Figure 11a. Logarithmic values of parameters are employed.

Figure 11c: Vertical cuts through the plot of Figure 11a. All cuts are along a line of constant Strouhal number fL/U, but at different values of a lying between the extreme values defined in Figure 11a.

Figure 11d: Zoomed-in view of vertical cut selected from series of Figure 11c. This cut corresponds to the largest amplitude, sharpest-peak response at larger values of inflow velocity. Parameters S_1 and S_2 are sharpness factors analogous to Q-quality factors.

Figure 12a: Plan view of pressure amplitude response on plane of velocity versus frequency corresponding to Figure 4f. Dashed line represents predominant Strouhal mode I. Solid lines correspond to boundaries of vertical cuts of three-dimensional plot of pressure amplitude – velocity – frequency. Values of a are extreme reference values for these cuts. Cavity length $L^* = L/D = 2.5$ and cavity depth $W^* = W/D = 0.125$, where D is pipe diameter. Long pipes of equal length are located at either end of the cavity.

Figure 12b: Vertical cuts through the plot of Figure 12a. All cuts are along a line of constant Strouhal number fL/U, but at different values of *a* lying between the extreme values defined in Figure 12a.

Figure 12c: Zoomed-in view of vertical cut selected from series of Figure 12b. Parameters S_1 and S_2 are sharpness factors analogous to Q-quality factors.

Figure 13a: Plan view of pressure amplitude response on plane of velocity versus frequency corresponding to Figure 5c. Dashed line represents predominant Strouhal mode I. Solid lines correspond to boundaries of vertical cuts of three-dimensional plot of pressure amplitude – velocity – frequency. Values of *a* are extreme reference values for these cuts. Cavity length $L^* = L/D = 2.5$ and depth $W^* = W/D = 0.5$, where D is pipe diameter. Short pipes of equal length are located at either end of the cavity.

Figure 13b: Vertical cuts through the plot of Figure 13a. All cuts are along a line of constant Strouhal number fL/U, but at different values of *a* lying between the extreme values defined in Figure 13a.

Figure 13c: Zoomed-in view of vertical cut selected from series of Figure 13b. Parameters S_1 and S_2 are sharpness factors analogous to Q-quality factors.

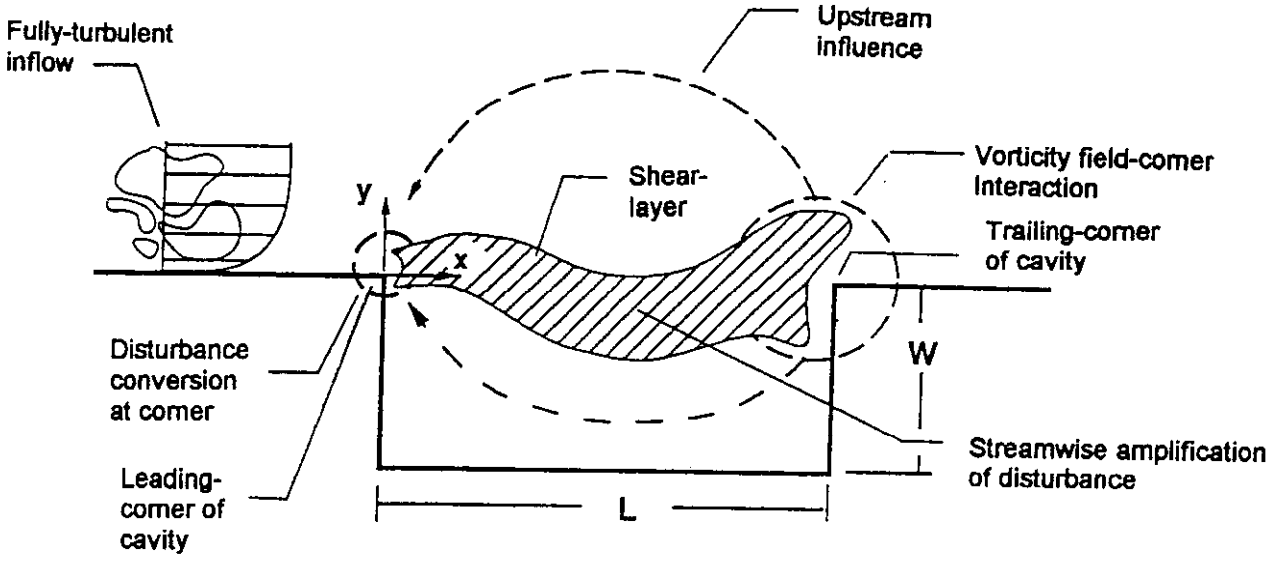

(a)

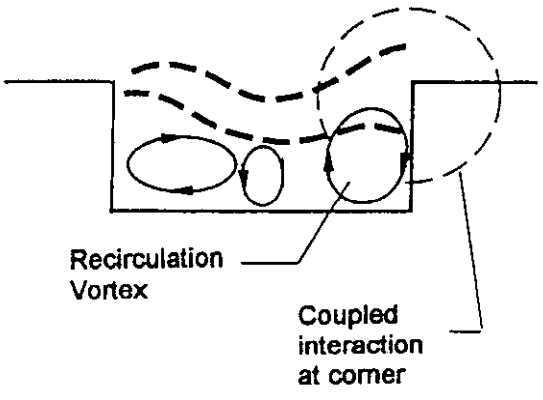

(b)

Figure 1: (a) Principal elements of self-sustaining oscillation of turbulent flow past cavity; and (b) hypothesized flow pattern within a very shallow cavity.

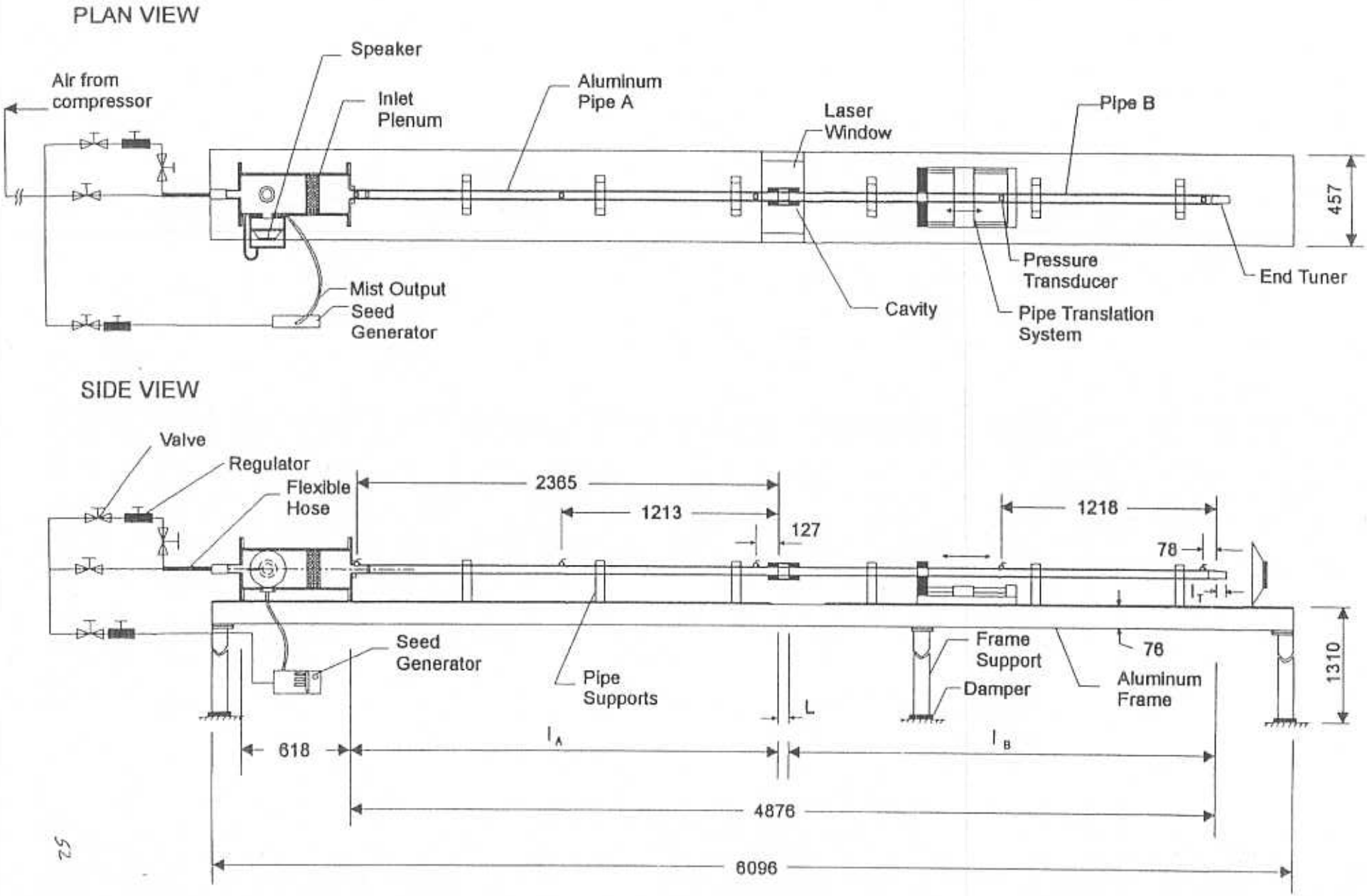

Figure 2a: Overview of pipeline-cavity system

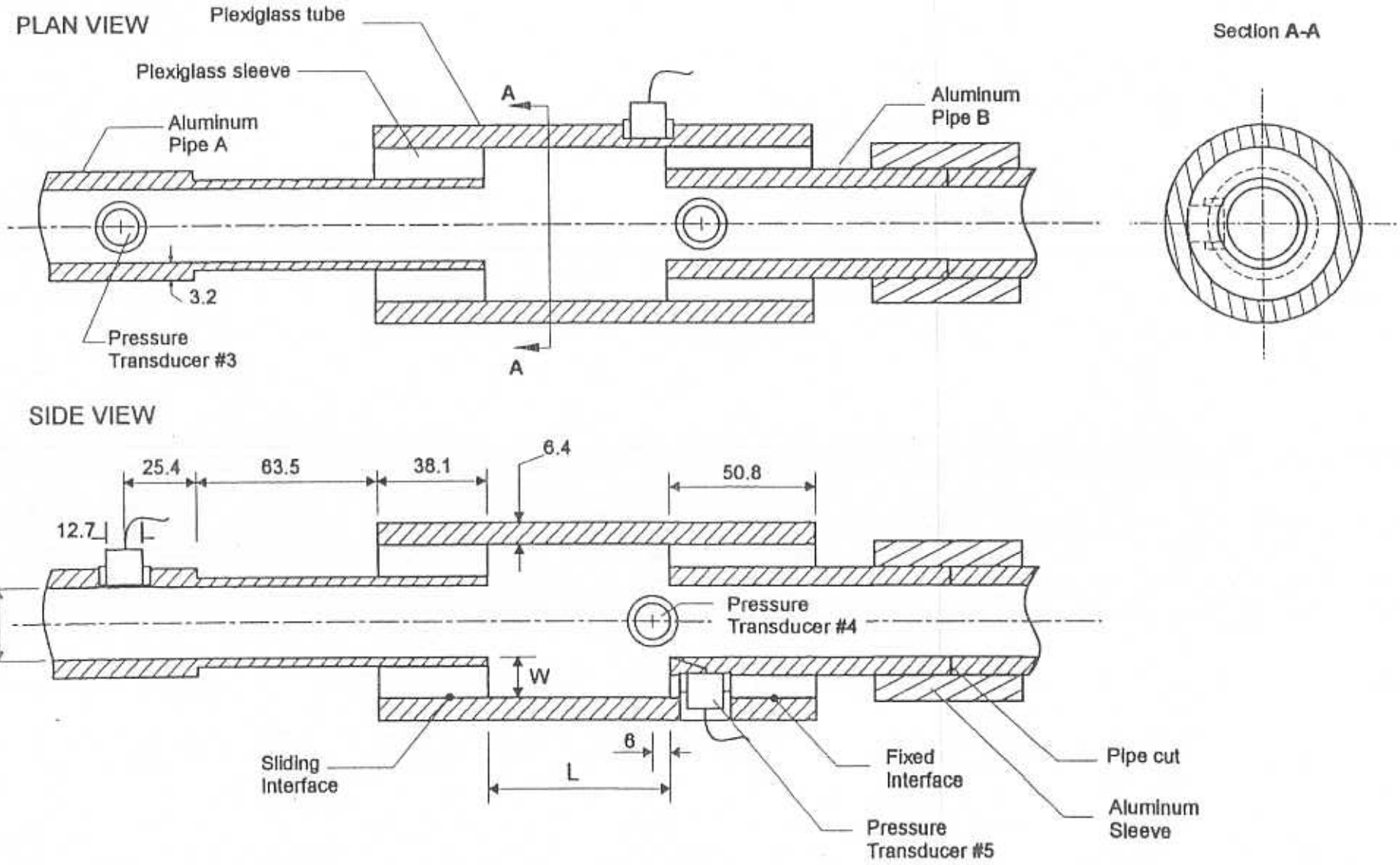

Figure 2b: Details of cavity subsystem.

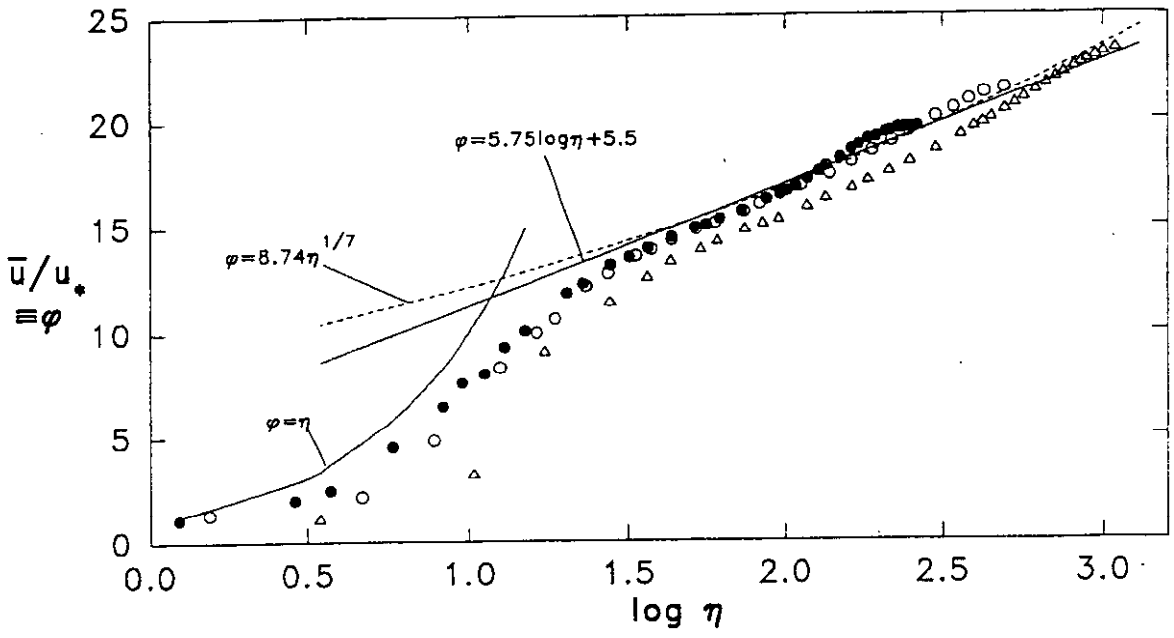

Figure 3a: Variation of normalized mean velocity across pipe on semi-log coordinates to emphasize region of logarithmic velocity variation.

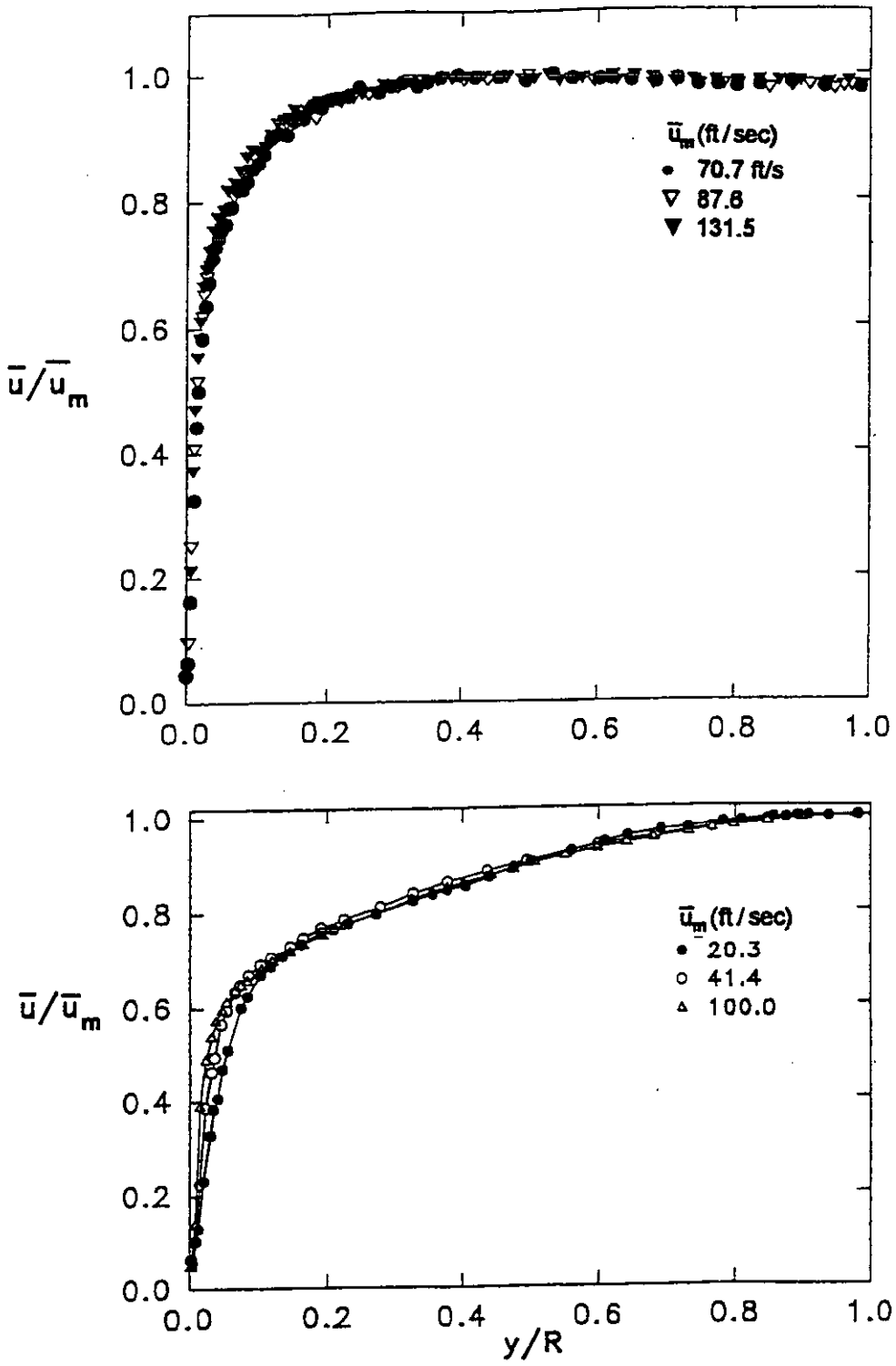

Figure 3b: Direct comparison of time-mean velocity variations across short inlet pipe (top plot) and long inlet pipe (bottom plot).

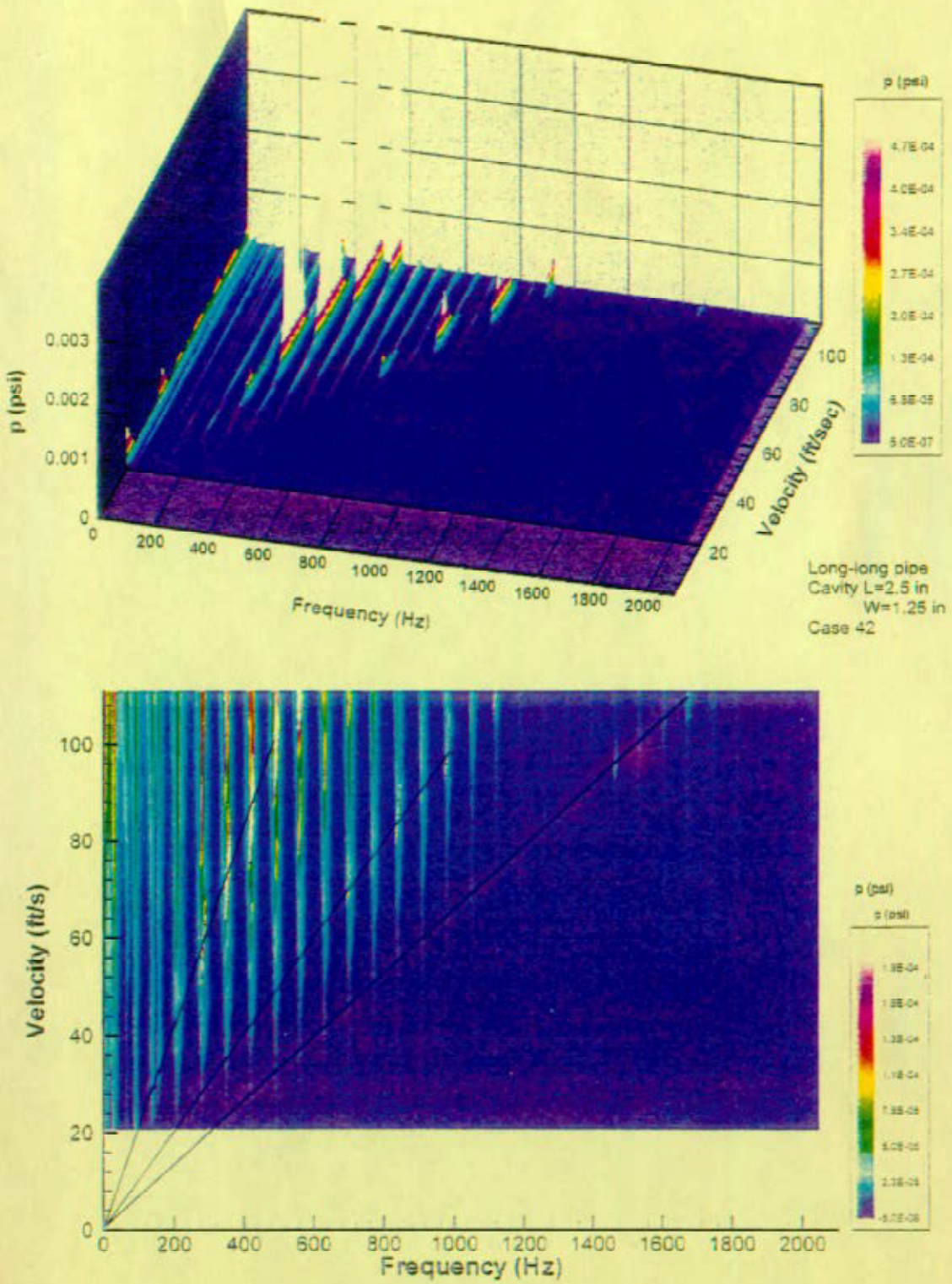

Figure 4a: Isometric view (top image) and plan view (bottom image) of pressure amplitude as a function of frequency and velocity. Lines shown on plan view represent fits through peak values of pressure amplitude. Cavity length $L^* = L/D = 2.5$ and depth $W^* = W/D = 1.25$, where D is pipe diameter. Long pipes of equal length are located at either end of the cavity.

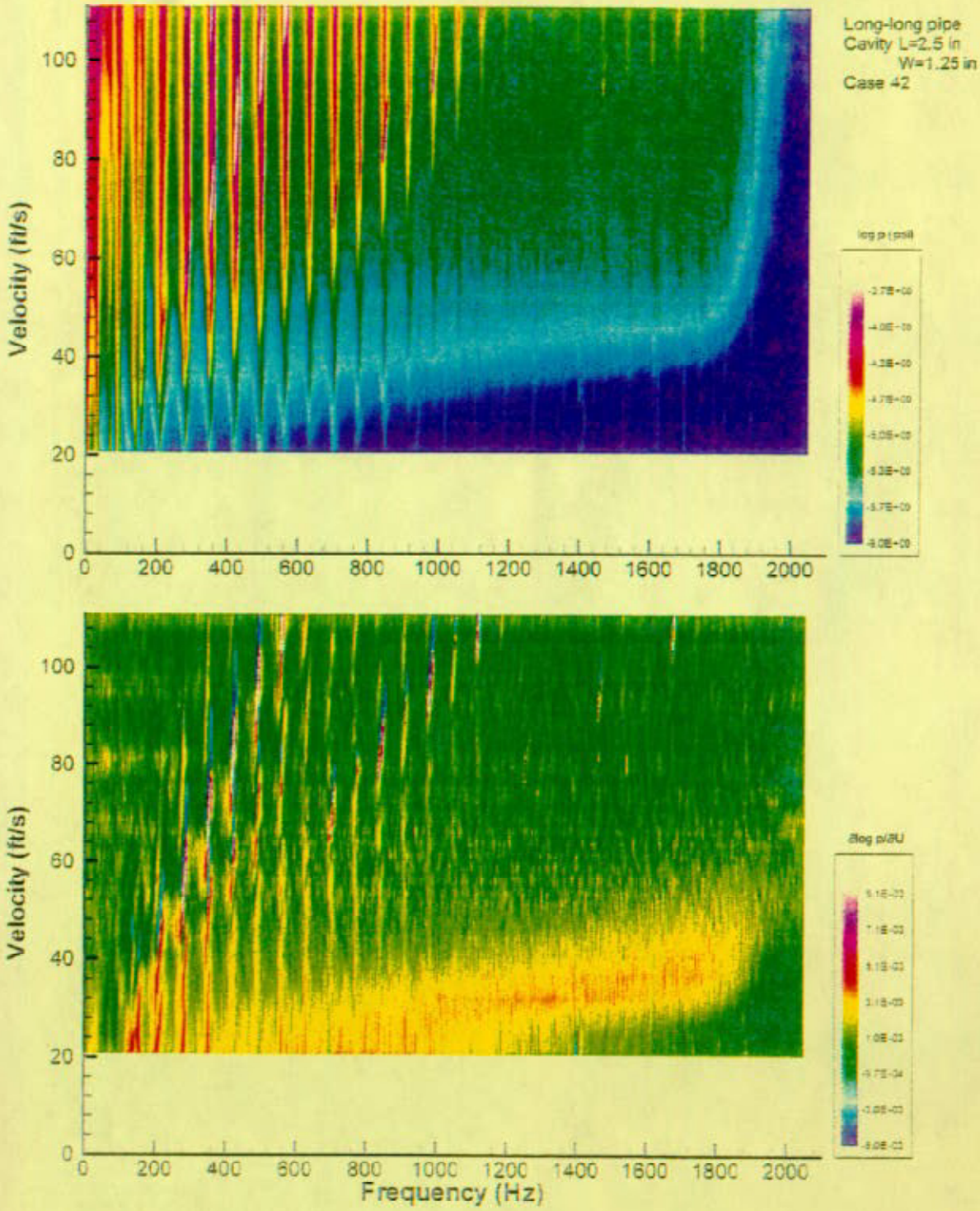

Figure 4b: Plan view of logarithmic pressure amplitude as a function of velocity and frequency (top image), and plan view of magnitude of the derivative of the logarithmic pressure amplitude with respect to velocity, $\partial(\log p)/\partial U$ (bottom image). Cavity length $L^* = L/D = 2.5$ and depth $W^* = W/D = 1.25$, where D is pipe diameter. Long pipes of equal length are located at either end of the cavity.

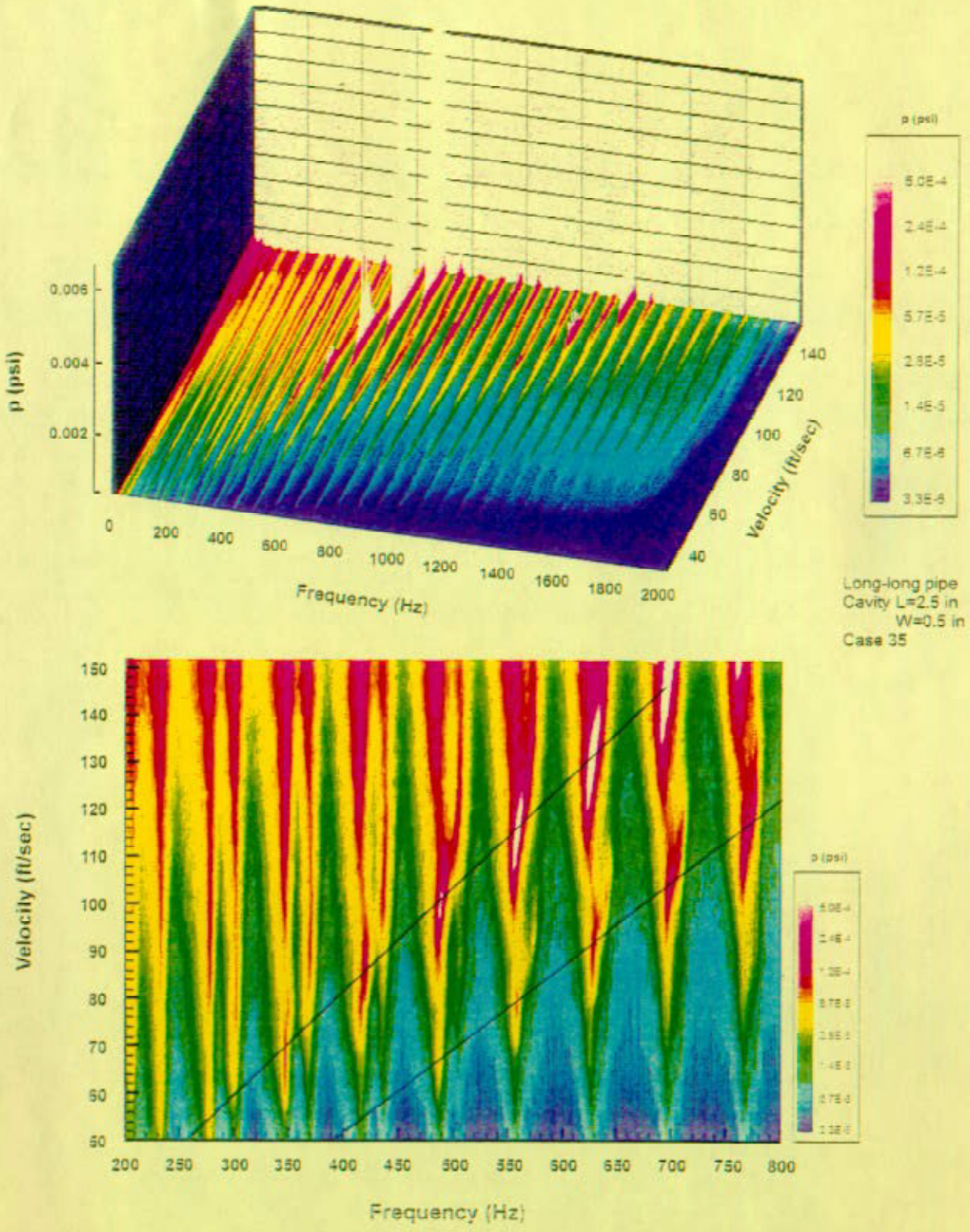

Figure 4c: Isometric view (top image) and plan view (bottom image) of pressure amplitude as a function of frequency and velocity. Lines shown on plan view represent fits through peak values of pressure amplitude. Cavity length $L' = L/D = 2.5$ and depth $W' = W/D = 0.5$, where D is pipe diameter. Long pipes of equal length are located at either end of the cavity.

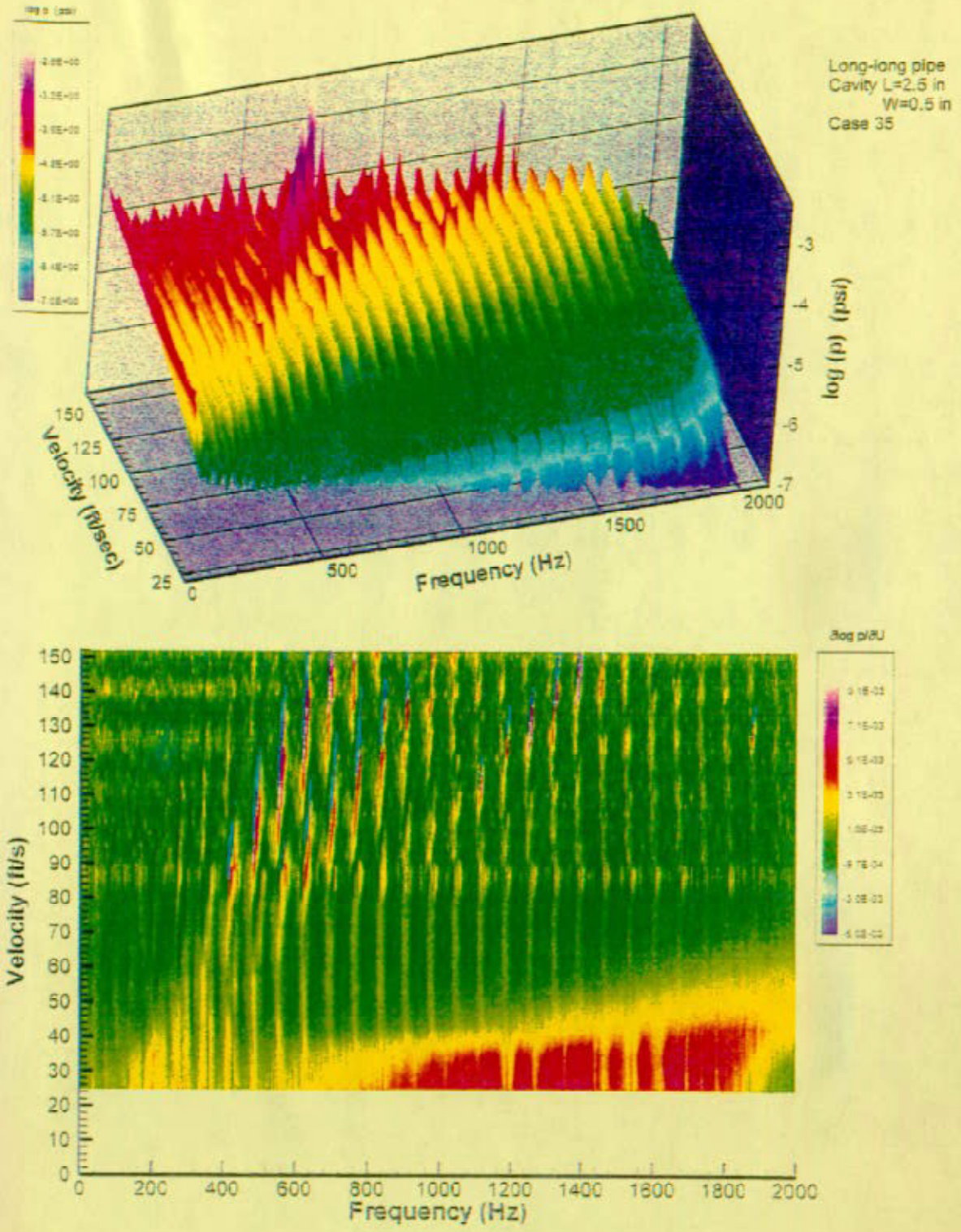

Figure 4d: Isometric view of logarithmic pressure amplitude as a function of velocity and frequency (top image); and plan view of magnitude of the derivative of the logarithmic pressure amplitude with respect to velocity, $\partial(\log p)/\partial U$ (bottom image). Cavity length $L^* = L/D = 2.5$ and depth $W^* = W/D = 0.5$, where D is pipe diameter. Long pipes of equal length are located at either end of the cavity.

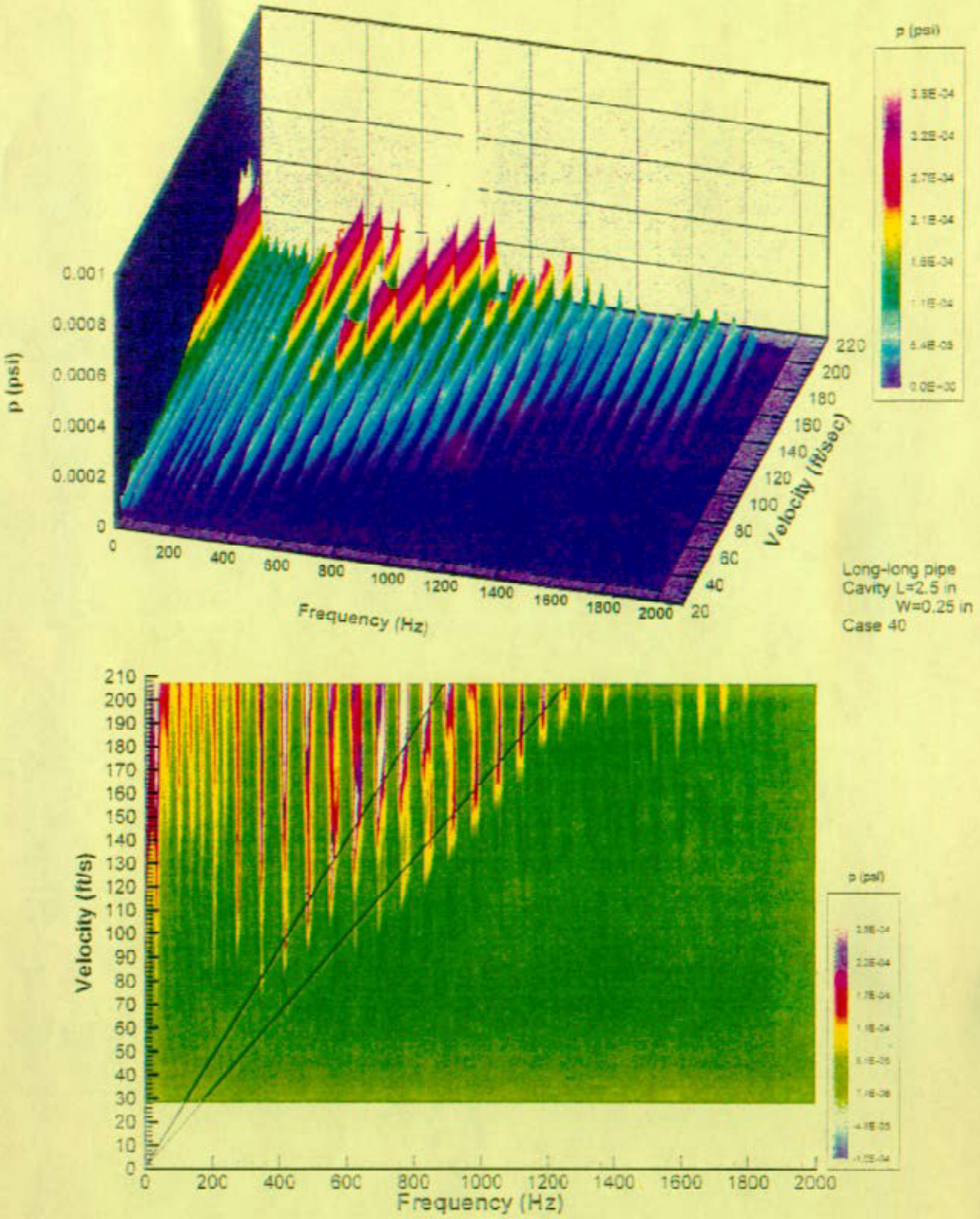

Figure 4e: Isometric view (top image) and plan view (bottom image) of pressure amplitude as a function of frequency and velocity. Lines shown on plan view represent fits through peak values of pressure amplitude. Cavity length $L^* = L/D = 2.5$ and depth $W^* = W/D = 0.25$, where D is pipe diameter. Long pipes of equal length are located at either end of the cavity.

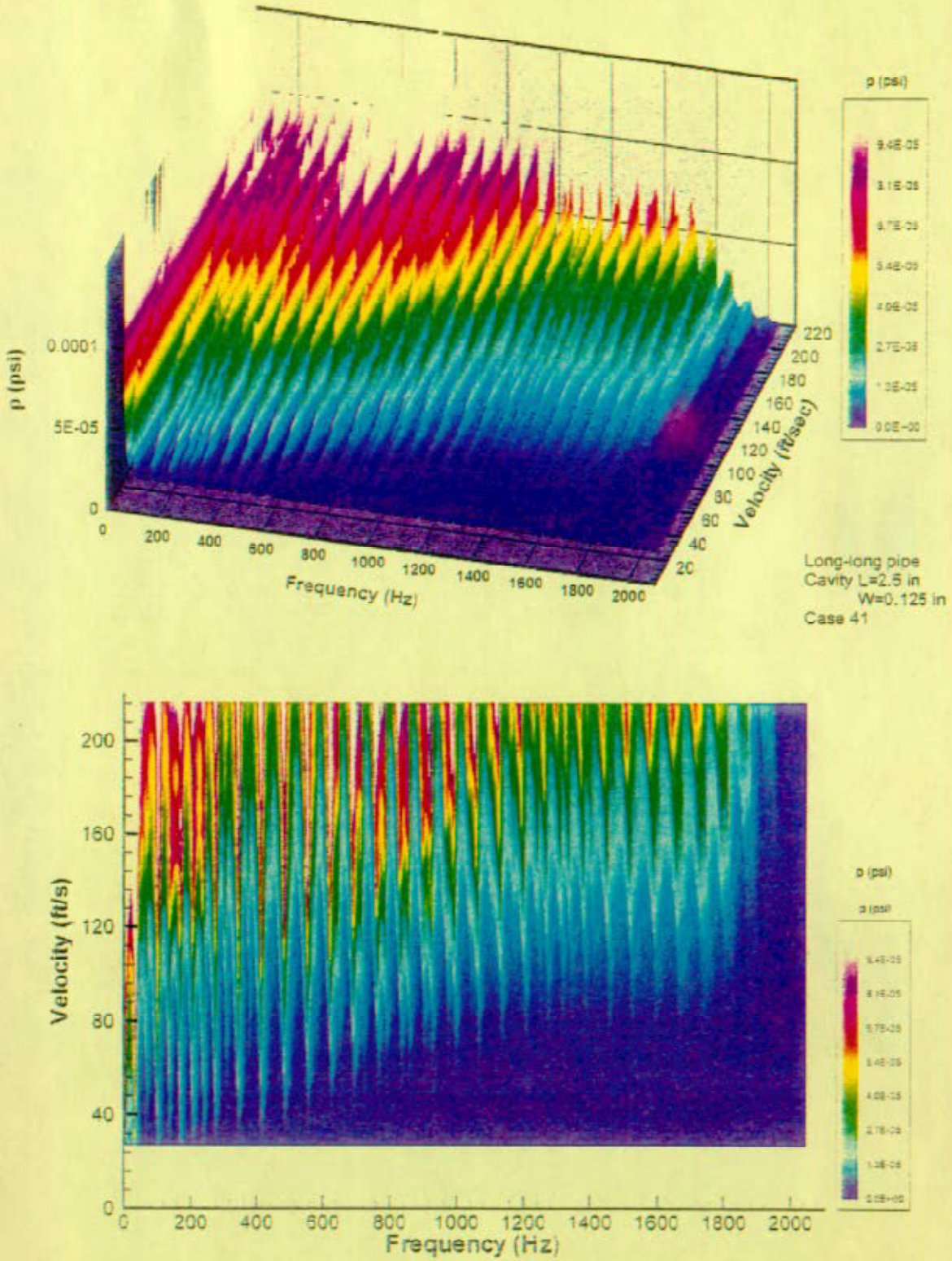

Figure 4f: Isometric view (top image) and plan view (bottom image) of pressure amplitude as a function of frequency and velocity. Cavity length $L^* = L/D = 2.5$ and depth $W^* = W/D = 0.125$, where D is pipe diameter. Long pipes of equal length are located at either end of the cavity.

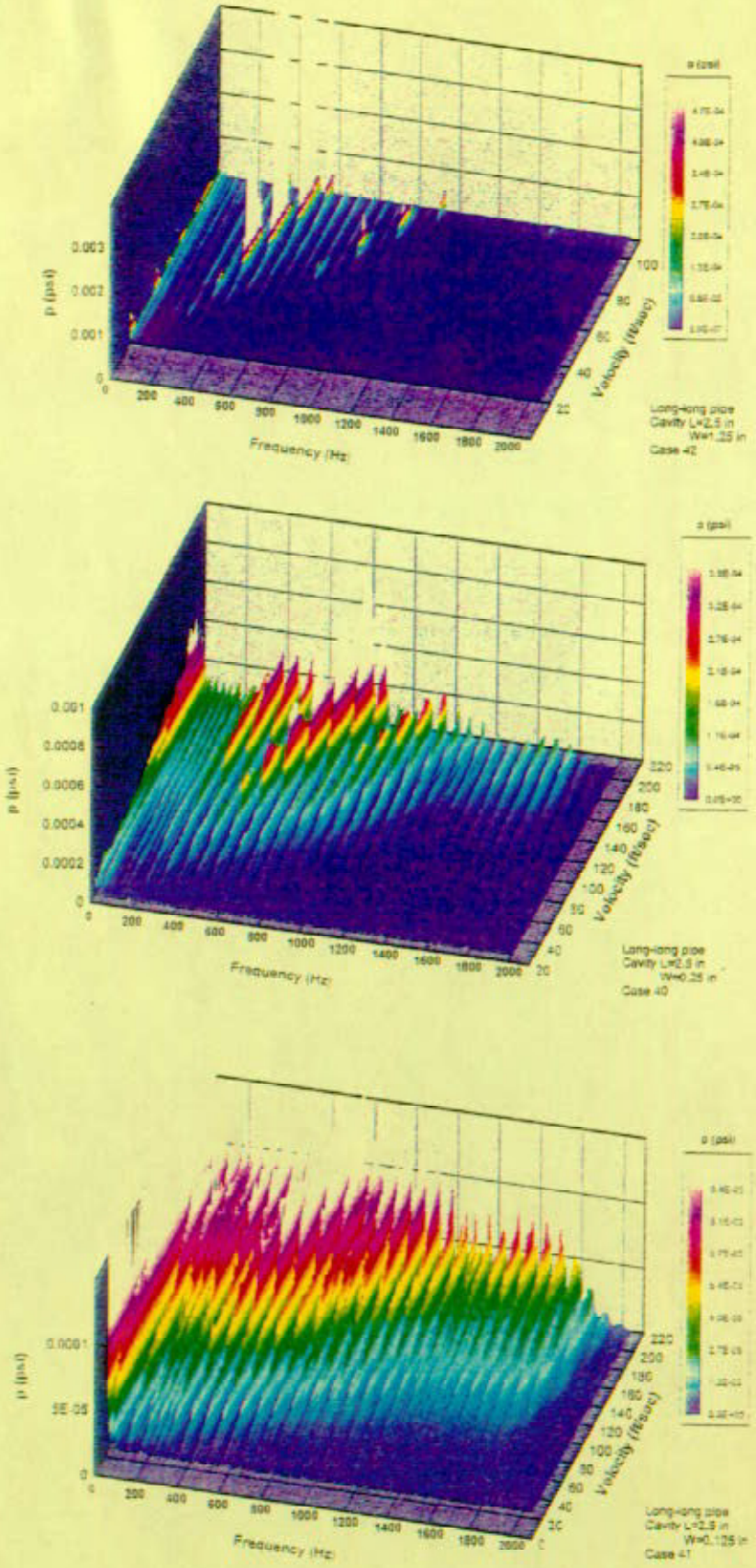

Figure 4g: Overview of effect of cavity depth on three-dimensional representation of pressure amplitude as a function of velocity and frequency. In all cases, cavity length is constant at $L^* = L/D = 2.5$. Cavity depth varies according to $W^* = W/D = 1.25$ (top image), $W^* = 0.25$ (middle image), and $W^* = 0.125$ (bottom image).

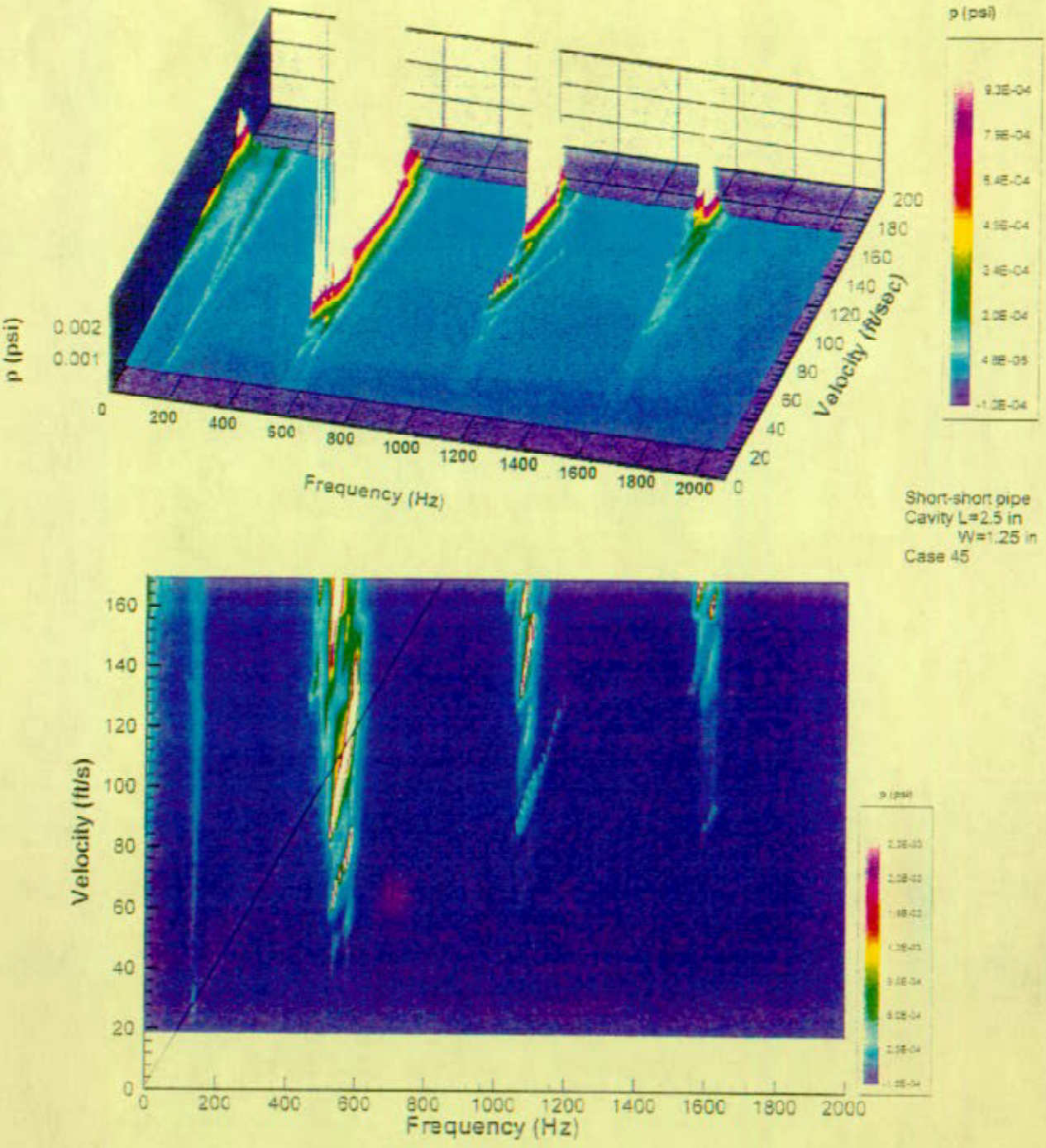

Figure 5a: Isometric view (top image) and plan view (bottom image) of pressure amplitude as a function of frequency and velocity. Line shown on plan view represents a fit through peak values of pressure amplitude. Cavity length $L^* = L/D = 2.5$ and depth $W^* = W/D = 1.25$, where D is pipe diameter. Short pipes of equal length are located at either end of the cavity.

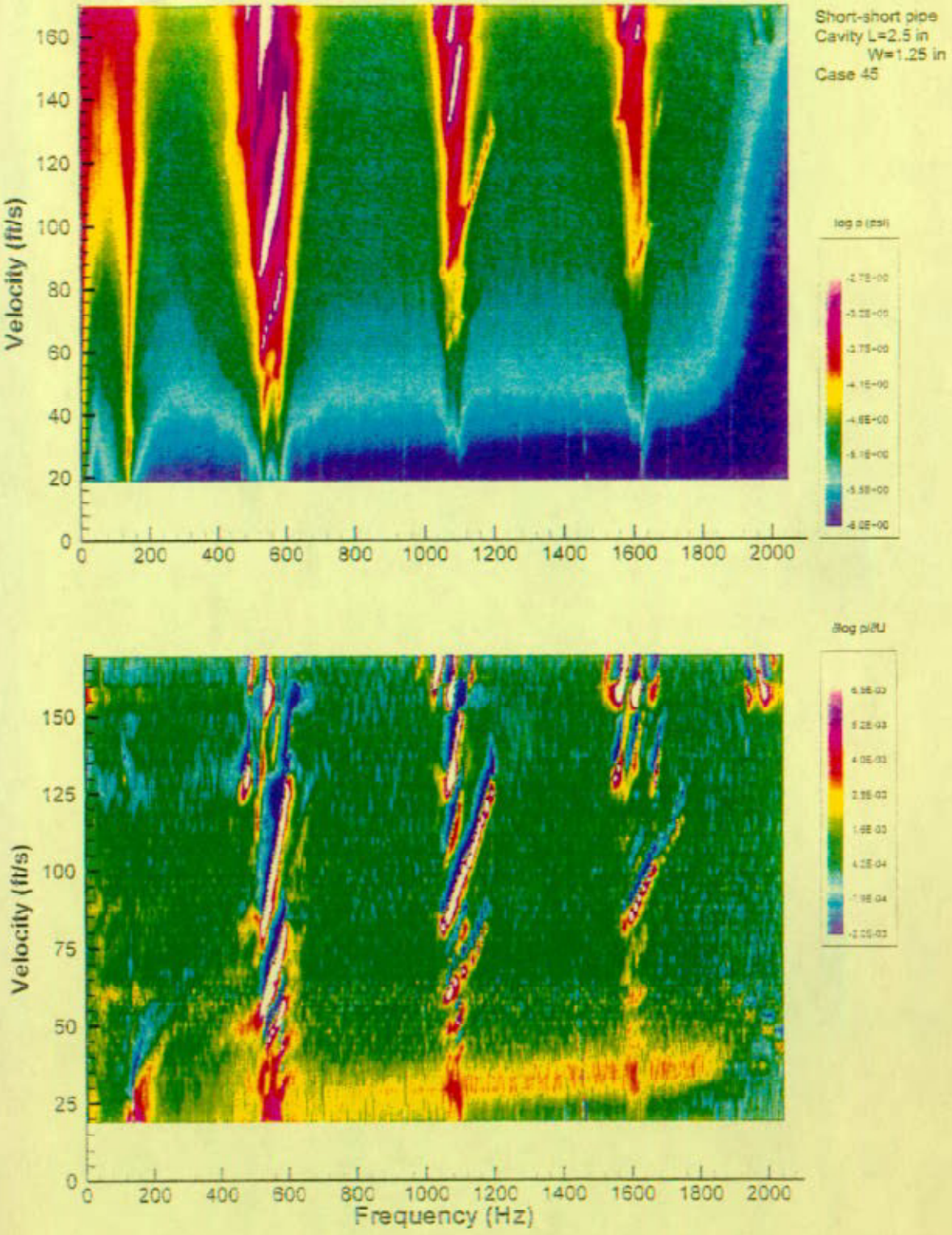

Figure 5b: Plan view of logarithmic pressure amplitude as a function of velocity and frequency (top image), and plan view of magnitude of the derivative of the logarithmic pressure amplitude with respect to velocity, $\partial(\log p)/\partial U$ (bottom image). Cavity length $L^* = L/D = 2.5$ and depth $W^* = W/D = 1.25$, where D is pipe diameter. Short pipes of equal length are located at either end of the cavity.

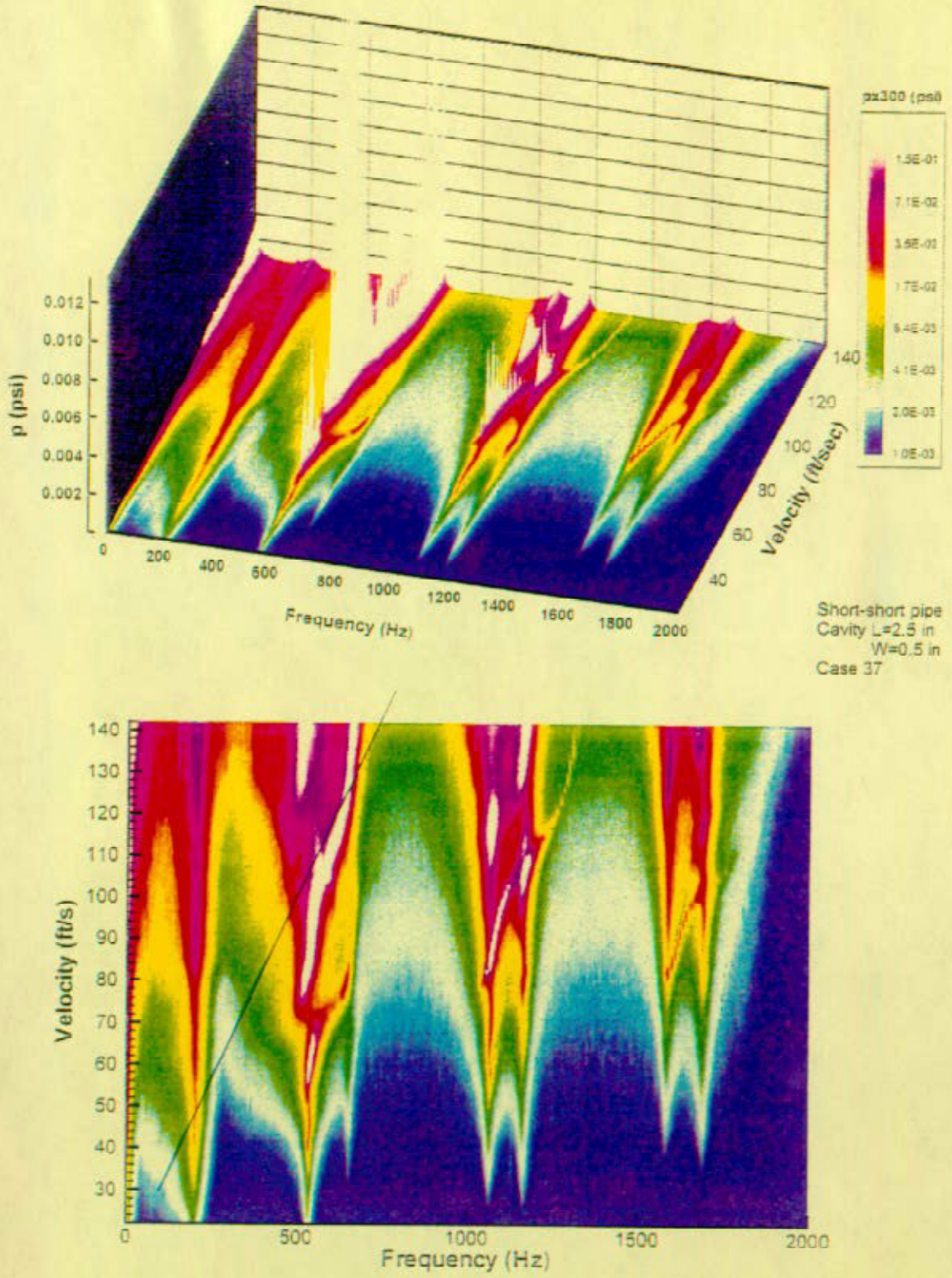

Figure 5c: Isometric view (top image) and plan view (bottom image) of pressure amplitude as a function of frequency and velocity. Line shown on plan view represents a fit through peak values of pressure amplitude. Cavity length $L^* = L/D = 2.5$ and depth $W^* = W/D = 0.5$, where D is pipe diameter. Short pipes of equal length are located at either end of the cavity.

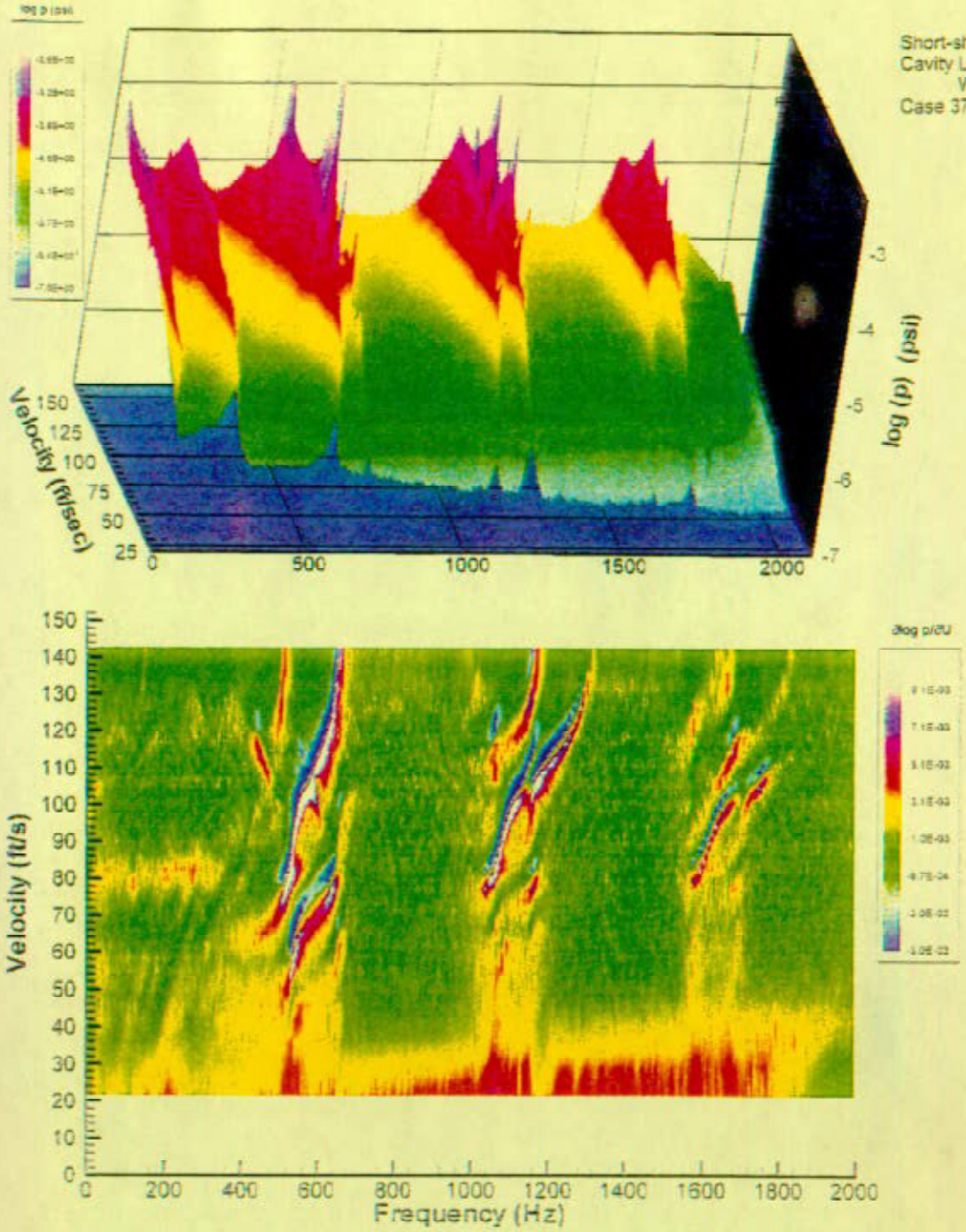

Figure 5d: Isometric view of logarithmic pressure amplitude as a function of velocity and frequency (top image), and plan view of magnitude of the derivative of the logarithmic pressure amplitude with respect to velocity, $\partial(\log p)/\partial U$ (bottom image). Cavity length $L^* = L/D = 2.5$ and depth $W^* = W/D = 0.5$, where D is pipe diameter. Short pipes of equal length are located at either end of the cavity.

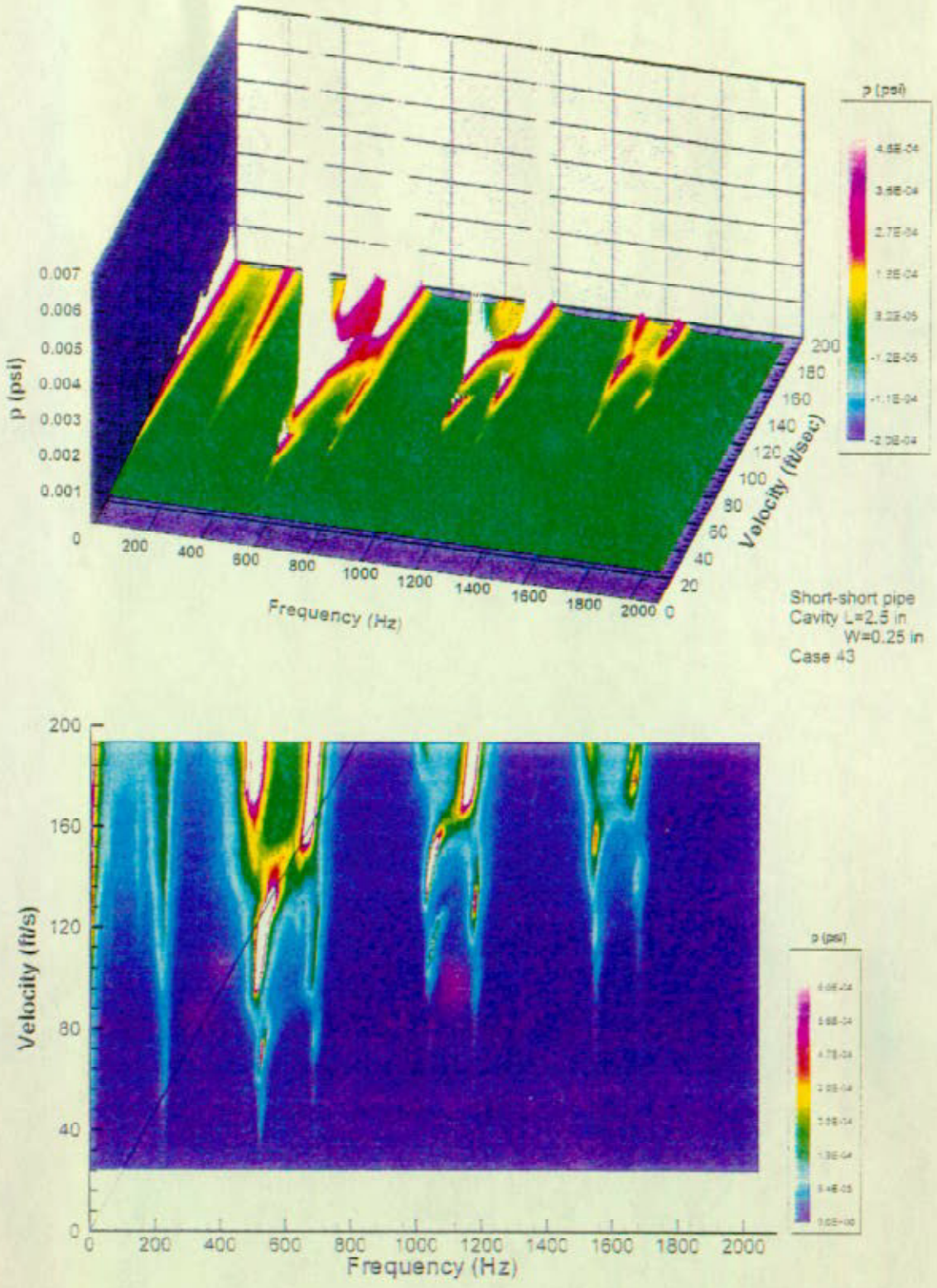

Figure 5e: Isometric view (top image) and plan view (bottom image) of pressure amplitude as a function of frequency and velocity. Line shown on plan view represents a fit through peak values of pressure amplitude. Cavity length $L^* = L/D = 2.5$ and depth $W^* = W/D = 0.25$, where D is pipe diameter. Short pipes of equal length are located at either end of the cavity.

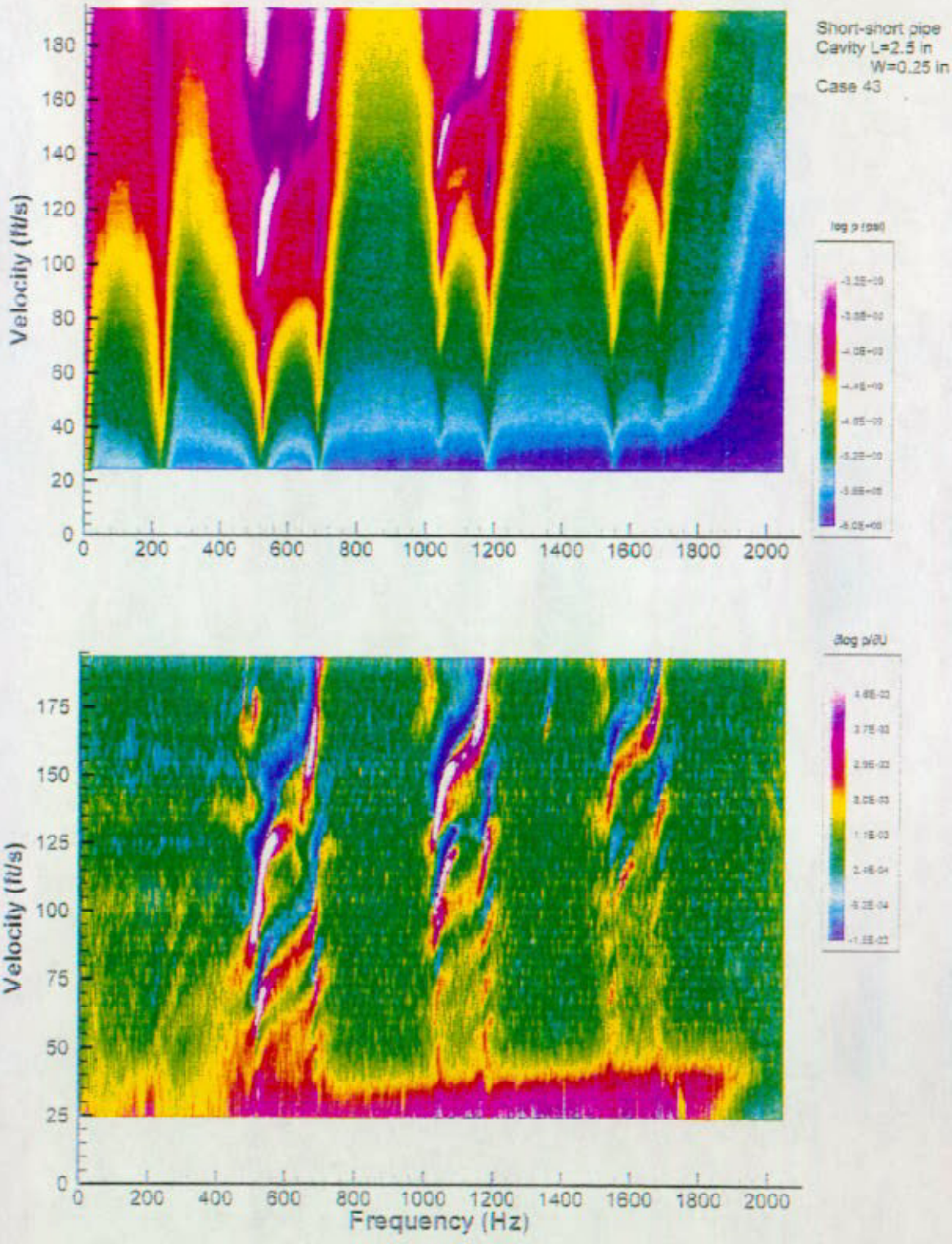

Figure 5f: Plan view of logarithmic pressure amplitude as a function of velocity and frequency (top image), and plan view of magnitude of the derivative of the logarithmic pressure amplitude with respect to velocity, $\partial(\log p)/\partial U$ (bottom image). Cavity length $L^* = L/D = 2.5$ and depth $W^* = W/D = 0.25$, where D is pipe diameter. Short pipes of equal length are located at either end of the cavity.

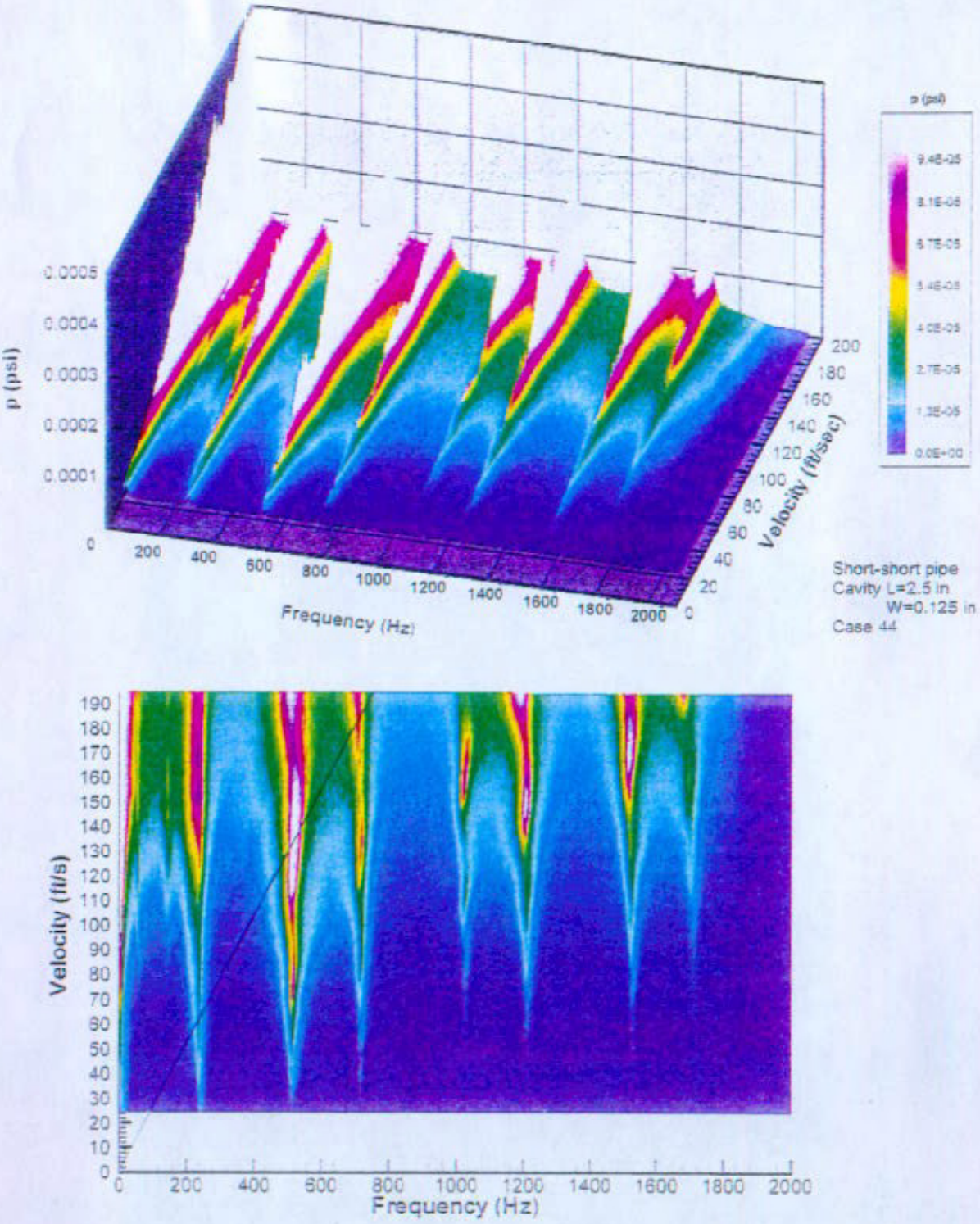

Figure 5g: Isometric view (top image) and plan view (bottom image) of pressure amplitude as a function of frequency and velocity. Line shown on plan view represents a fit through peak values of pressure amplitude. Cavity length $L^* = L/D = 2.5$ and depth $W^* = W/D = 0.125$, where D is pipe diameter. Short pipes of equal length are located at either end of the cavity.

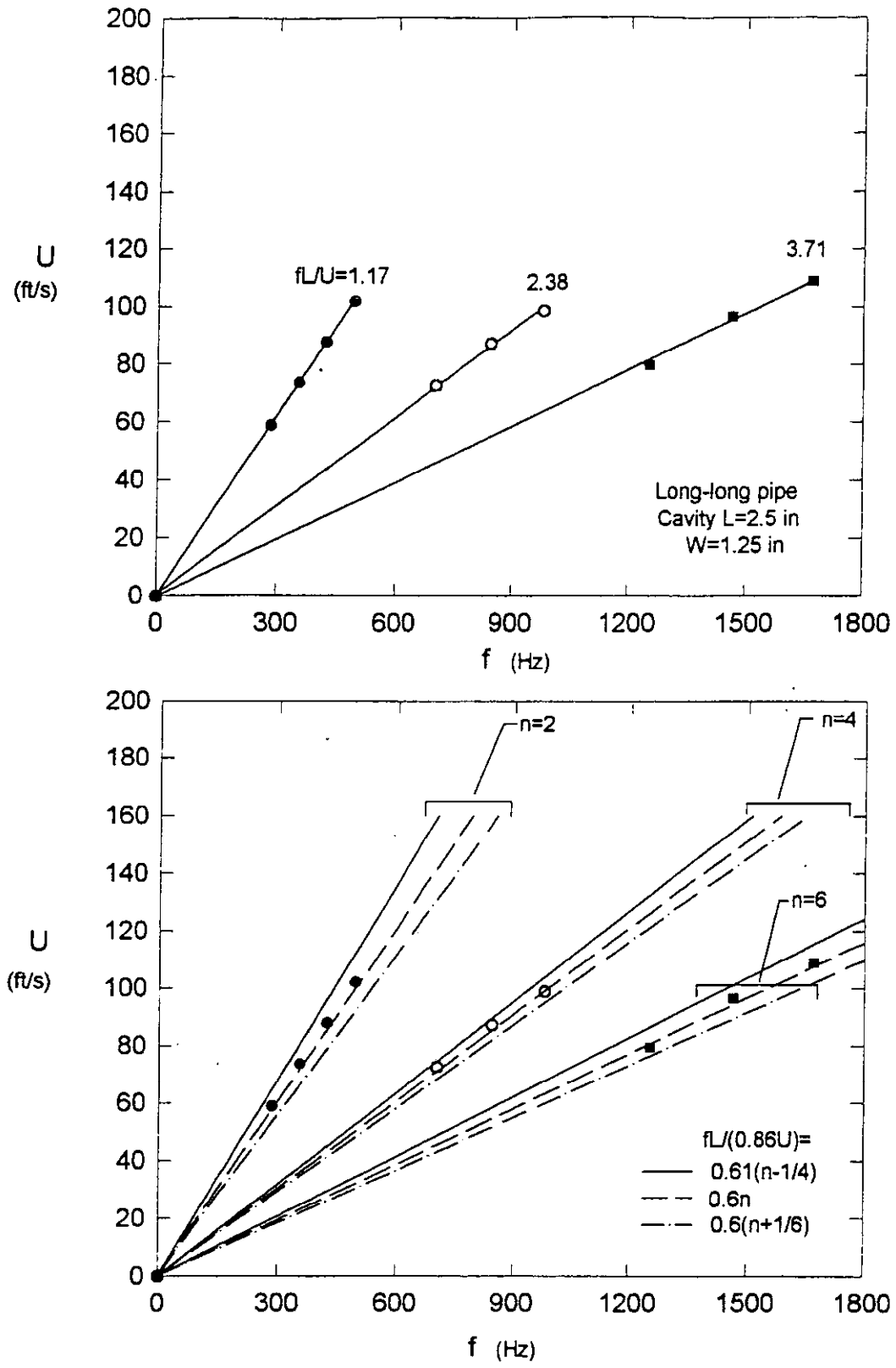

Figure 6a: Plots of values of frequency corresponding to amplitude peaks in Figures 4a and 4b. Top plot shows lines corresponding to the best fit of the dimensionless frequency fL/U through each set of data points. Bottom plot shows lines corresponding to three different correlations for fL/U. Velocity U corresponds to the time-mean centerline velocity at the center of the pipe, i.e., $U = \overline{u}_c$. In the lower plot, the bulk velocity of the pipe flow, 0.86 U, is employed as the normalization velocity.

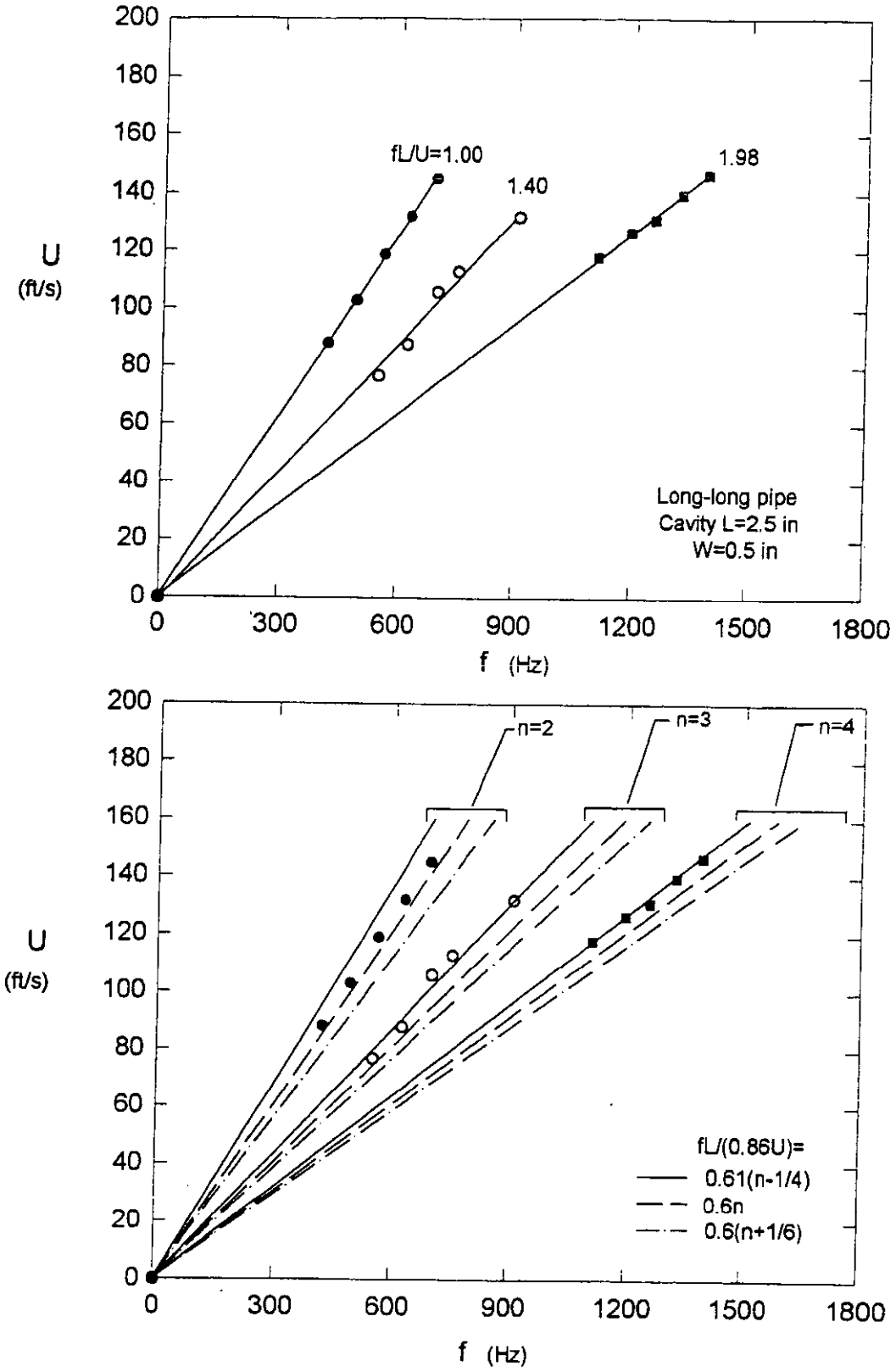

Figure 6b: Plots of values of frequency corresponding to amplitude peaks in Figures 4c and 4d. Top plot shows lines corresponding to the best fit of the dimensionless frequency fL/U through each set of data points. Bottom plot shows lines corresponding to three different correlations for fL/U. Velocity U corresponds to the time-mean centerline velocity at the center of the pipe, i.e., $U = \bar{u}_{\infty}$. In the lower plot, the bulk velocity of the pipe flow, 0.86 U, is employed as the normalization velocity.

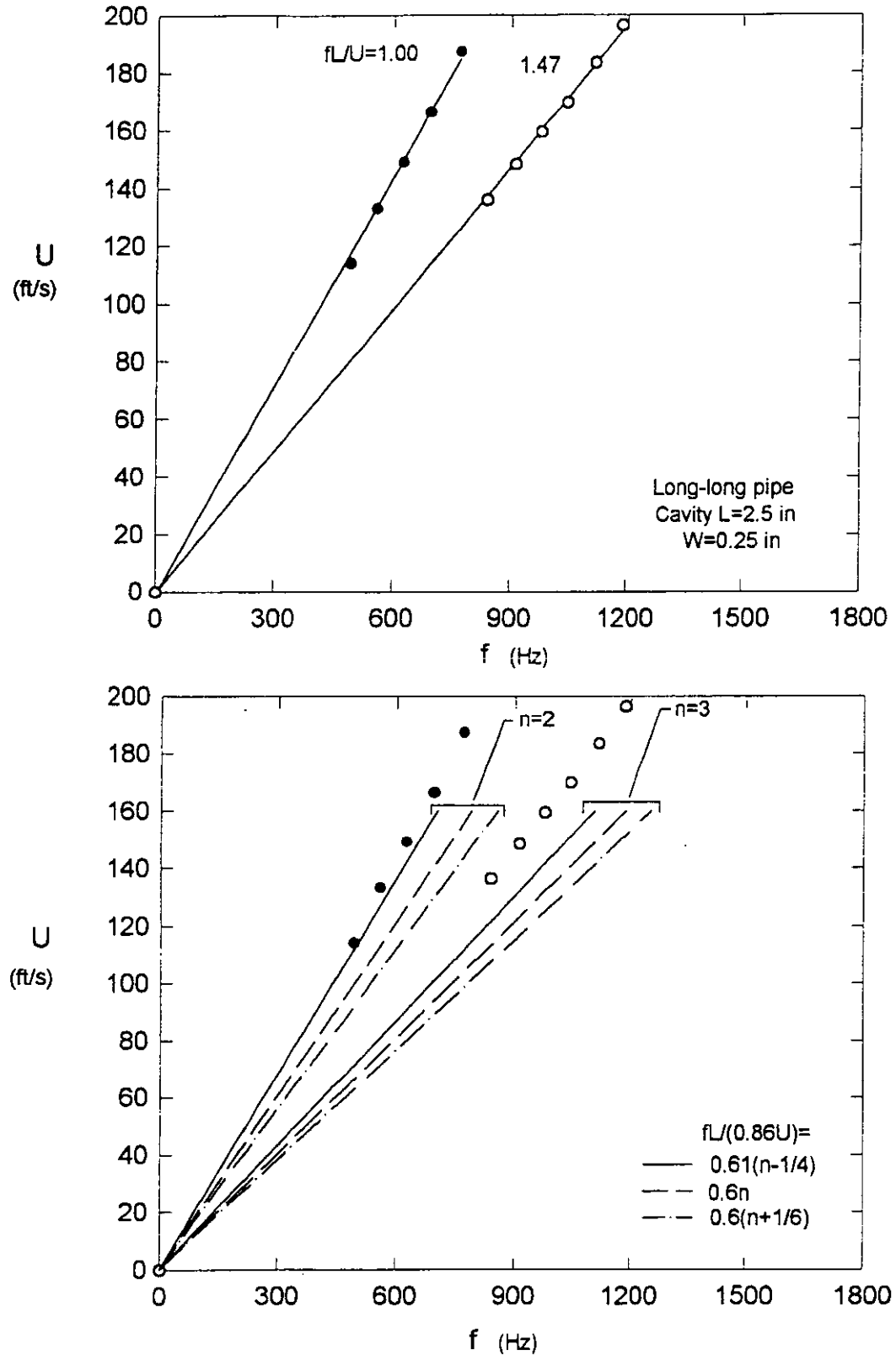

Figure 6c: Plots of values of frequency corresponding to amplitude peaks in Figure 4e. Top plot shows lines corresponding to the best fit of the dimensionless frequency fL/U through each set of data points. Bottom plot shows lines corresponding to three different correlations for fL/U. Velocity U corresponds to the time-mean centerline velocity at the center of the pipe, i.e., $U = \bar{u}_m$. In the lower plot, the bulk velocity of the pipe flow, 0.86 U, is employed as the normalization velocity.

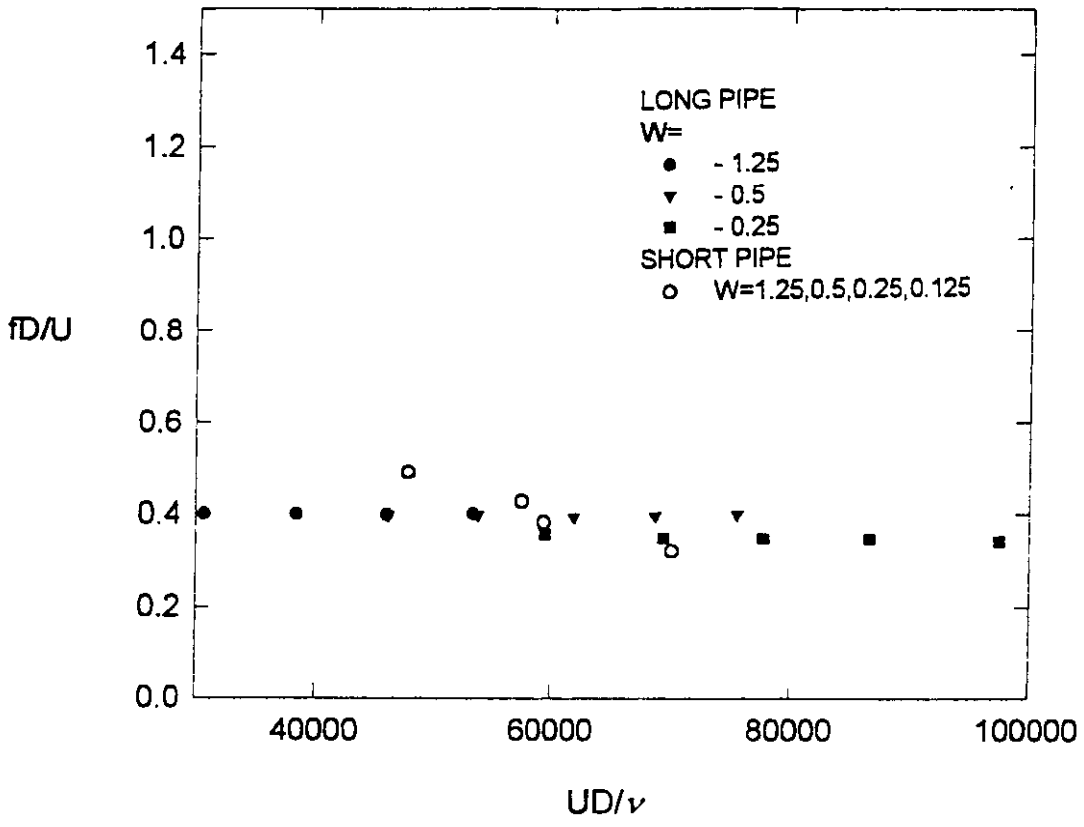

Figure 7: Superposition of values of dimensionless frequency corresponding to the maximum amplitude peaks for each cavity configuration.

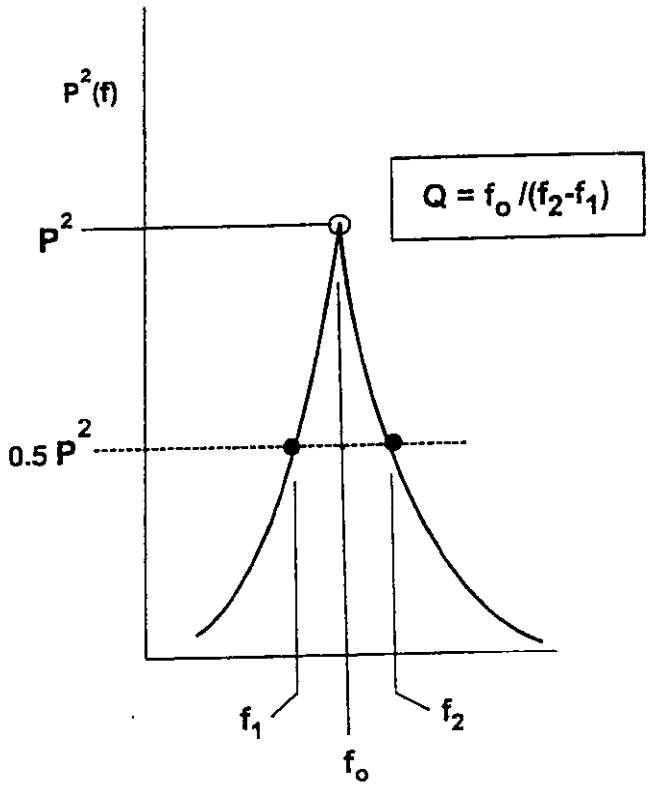

Figure 8: Schematic illustrating definition of Quality (Q) factor based on pressure spectrum $p^2(f)$.

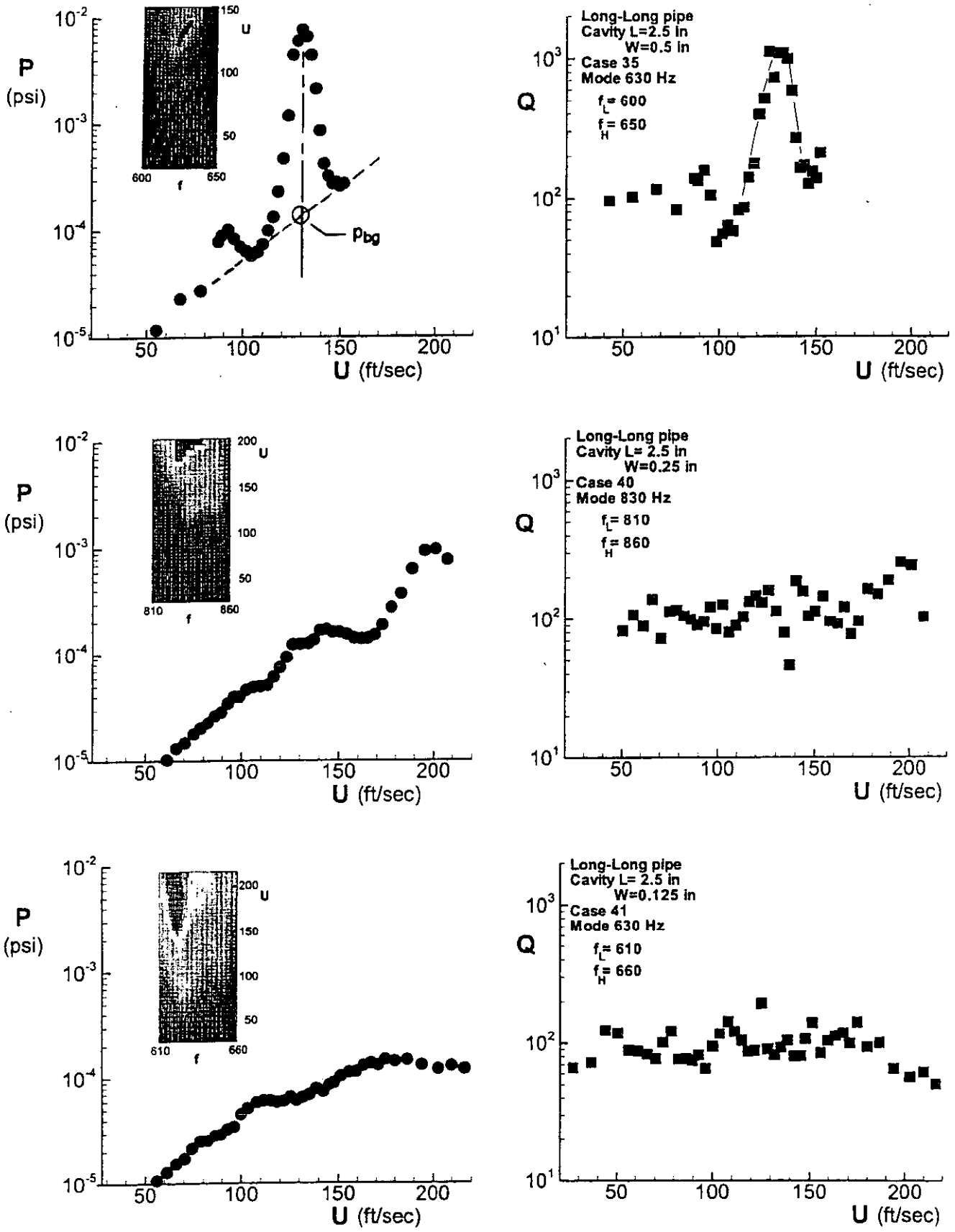

Figure 9a: Effect of cavity depth on onset of flow tones. Plots show peak pressure amplitude P and quality factor Q as a function of centerline velocity U for data corresponding to Figures 4c,d (top set of plots), 4e (middle set of plots), and 4f (bottom set of plots). Images in the inset of each

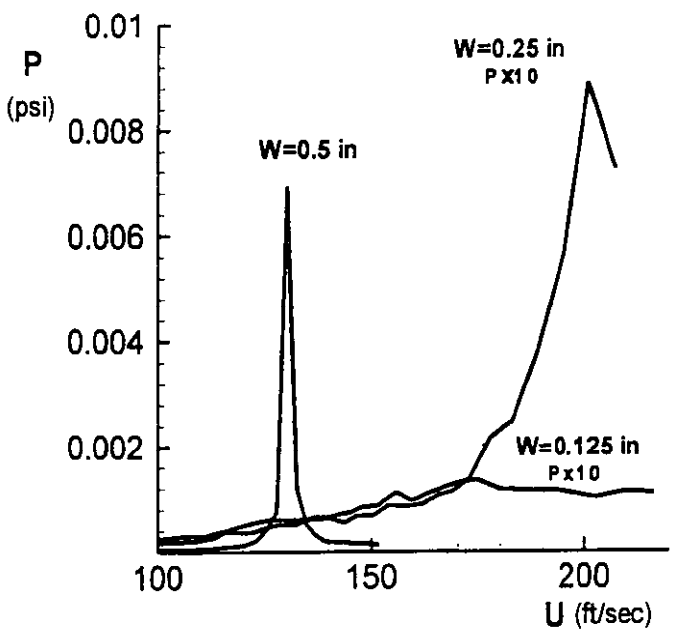

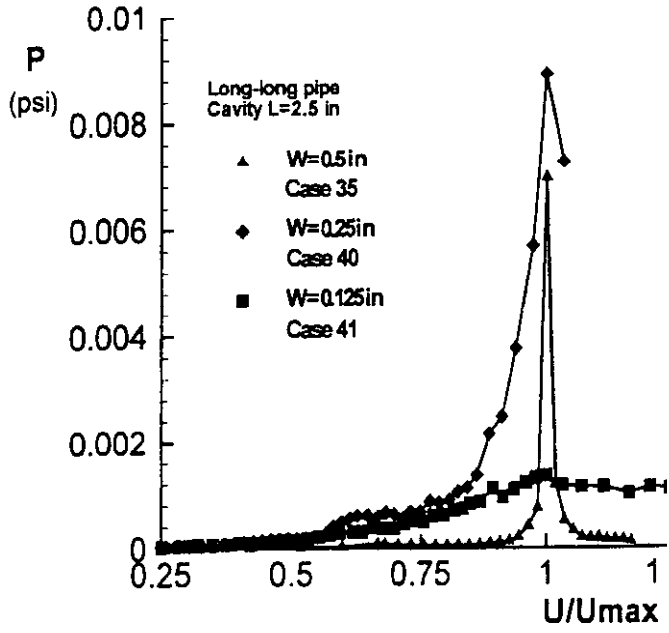

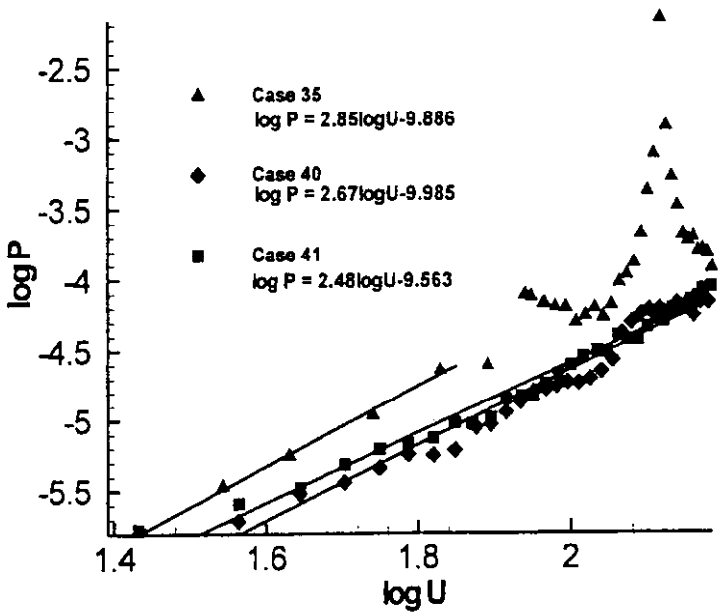

Figure 9b: Direct comparison of variations of peak pressure amplitude P with centerline velocity U corresponding data of Figure 9a.

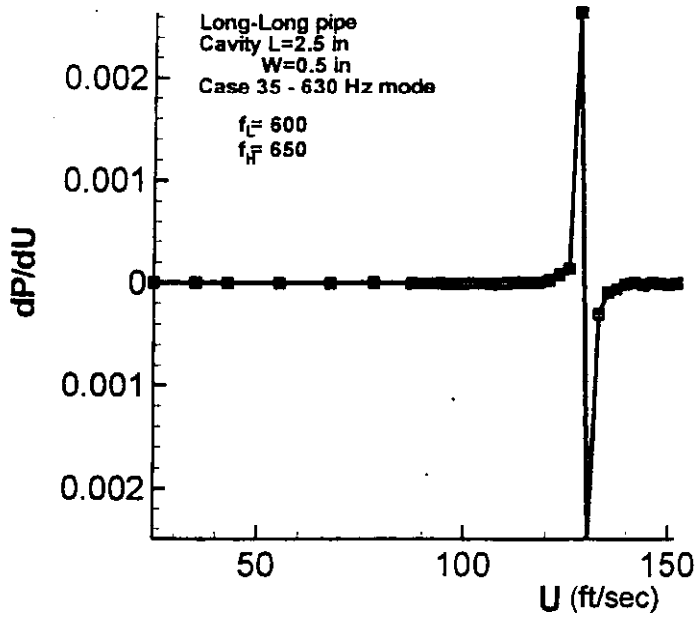

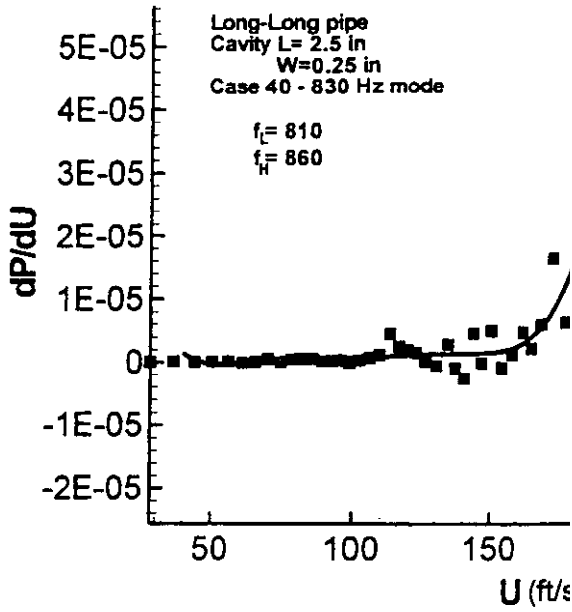

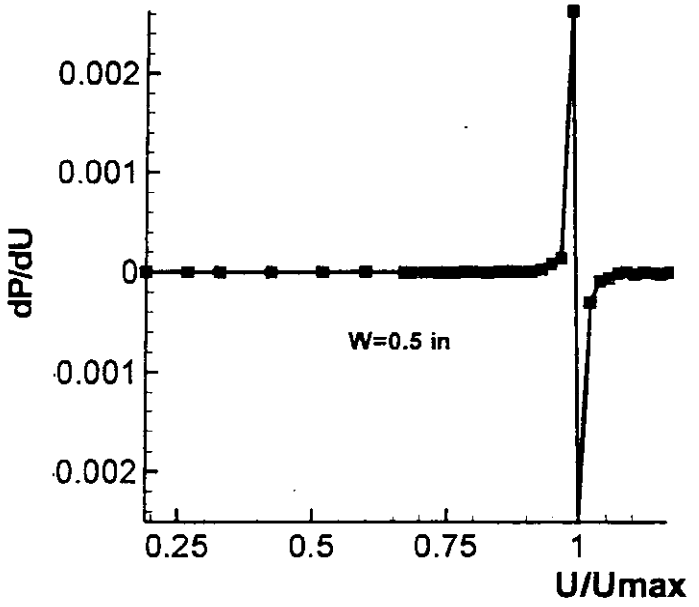

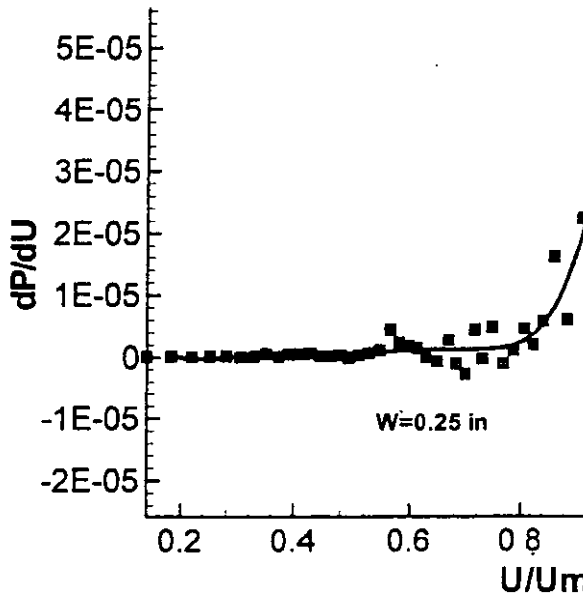

Figure 9c: Variation of slope of peak pressure amplitude P as a function of velocity U for data corresponding to the
and middle sets of plots in Figure 9a.

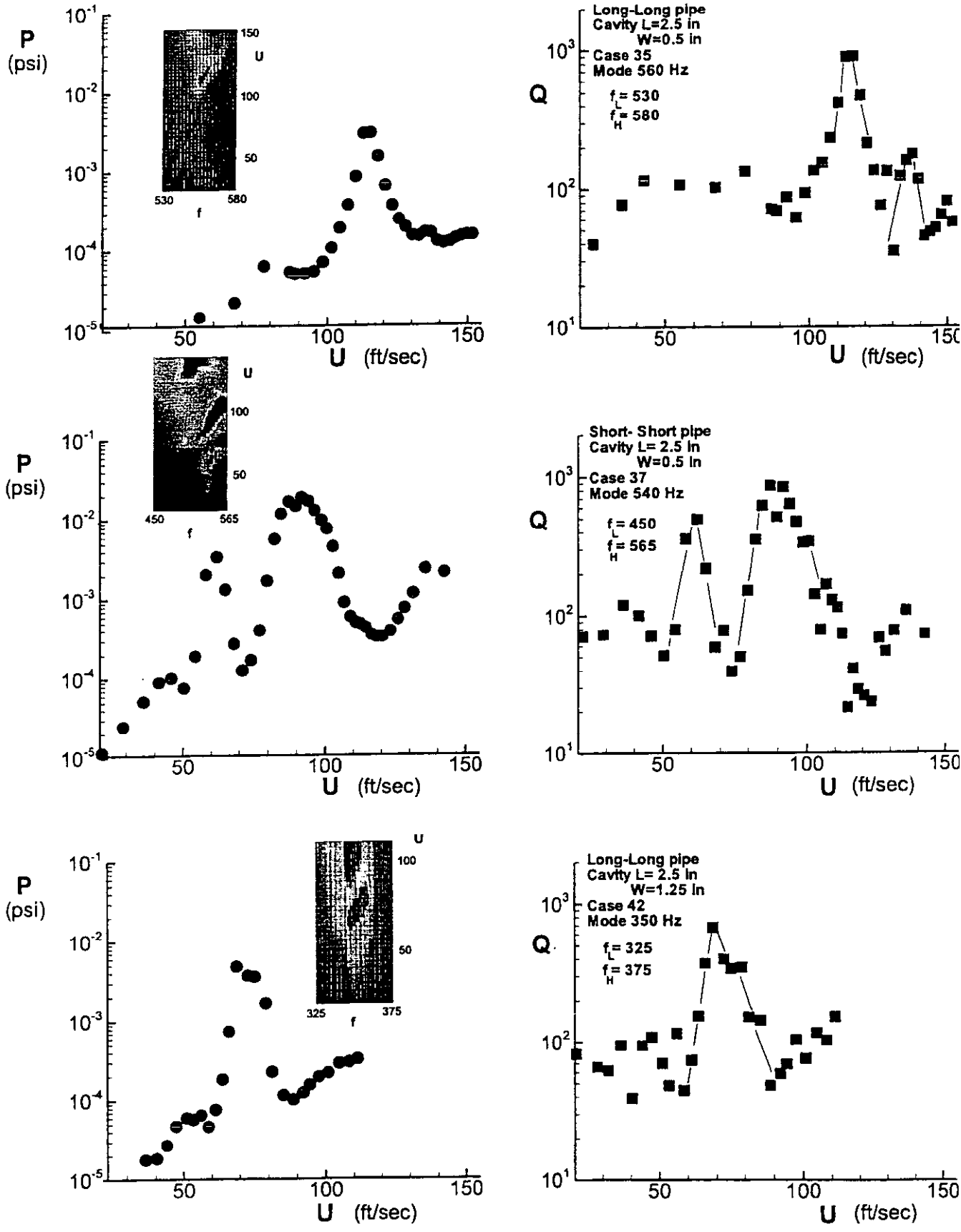

Figure 10: Onset of initial flow tones. Plots show peak pressure amplitude P and quality factor Q as a function of centerline velocity U for data corresponding to Figures 4c,d (top set of plots),

Case 35
Long pipe: W=0.5, L=2.5
35-stage1.cdr

$$U = b^{af}$$
$$\log U = \log f + a$$

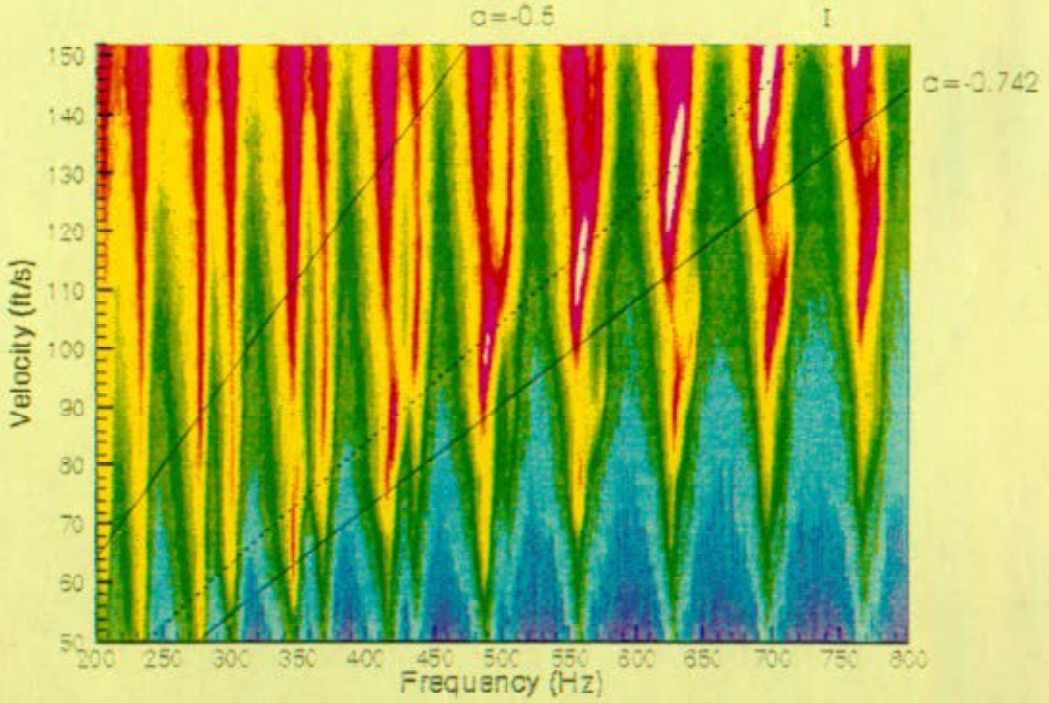

Figure 11a: Plan view of pressure amplitude response on plane of velocity versus frequency corresponding to Figure 4c. Dashed line represents predominant Strouhal mode I. Solid lines correspond to boundaries of vertical cuts through three-dimensional plot of pressure amplitude velocity frequency. Values of *a* are extreme reference values for these cuts. Cavity length $L' = L/D = 2.5$ and depth $W' = W/D = 0.5$, where D is pipe diameter. Long pipes of equal length are located at either end of the cavity.

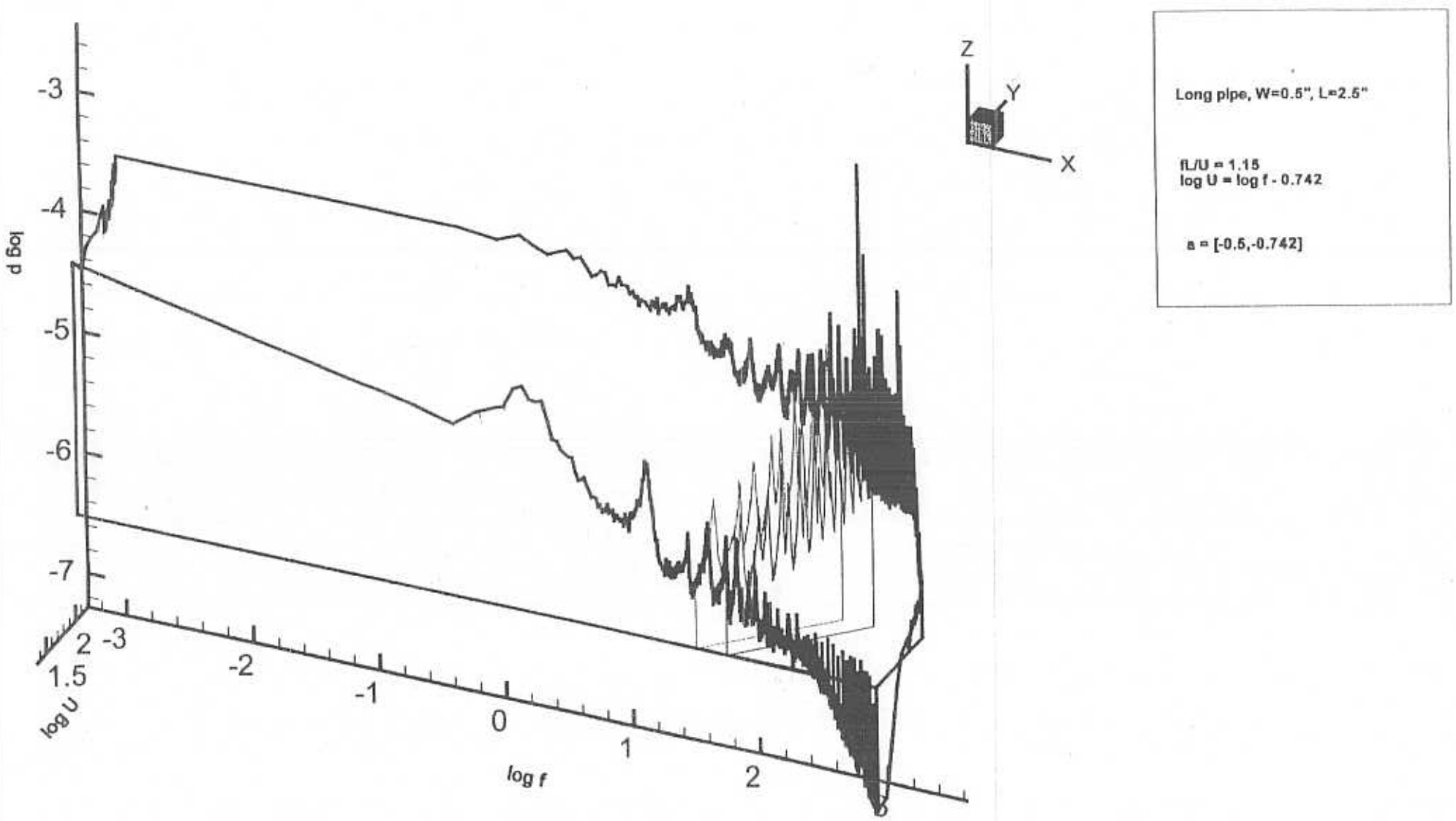

Figure 11b: Three-dimensional representation of vertical cuts defined by extreme values of a in Figure 11a. Bold lines represent spectra. Thin lines are vertical cuts coincident with the constant value of a in Figure 11a. Logarithmic values of parameters are employed.

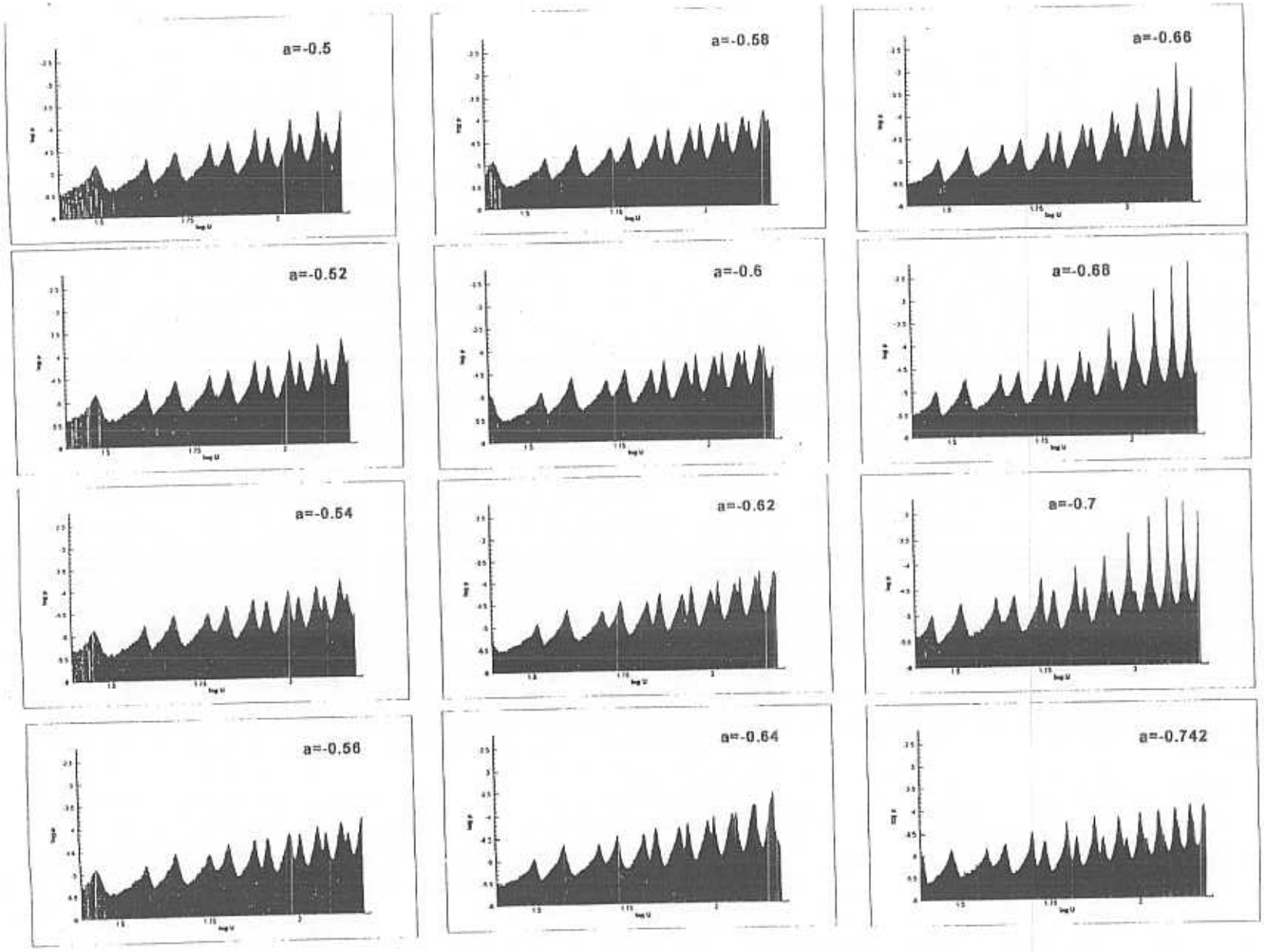

Long pipe; W=0.5", L=2.5"

log U = log f + a
a=[-0.5,-0.742]

Figure 11c: Vertical cuts through the plot of Figure 11a. All cuts are along a line of constant Strouhal number fL/U, but at different values of *a* lying between the extreme values defined in Figure 11a.

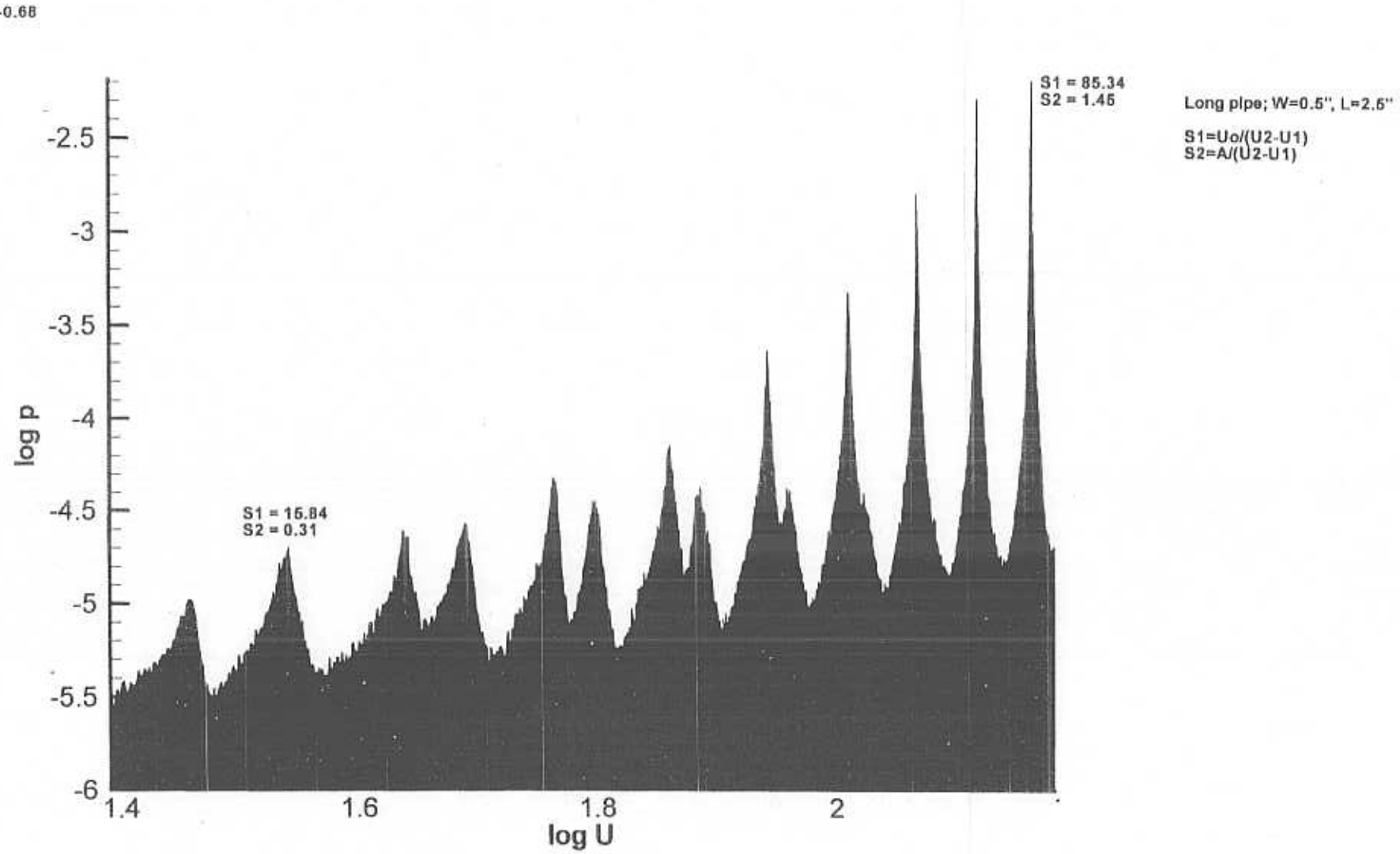

Figure 11d: Zoomed-in view of vertical cut selected from series of Figure 11c. This cut corresponds to the largest amplitude, sharpest-peak response at larger values of inflow velocity. Parameters S_1 and S_2 are sharpness factors analogous to Q-quality factors.

Case 41
Long pipe: W=0.125, L=2.5
41-stage1.cdr

$$U = b^{af}$$
$$\log U = \log f - a$$

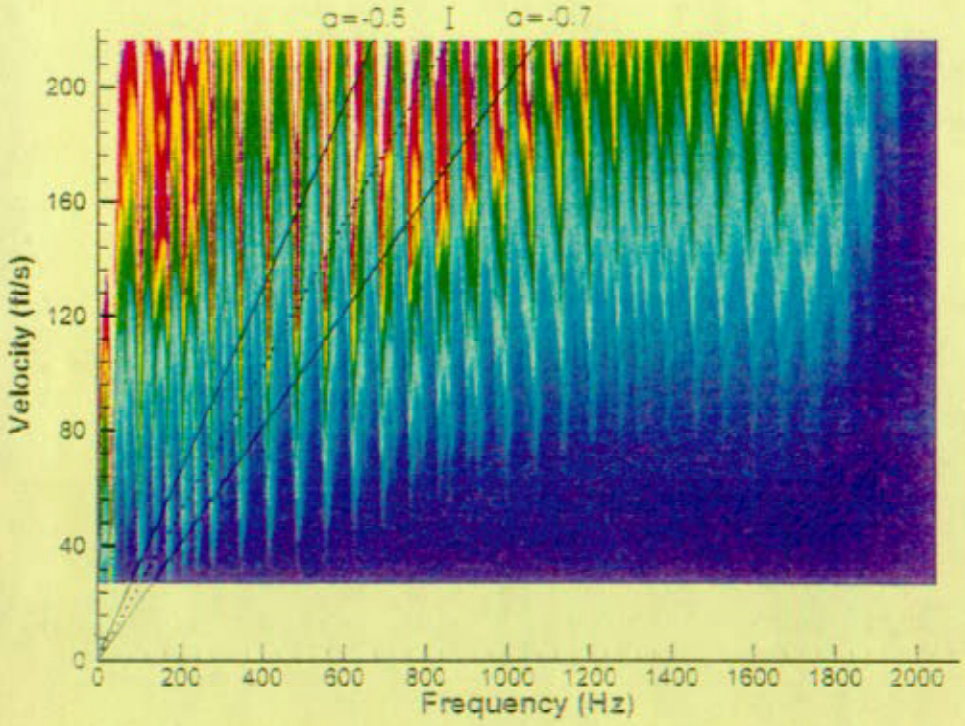

Figure 12a: Plan view of pressure amplitude response on plane of velocity versus frequency corresponding to Figure 4f. Dashed line represents predominant Strouhal mode I. Solid lines correspond to boundaries of vertical cuts of three-dimensional plot of pressure amplitude velocity frequency. Values of a are extreme reference values for these cuts. Cavity length $L^* = L/D = 2.5$ and cavity depth $W^* = W/D = 0.125$, where D is pipe diameter. Long pipes of equal length are located at either end of the cavity.

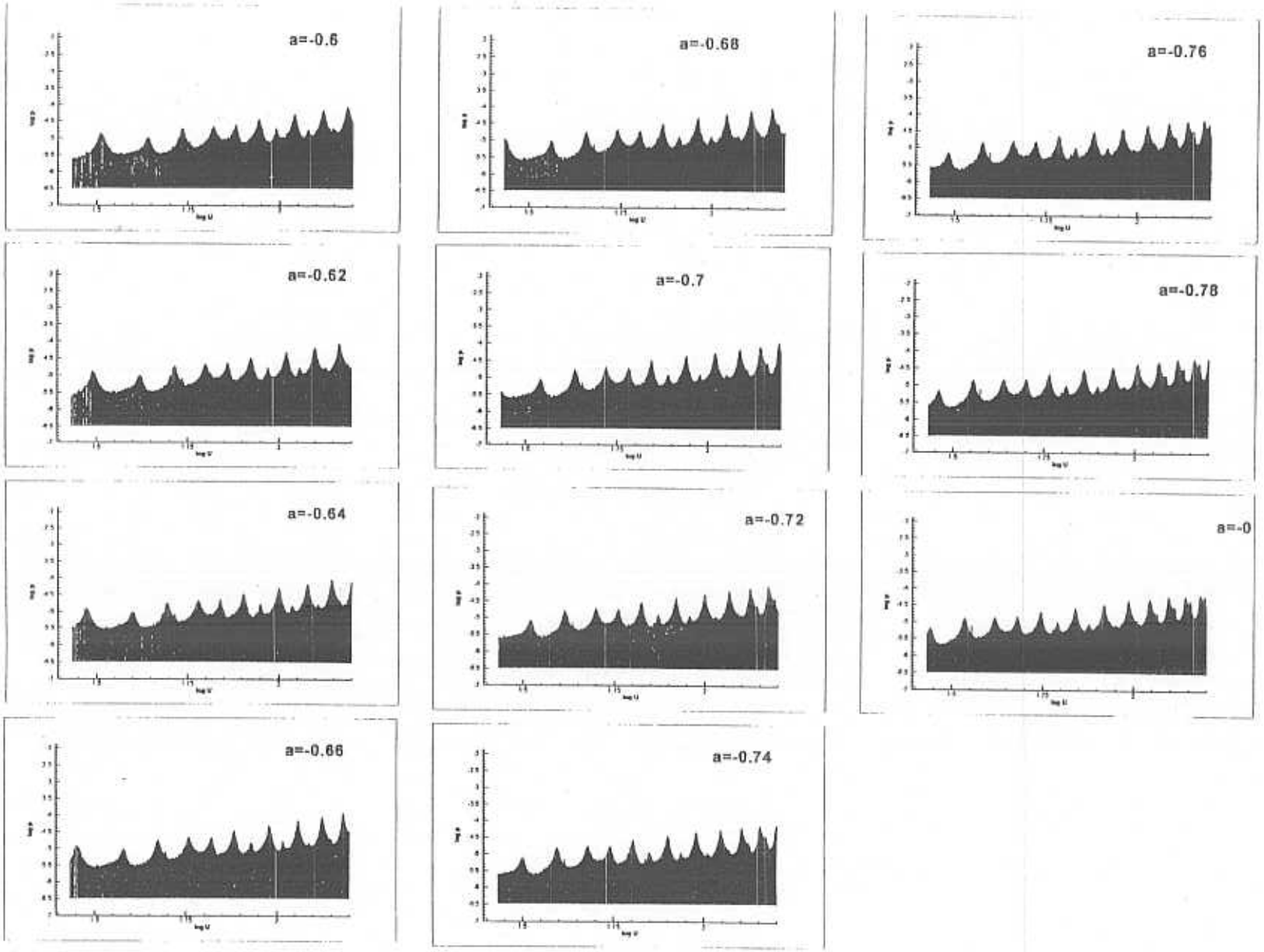

Figure 12b: Vertical cuts through the plot of Figure 12a. All cuts are along a line of constant Strouhal number fL/U, but at different values of a lying between the extreme values defined in Figure 12a.

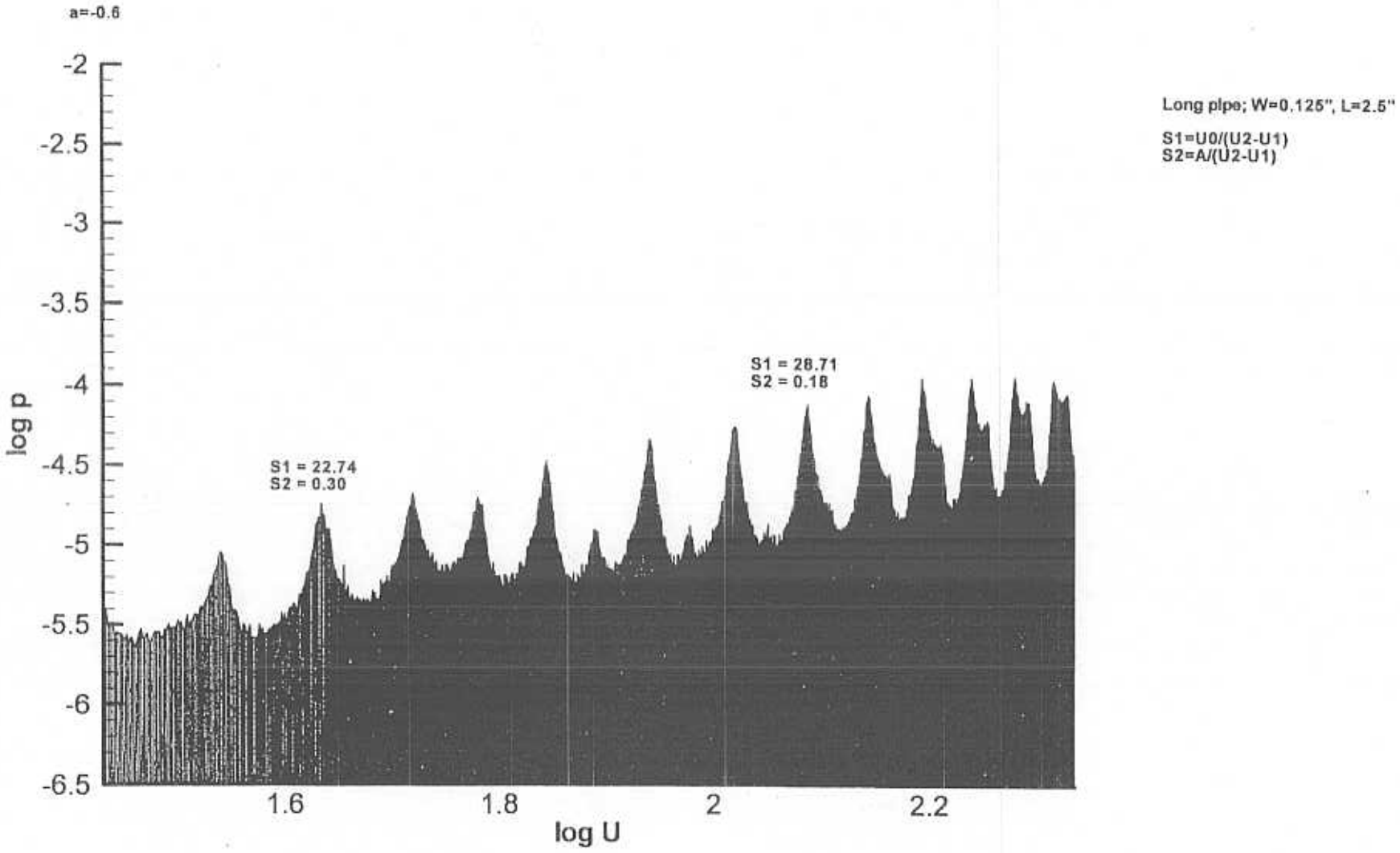

Figure 12c: Zoomed-in view of vertical cut selected from series of Figure 12b. Parameters S_1 and S_2 are sharpness factors analogous to Q-quality factors.

Case 37
Short pipe: W=0.5, L=2.5
37-stage1.cor

$$U = b^{*}f$$
$$\log U = \log f - a$$

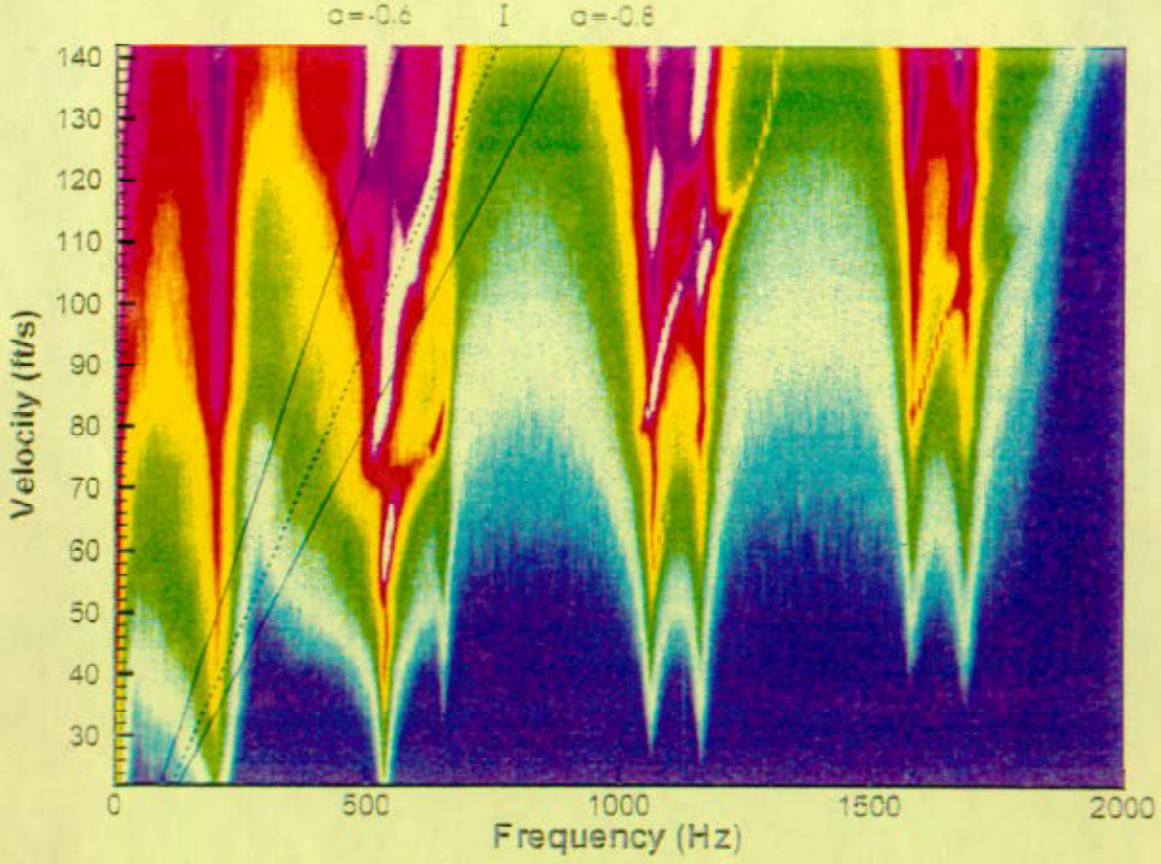

Figure 13a: Plan view of pressure amplitude response on plane of velocity versus frequency corresponding to Figure 5c. Dashed line represents predominant Strouhal mode I. Solid lines correspond to boundaries of vertical cuts of three-dimensional plot of pressure amplitude velocity frequency. Values of a are extreme reference values for these cuts. Cavity length $L^{*} = L/D = 2.5$ and depth $W^{*} = W/D = 0.5$, where D is pipe diameter. Short pipes of equal length are located at either end of the cavity.

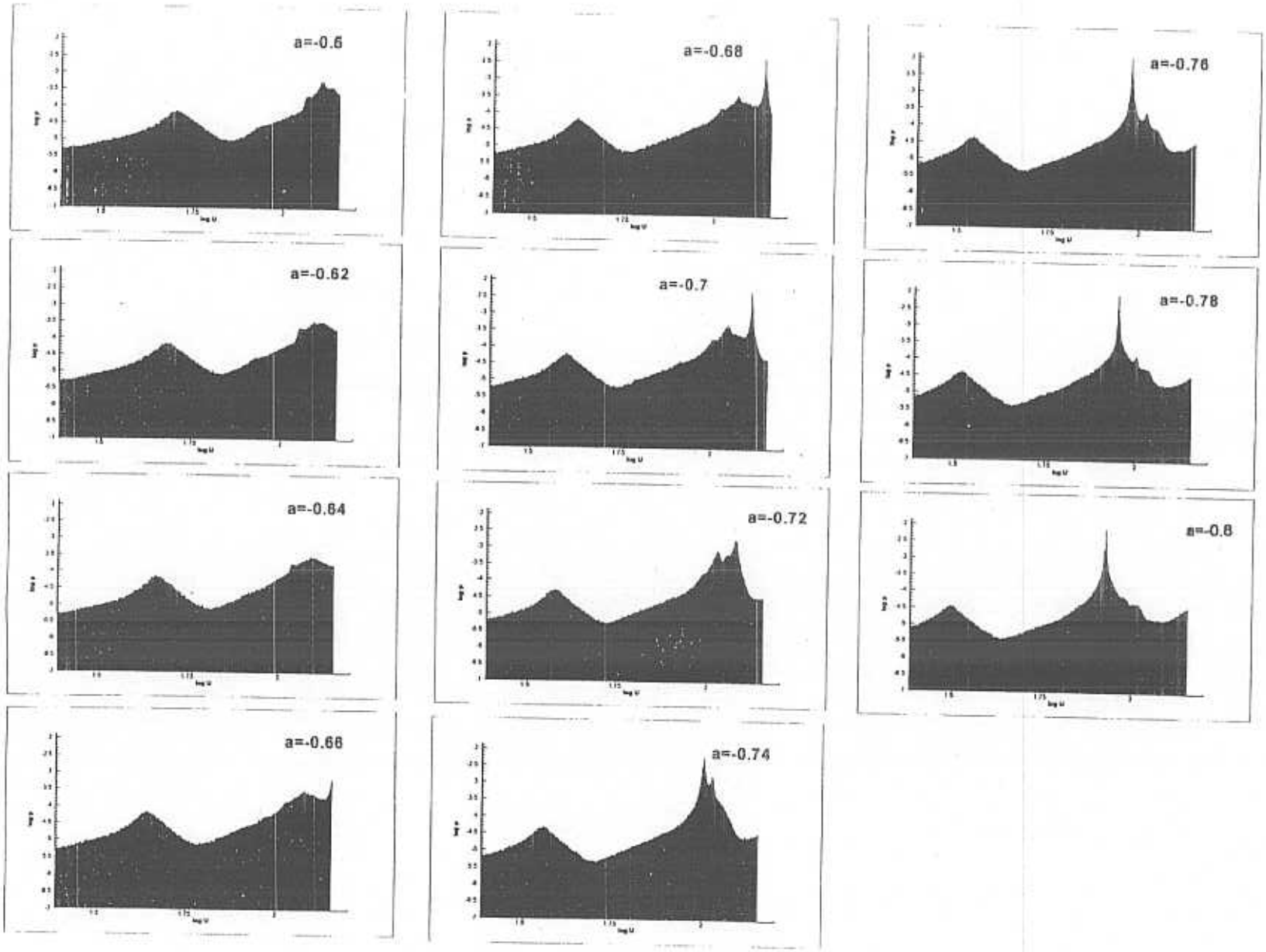

Short pipe; W=0.5", L=2.6"

log U = log f + a
a=[-0.6,-0.8]

Figure 13b: Vertical cuts through the plot of Figure 13a. All cuts are along a line of constant Strouhal number fL/U, but at different values of a lying between the extreme values defined in Figure 13a.

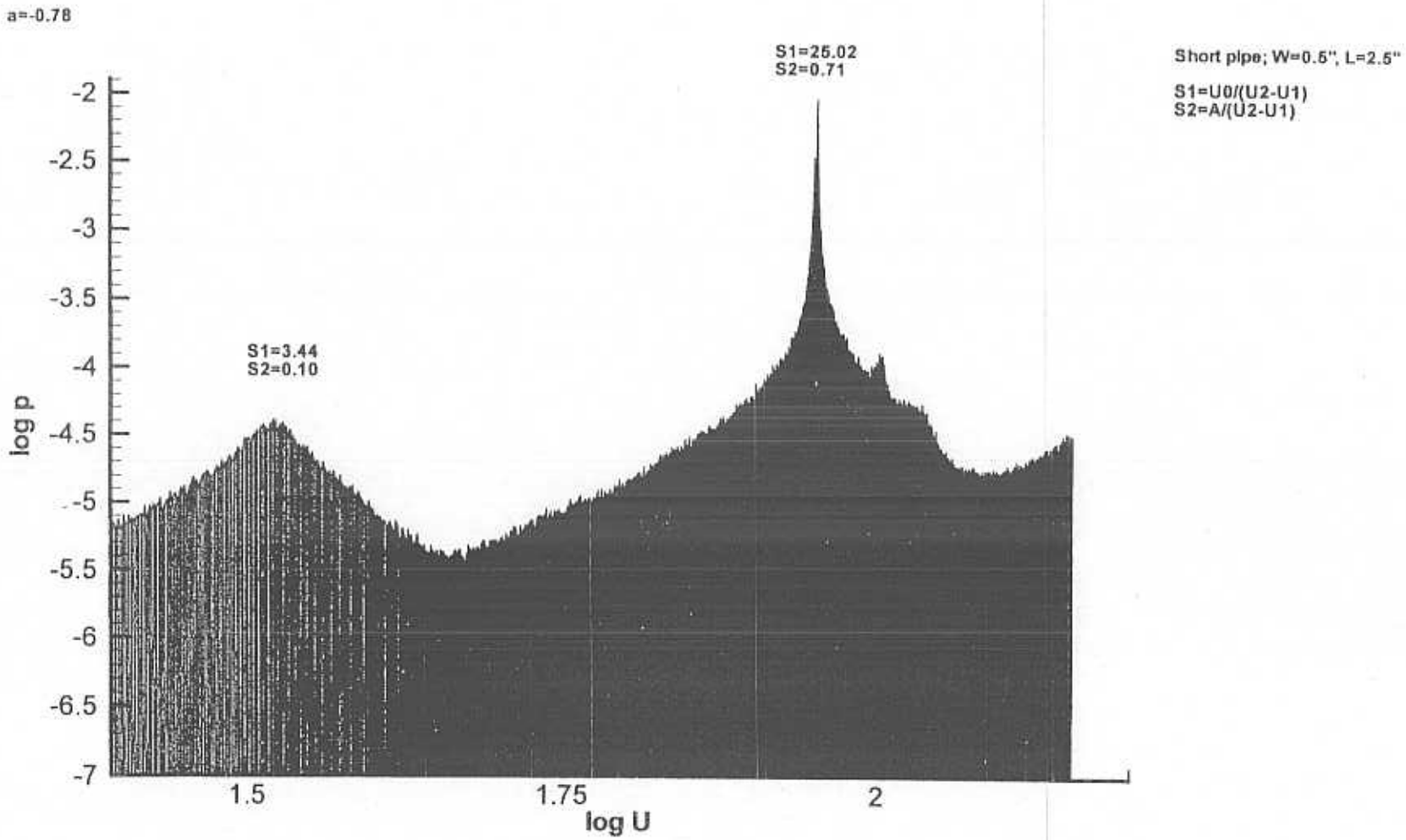

Figure 13c: Zoomed-in view of vertical cut selected from series of Figure 13b. Parameters S_1 and S_2 are sharpness factors analogous to Q-quality factors.